약학박사학위논문

Protective Role of Ninjurin1 in the Development of Intestinal Inflammation

대장 염증 발생 과정에서 Ninjurin1 단백질의 대장 보호 기능에 관한 연구

2020 년 8 월

서울대학교 대학원

약학과 의약생명과학전공

최 훈

Protective Role of Ninjurin1 in the Development of Intestinal Inflammation

대장 염증 발생 과정에서 Ninjurin1 단백질의 대장 보호 기능에 관한 연구

지도교수 서 영 준

이 논문을 약학박사 학위논문으로 제출함
2020년 6월

서울대학교 대학원
약학과 의약생명전공
최 훈

최 훈의 약학박사 학위논문을 인준함
2020년 6월

위 원 장 이 정 원 (印)

부위원장 차 혁 진 (印)

위 원 홍 순 선 (印)

위 원 정 규 원 (印)

위 원 서 영 준 (印)

ABSTRACT

Protective Role of Ninjurin1 in the Development of Intestinal Inflammation

Hoon Choi

Division of Pharmaceutical Bioscience
College of Pharmacy
The Graduate School
Seoul National University

Disruption of colonic homeostasis caused by aberrant M1/M2 macrophage polarization and dysbiosis contributes to inflammatory bowel disease (IBD) pathogenesis. However, the molecular factors mediating colonic homeostasis are not well characterized. Here, I found that Ninjurin1 (Ninj1) limits colon inflammation by regulating macrophage polarization and microbiota composition under homeostatic conditions and during colitis development. Ninj1 deletion in mice induced hypersusceptibility to colitis, with increased prevalence of colitogenic *Prevotellaceae* strains and decreased immunoregulatory *Lachnospiraceae* strains. Upon co-housing with WT mice, *Ninj1*$^{-/-}$ mice showed increased *Lachnospiraceae* and decreased *Prevotellaceae*

abundance, with subsequent improvement of colitis. Under homeostatic conditions, M1 macrophage frequency was higher in the *Ninj1*$^{-/-}$ mouse colons than WT mouse colons, which may contribute to increased basal colonic inflammation and microbial imbalance. Following colitis induction, Ninj1 expression was increased in macrophages; meanwhile *Ninj1*$^{-/-}$ mice showed severe colitis development and impaired recovery, associated with decreased M2 macrophages and escalated microbial imbalance. *In vitro*, Ninj1 knockdown in mouse and human macrophages activated M1 polarization and restricted M2 polarization. Finally, the transfer of WT macrophages ameliorated severe colitis in *Ninj1*$^{-/-}$ mice. These findings suggest that Ninj1 mediates colonic homeostasis by modulating M1/M2 macrophage balance and preventing extensive dysbiosis, with implications for IBD prevention and therapy.

Keywords : Ninjurin1; inflammatory bowel disease; inflammation; M1 macrophages; M2 macrophages; homeostasis; dysbiosis; colitis development; colitis recovery

Student Number **: 2015-30513**

TABLE OF CONTENTS

LIST OF FIGURES

LIST OF TABLES

LIST OF ABBREVIATIONS

ABX: antibiotic cocktails

APC: allophycocyanin

AOM: azoxymethane

BF: *Bacteroides fragilis*

BMDMs: bone marrow-derived macrophages

CAC: colitis-associated colon cancer

CAM: cell adhesion molecule

CD: Crohn's disease

CD: cluster of differentiation

CFSE: carboxyfluorescein succinimidyl ester

CoH: co-housing (housed)

COX: cyclooxygenase

DAI: disease activity index

DSS: dextran-sulfate sodium

EB: *Escherichia coli 0111:B4*

FACS: flow cytometry

FM: fecal microbiota

FMT: fecal microbiota transplantation

GR: glucocorticoid receptor

H&E: hematoxylin and eosin

HK: heat-killed

IBD: inflammatory bowel disease

Ig: immunoglobulin

IKK: IκB kinase

IL: interleukin

iNOS: inducible nitric oxide synthase

JNK: Janus kinase

L: lamina propria

LM: *Listeria monocytogenes*

LPS: lipopolysaccharide

LR: *Lactobacillus rhamnosus*

M: muscularis externa

MAPK: mitogen-activated protein kinase

MHC: major histocompatibility complex

MR: mannose receptor

Mrc1: mannose receptor c-type 1

MΦ: macrophage(s)

NF-κB: nuclear factor kappa-light-chain-enhancer of activated B cells

Ninjurin1: nerve injury-induced protein 1

Ninj1$^{-/-}$: Ninj1 knockout

NLRP: nucleotide-binding oligomerization domain Leucine rich repeat and pyrin domain containing

NOD: nucleotide-binding oligomerization domain-containing protein

NS: non-significance

PE: phycoerythrin

PerCP/Cy5.5: peridinin-chlorophyll protein complex-Cyanine5.5

p-IKKα/β$^{S176/180}$: phosphorylation of IKKα/β at serine 176 or 180

p-JNK$^{T183/Y185}$: phosphorylation of JNK at threonine 183 or tyrosine 185

p-p38$^{T180/Y182}$: phosphorylation of p38 at threonine 180 or tyrosine 182

p-p65^{S536}: phosphorylation of p65 at serine 536

OCD: obsessive-compulsive disorder

OTU: operational taxonomic unit

PCoA: principal coordinates analysis

PG: *Porphyromonas gingivalis*

qPCR: quantitative polymerase chain reaction

S: submucosa

SCFAs: short-chain fatty acids

SR: scavenger receptor

R: receptor

Retnla: resistin like alpha

RNI: reactive nitrogen intermediates

ROI: reactive oxygen intermediates

rRNA: ribosomal ribonucleic acid

SiH: single (singly) housing (housed)

ST: *Salmonella typhimurium*

TGF: tumor growth factor

TLR: toll-like receptor

TNF: tumor necrosis factor

T_{reg}: regulatory T cells

UC: unclassified

UC: ulcerative colitis

WT: wild-type.

INTRODUCTION

1. Macrophage plasticity and polarization

Macrophages are one of the multifunctional innate immune cells, and play a role in many biological process ranging from development, homeostasis and immune response to pathogen (Amit et al., 2016). Macrophages are heterogeneous and plastic cells which can switch from one to another phenotype, and their phenotype are regulated by the prevailing microenvironment (Mosser and Edwards, 2008). Macrophages are generally or simply categorized into two subsets, by activation state, as either classically activated (M1 or pro-inflammatory) or alternatively activated macrophages (M2 or anti-inflammatory and tissue repair) (Figure 1) (Sica and Mantovani, 2012). M1 macrophages are generally polarized by bacterial products including lipopolysaccharide or by Th1 cytokines such TNF-α and IFN-γ, produce and secrete higher levels of pro-inflammatory mediators such as TNF-α, IL-6, IL-1β, and iNOS, and lower levels of IL-10 (Figure 1). M2 macrophages are induced by Th2 cytokines IL-4 and IL-13, produce and secrete anti-inflammatory or tissue repair promoting mediators such as IL-10 and TGF-β (Figure 1) (Gordon and Martinez, 2010). Persistence of M1 macrophage polarization can cause extensive tissue damage by secreting of chronic pro-inflammatory mediators (Shapouri-Moghaddam et al., 2018). The activity of

M1 macrophages is balanced by M2 macrophage, which are primarily involved in downregulating inflammation and initiating tissue repair (Sica et al., 2015). Therefore, the balance of M1-M2 macrophage phenotype is important for the maintenance of tissue homeostasis.

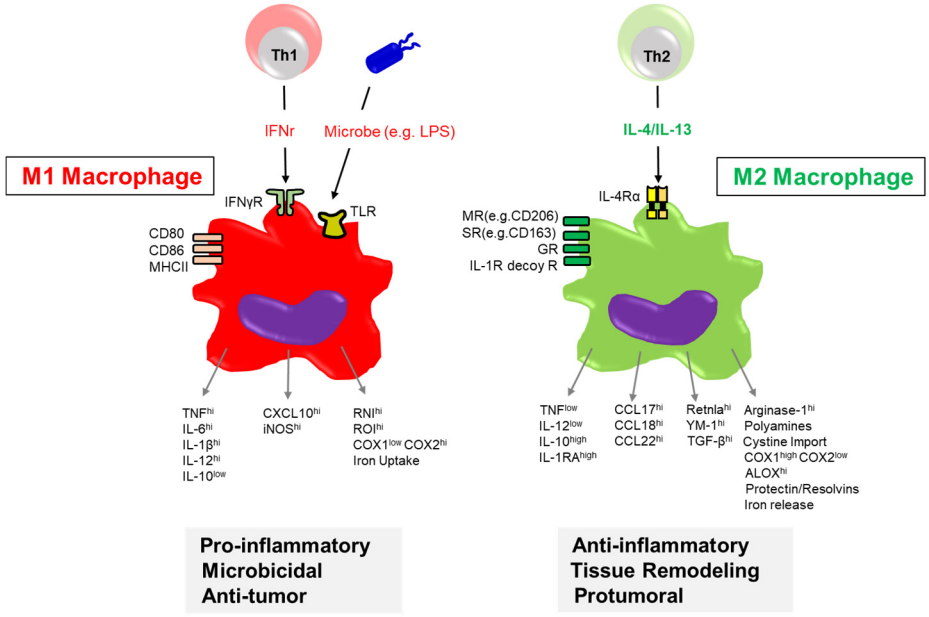

Figure 1. Schematic representation of M1/M2 macrophage polarization.

2. Macrophages and intestine homeostasis

The intestinal mucosa is a dynamic environment in which the host immune systems constantly interact with trillions of microbiota, and maintain a balance between commensal tolerance and pathogen recognition (Figure 2) (Belkaid and Hand, 2014; Hooper et al., 2012). Colonic macrophages are one of the important immune sentinels and effector population in the lamina propria; their close proximity to the epithelial layers suggest that they can sense and respond to the gut microbiota and its metabolites (Cerovic et al., 2014; Hume et al., 1984; Postler and Ghosh, 2017). Although lamina propria macrophages are characterized by highly phagocytic and bactericidal properties in response to bacteria, they show hyporesponsiveness to microbial stimulation under homeostatic conditions (Smythies et al., 2005) (Denning et al., 2007). This is a critical feature to maintain immune tolerance toward the high commensal bacterial load by preventing aberrant inflammatory response.

In addition, colonic macrophages initially develop a M1/pro-inflammatory phenotype but gradually acquire a M2/anti-inflammatory phenotype to maintain immune homeostasis (Bain et al., 2013; Isidro and Appleyard, 2016). The signals that cause the colonic macrophages to replace the initial pro-inflammatory/M1 phenotype with a tolerogenic and anti-inflammatory profiles are incompletely understood, but can include IL-10 secreted from macrophages and regulatory T (T_{reg}) cells (Figure 2) (Hoshi et al., 2012; Mowat, 2018).

However, in the presence of pathogenic bacteria, macrophages can elicit proper inflammation and protective host defense responses (Tanoue et al., 2010). It remains unknown whether these macrophages can selectively promote host defense against pathogenic bacteria in the intestine. Therefore, maintenance of a balance between commensal tolerance and pathogen elimination is important for the promotion of intestine homeostasis.

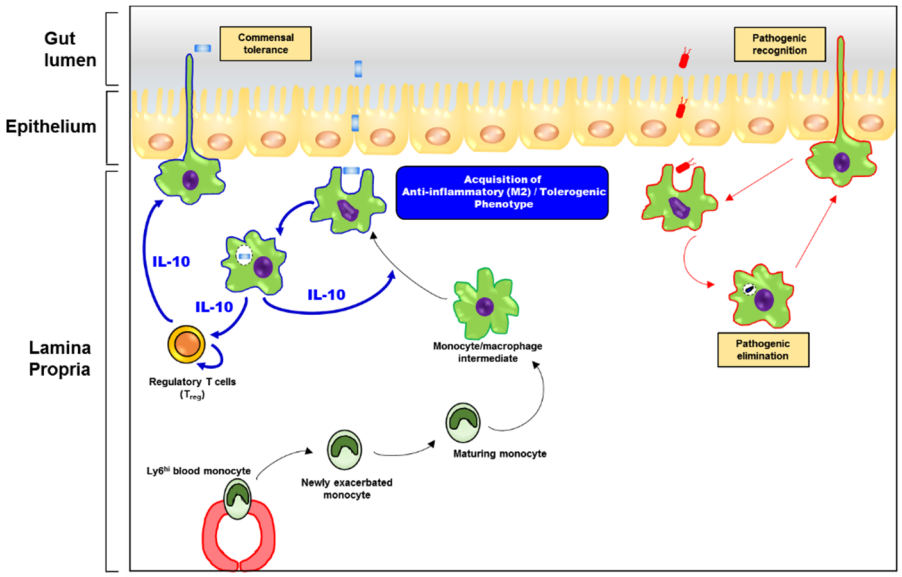

Figure 2. Maintenance of anti-inflammatory or tolerogenic phenotype of macrophage for colonic homeostasis.

3. Macrophage phenotype in IBD

Inflammatory bowel disease (IBD) is a chronic inflammatory conditions of the colon and small intestine. Crohn's disease (CD) and Ulcerative colitis (UC) are the two main types of IBD. The etiology of IBD is complex, but generally believed to arise from the interaction of environmental, genetic factors, leading to abnormal immunological response and inflammation in the intestine (Khor et al., 2011).

In IBD-prone mice and patients, colonic macrophages robustly respond to resident bacteria and their products, which results in the production of large amounts of pro-inflammatory factors (Hoshi et al., 2012; Kamada et al., 2008). Thus, the abnormal activation of resident colonic macrophages by commensal bacteria might facilitate the pathogenesis of IBD. Indeed, several studies reported that the accumulation of M1 macrophages are frequently observed in inflammatory bowel disease (IBD) patients (Figure 3) and animal models, and exacerbate the IBD pathogenesis by promoting the release of pro-inflammatory cytokines (Bernardo et al., 2018; Zhou et al., 2019).

Alternatively, M2 macrophages secrete anti-inflammatory or tissue repair-related mediator, alleviating the development of severe IBD (Hunter et al., 2010; Lin et al., 2014). Because the state of macrophage polarization is closely linked to the incidence and progression of IBD, it has recently been postulated as a

target of potential therapeutic intervention (Na et al., 2019).

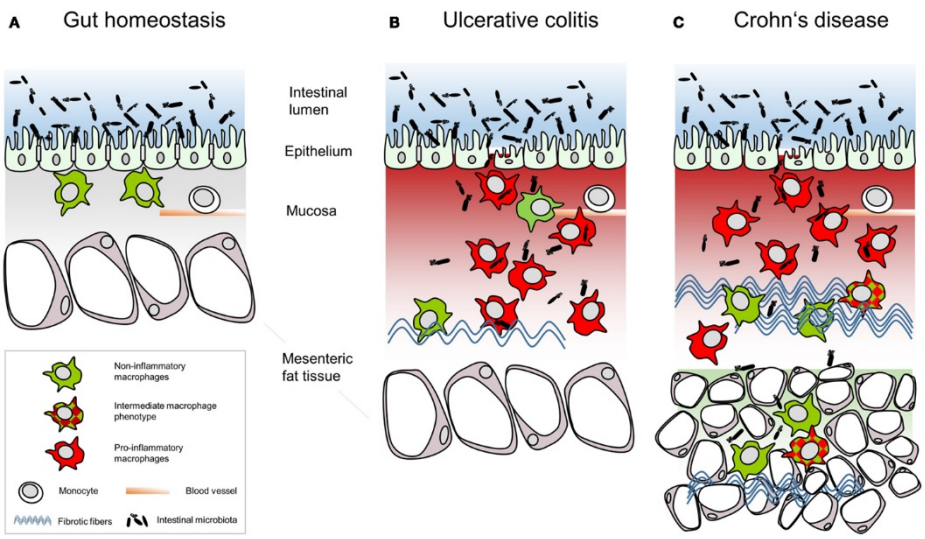

Figure 3. Schematic summary of the relative intestinal macrophage phenotype distribution in gut homeostasis, ulcerative colitis and Crohn's disease.

4. Gut microbiota and immune homeostasis

The intestinal mucosal surface of mammalian are colonized by microorganisms, including bacteria, fungi and viruses, commonly referred to as the gut microbiota. The mammalian gut microbiota is composed of more than 500 species within 4 dominant phylum: Actinobacteria, Bacteriodetes, Firmicutes, and Proteobacteira. Bacteriodetes and Firmicutes contain more than 90% of the bacterial population, but Actinobacteria and Proteobacteria are unusual in the colon. The main contributions of the microbiota to the host include the digestion and fermentation of carbohydrates, vitamin synthesis, polarization of gut-specific immune responses, and the prevention of colonization by pathogenic bacteria (Flint et al., 2012).

In particular, the short-chain fatty acids (SCFAs), including acetate, butyrate and propionate, produced by microbial fermentation of undigested carbohydrates play a crucial role in gut physiology and immunity (Figure 4) (Rooks and Garrett, 2016). SCFAs are inhibitors of histone deacetylases (HDACs) and ligands for G protein-coupled receptor (GPCR), thereby act as a signaling molecules. SCFAs-driven inhibition of HDACs tends to promote an anti-inflammatory or tolerogenic cell phenotype that is crucial for immune homeostasis. For example, exposure of lipopolysaccharide (LPS)-stimulated macrophages to butyrate, downregulated production of the pro-inflammatory factors (Chang et al., 2014). Recently, butyrate enhances anti-inflammatory

programming in macrophages (Figure 4) (Ji et al., 2016). These results indicate that butyrate promote M2 macrophage phenotype, and suppress M1 macrophage phenotype.

Additionally, SCFAs promotes the expansion of interleukin (IL)-10-producing regulatory T cells (T_{reg}) in a HDAC-dependent manner (Figure 4) (Smith et al., 2013). These findings suggest that reduced levels of SCFAs affect the anti-inflammatory or tolerogenic phenotype in macrophages, resulting in disruption of immune tolerance against commensal bacteria.

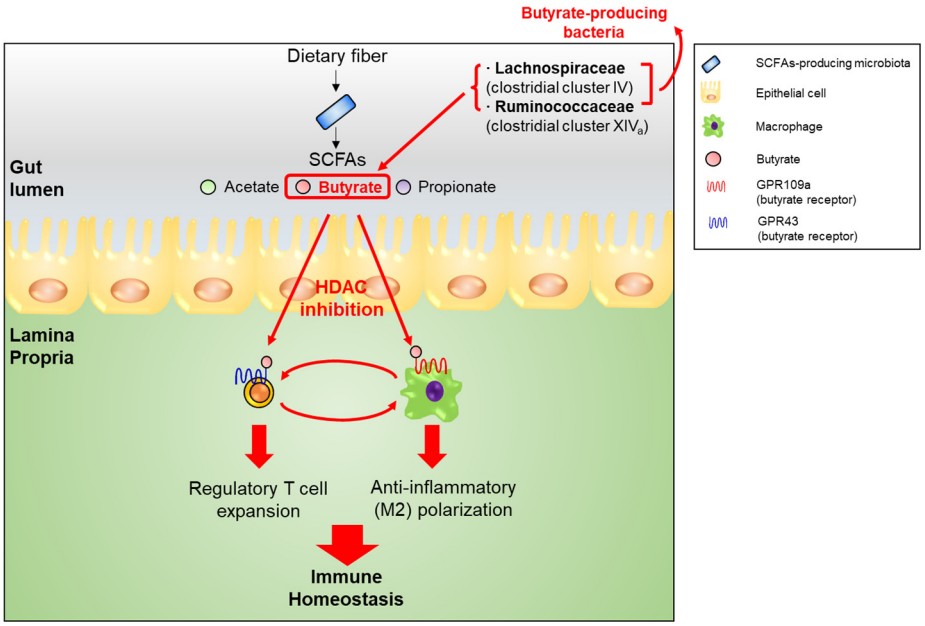

Figure 4. Immunomodulatory role of butyrate on macrophage and T_{reg} cell.

5. Dysbiosis and IBD

The breakdown of gut homeostasis caused by dietary changes, aging, or genetic deficiency can lead to compositional and functional changes in the gut microbiota, referred to as gut dysbiosis, contributing to aberrant immune response and hyperinflammation (Figure 5) (Belkaid and Hand, 2014). Gut dysbiosis has recently been associated with IBD as well as other immunological diseases such as atherosclerosis, asthma and central nervous system diseases (Levy et al., 2017).

Dysbiotic microbiome involves decreased non-pathogenic commensal bacteria and abnormal accumulation or increased virulence of certain commensal population of bacteria (Figure 5). Pathobionts are typically colitogenic in that they can trigger gut inflammation; therefore, there has been considerable interest in the identification of colitogenic pathobionts to understand the pathogenesis of IBD. Furthermore, a decreased abundance of SCFAs-producing immunoregulatory commensal bacteria, such as *Lachnospiraceae* and *Ruminococcaceae* families in patients with IBD was observed (Halfvarson et al., 2017; Kostic et al., 2014; Mottawea et al., 2016), suggesting that SCFAs treatment could lend clinical benefits to patients with colitis (Di Sabatino et al., 2005; Scheppach et al., 1992).

The immune system is considered one of the most important forces by which the host shapes the composition of the normal and dysbiotic microbiota

(Robertson et al., 2018). For example, mice with innate immune defects, such as NLRP6-, TLR5-, or NOD2-deficiency, display gut dysbiosis, which contributes to exacerbated colitis (Carvalho et al., 2012; Couturier-Maillard et al., 2013; Elinav et al., 2011). Therefore, interactions of dysbiotic microbiota with M1-polarized macrophages may accelerate aberrant immune activation and chronic inflammation.

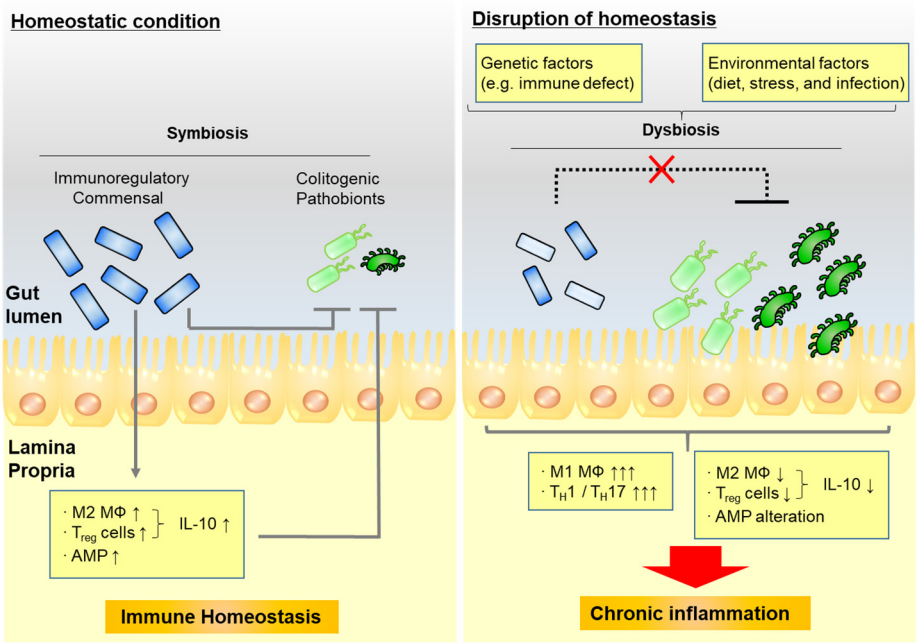

Figure 5. Dysbiosis and chronic inflammation.

6. Ninjurin1

Nerve injury-induced protein 1 (Ninjurin1, Ninj1) is a homophilic cell adhesion molecule (CAM) and originally identified as a transmembrane protein to be highly induced by nerve injury in dorsal root ganglion and Schwann cells (Araki and Milbrandt, 1996). Ninj1 is composed of two transmembrane regions, an intracellular region, and extracellular region at the N- and C-termini (Figure 6). In addition, 12 amino acid residues, from Pro^{26} to Asn^{37} positioned in the extracellular region of the N-terminus, were identified as a domain with homophilic binding affinity in a trans-interaction (Araki et al., 1997).

Ninj1 is widely expressed in several tissues and cells, and is especially known to be highly expressed in myeloid cells, including macrophages (Ahn et al., 2009; Araki et al., 1997; Ifergan et al., 2011; Lee et al., 2009; Woo et al., 2016). Ninj1 has been reported to play an important role in maintain bone and muscle homeostasis (Bae et al., 2019; Kny et al., 2019).

Furthermore, it is widely involve in inflammation-related diseases. For example, Ninj1 deficiency or repression attenuates the severity of experimental autoimmune encephalomyelitis (EAE) or in a rat middle cerebral artery occlusion (MCAO) mice by suppressing leukocyte infiltration (Ahn et al., 2014; Ifergan et al., 2011; Lee et al., 2018). Additionally, Ninj1 promotes the development of pulmonary fibrosis by promoting interaction between

macrophage and alveolar epithelial cells (Choi et al., 2018).

On the other hands, Ninj1 contributes nerve regeneration in response to sciatic nerve injury by promoting neurite outgrowth from the dorsal root ganglion (Araki and Milbrandt, 1996). In addition, Ninj1 deficiency increases systemic inflammation and reduces survival rate of mice with age (Yang et al., 2017). Furthermore, pericyte-specific Ninj1 deletion attenuates vascular maturation and blood flow recovery after hindlimb ischemia induction (Minoshima et al., 2018). Interestingly, Ninj1 overexpression on macrophages suppress the development of colitis-associated colon cancer by limiting infiltration of tumor-associated macrophages (TAMs) (Woo et al., 2016). However, the biological role of Ninj1 in gut microbiota-associated colitis has not yet been well characterized.

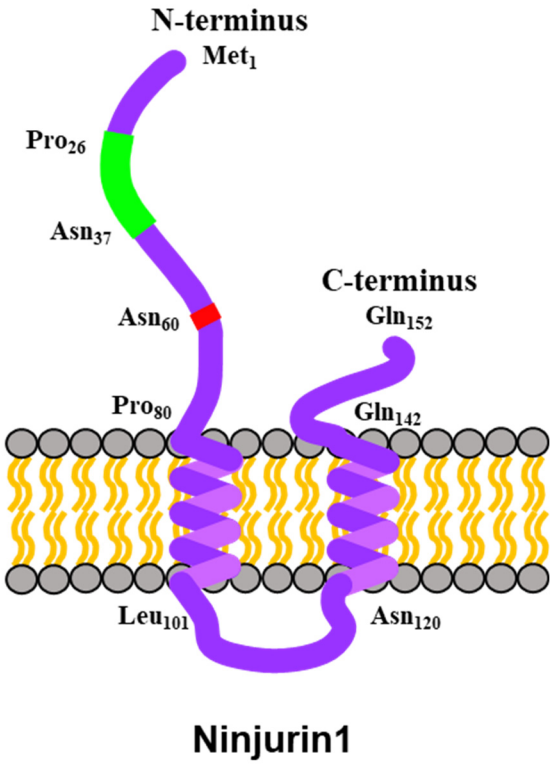

Figure 6. Diagrammatic description of Ninjurin1.

7. Dextran sulfate sodium (DSS)-induced colitis

Dextran sulfate sodium (DSS) is a water-soluble, negatively charged sulfated polysaccharide with a highly variable molecular weight ranging from 5 to 1400 kDa. DSS-induced colitis is a murine model that chemically induces the intestinal inflammation, and histological damage is confined to the large intestine, specifically the distal colon where an enormous number of microorganisms live (Figure 7) (Chassaing et al., 2014; Perse and Cerar, 2012). It is directly toxic to colonic epithelium causes disruption of the colon epithelial barrier and thereby entry of luminal bacteria and their products, contributing the development of colon inflammation (Kiesler et al., 2015). Intriguingly, this inflammation develops in the absence of B or T cells mediating adaptive immunity (Krieglstein et al., 2002; Okayasu et al., 1990), suggesting that innate immune cells including macrophages are sufficient to cause colon inflammation. On this basis, DSS-induced colitis has become a useful animal models for the study of the innate immune mechanisms during the development of colon inflammation.

Recently, DSS-induced colitis has provided a platform for the investigation of the effect of host-microbiota interactions on colitis development. For example, NLRP6-deficient mice are hypersusceptibility to colitis with increased abundance of *Prevotellaceae* species via reduction of IL-18. In addition, NLRP6-deficient fecal microbiota colonized with WT mice

accelerate the development of colitis (Elinav et al., 2011).

In this study, I induced experimental colitis via DSS administration to WT and *Ninj1*$^{-/-}$ mice to investigate the effects of Ninj1 on macrophage polarization and microbial composition during colitis development.

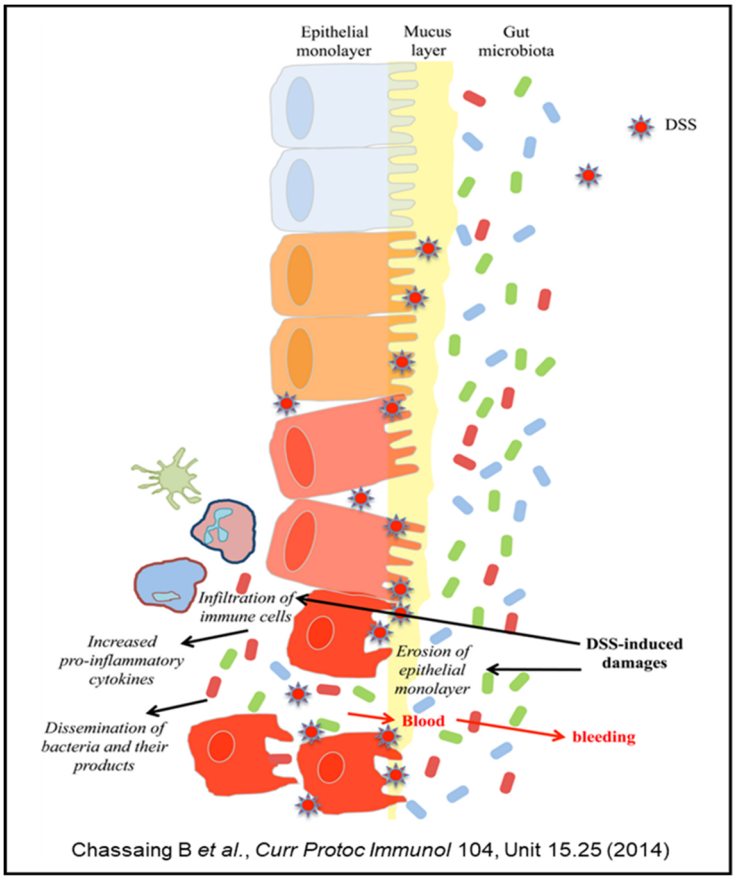

Figure 7. Schematic representation of DSS-induced colitis.

PURPOSE OF THIS STUDY

Disruption of colonic homeostasis caused by aberrant M1/M2 macrophage polarization and dysbiosis contribute to the pathogenesis of inflammatory bowel disease (IBD). However, the molecular factors that mediate macrophage polarization and microbial homeostasis for the maintenance of colonic homeostasis are not well characterized.

In the present study, I sought to investigate the role of Ninj1 in mediating colonic homeostasis via modulation of M1/M2 macrophage polarization and microbial compostion under homeostatic conditions and during colitis development. To define this, I induced experimental colitis via dextran sulfate sodium (DSS) administration to *Ninj1*$^{-/-}$ mice. Results show that under homeostatic conditions, Ninj1 deficiency increased the frequency of M1 macrophages and microbial imbalance, inducing hypersusceptibility to colitis. Further, during colitis development, Ninj1 deficiency accelerates M1 macrophage accumulation and escalates dysbiosis, contributing to severe colitis development and impaired recovery. Thus, these findings suggest that Ninj1 plays a critical role in maintenance and restoration of colonic homeostasis by influencing macrophage polarization and microbial composition.

MATERIALS AND METHODS

1. Mice

The *Ninj1*$^{-/-}$ mice has been described previously (Ahn et al., 2014). All animal experiments were performed with male, age-matched mice of similar weight (age: 10–12-week-old, starting weight: 24–27 g) for the respective experimental groups. All mice were maintained under specific pathogen-free conditions in the animal-housing facility at the Seoul National University. Animal experiments were approved by the Institutional Animal Care and Use Committees of Seoul National University and performed in accordance with the Guide for Animal Experiments of the Korean Academy for Medical Sciences.

2. DSS-induced colitis

The mice were provided 2 or 2.5 % dextran sulfate sodium (DSS, 36,000–50,000 Da; MP Biomedicals, Illkirch, France) in their drinking water for six days, followed by the administration of normal water for 2–6 days. Body weight and survival were monitored every 24 h, and the disease activity index (DAI) was calculated daily for each mouse. The maximum DAI score was 12, according to the following parameters: weight loss (score 0 = no loss from the initial body weight; score 1 = 1%–5% weight loss; score 2 = 6%–10% weight loss; score 3 = 11%–20% weight loss; score 4 = more than 20% weight loss),

stool consistency (score 0 = normal stool, score 2 = loose stool; stool that readily becomes a paste upon handling, score 4 = diarrhea; liquid that adheres to the anus), and rectal bleeding (score 0 = no bleeding. score 2 = slight bleeding, score 4 = gross bleeding).

3. Histopathological Score

Disease severity was determined by histopathologic scoring of a hematoxylin and eosin (H&E)-stained colon, which is characterized by inflammation severity (score 0–3), crypt damage (score 0–5), and ulceration (score 0–3). The presence of occasional inflammatory cells in the lamina propria was scored as 0, increased numbers of inflammatory cells in the lamina propria was scored as 1, infiltration of inflammatory cells into the submucosa was scored as 2, and transmural extension of the infiltrate was scored as 3. Intact crypt was scored as 0, loss of the basal one-third was scored as 1, loss of the basal two-thirds was scored as 2, 100% crypt loss was scored as 3, change of epithelial surface with erosion was scored as 4, and confluent erosion was scored as 5. Absence of ulcers was scored as 0, 1–2 ulceration foci was scored as 1, 3–4 ulceration foci was scored as 2, and confluent or extensive ulceration was scored as 3. Data of the three distal colon regions were then averaged to obtain an overall score.

4. Antibiotic treatment

Gut microbiota depletion by antibiotic cocktails was achieved as described previously (Wellman et al., 2017). Briefly, the mice were administered antibiotic cocktails for four weeks prior to DSS treatment. The antibiotic cocktails consisted of ampicillin (1 g/L; Sigma-Aldrich, St. Louis, MO, USA), vancomycin (0.5 g/L; Sigma-Aldrich), neomycin (1 g/L; Sigma-Aldrich), and metronidazole (1 g/L; Sigma-Aldrich) in the drinking water.

5. Bacterial 16S rRNA sequencing and data analysis

A 16S rRNA sequencing library was constructed according to the 16S metagenomics sequencing library preparation protocol (Illumina, San Diego, CA, USA) targeting the V3 and V4 hypervariable regions of the 16S rRNA gene. KAPA HiFi HotStart ReadyMix (KAPA Biosystems, Wilmington, MA, USA) and Agencourt AMPure XP system (Beckman Coulter Genomics, Brea, CA, USA) were used for PCR and purification of the PCR products, respectively. Genomic DNA was isolated from the mouse stool using the PowerSoil DNA Isolation Kit (Mo Bio, Carlsbad, CA, USA). The initial PCR was performed with 12 ng of template using region-specific primers shown to have compatibility with the Illumina index and sequencing adapters (forward primer: 5′-

TCGTCGGCAGCGTCAGATGTGTATAAGAGACAGTCGTCGGCAGCGT

CAGATGTGTATAAGAGACAGCCTACGGGNGGCWGCAG-3′; reverse primer: 5′-GTCTCGTGGGCTCGGAGATGTGTATAAGAGACAGGTCTCGTGGGCTCGGAGATGTGTATAAGAGACAGGACTACHVGGGTATCTAATCC-3′).

After magnetic bead-based purification of PCR products, the second PCR was performed using primers from the Nextera XT Index Kit (Illumina) with a limited cycle. Purified PCR products were visualized by gel electrophoresis and quantified using the Qubit dsDNA HS Assay Kit (Thermo Fisher Scientific, Waltham, MA, USA) on a Qubit 3.0 fluorometer. The pooled samples were run on an Agilent 2100 Bioanalyzer (Agilent) for quality analysis prior to sequencing. The libraries were quantified by qPCR using the CFX96 Real-Time System (BioRad, Hercules, CA, USA). After normalization, the library was sequenced using the MiSeq system (Illumina) with 300-bp paired-end reads. Sequence processing and cleanup were performed using QIIME. Paired-end duplex sequence reads were combined into contigs using fastq-join. Chimeric sequences were identified and removed using VSEARCH. The sequences were then aligned to the SILVA 16S rRNA gene reference alignment database. Finally, the sequences with 97% similarity were clustered into operational taxonomic units. Then, the composition of microbial composition and differences in microbial diversity was determined.

6. Co-housing experiment

Prior to DSS treatment, 4-week-old WT and *Ninj1*$^{-/-}$ mice were placed in single (SiH) or co-housing (CoH) conditions for six weeks, to allow the natural transfer of the gut microbiota. Microbial diversity and composition were compared in feces from WT and *Ninj1*$^{-/-}$ mice. Co-housed mice were compared with single-housed mice as controls.

7. Tissue harvesting

Anaesthetized mice were transcardially perfused with 0.1 M PBS (pH 7.4). The colon samples were prepared using the Swiss-rolled method as described previously (Moolenbeek and Ruitenberg, 1981). The colon was excised, opened longitudinally, and washed with cold PBS. The opened colon was rolled on a wooden stick and fixed with 4% paraformaldehyde (PFA) at 4 °C. After dehydration with serial gradients of sucrose, the colon was embedded in optimal cutting temperature (O.C.T) compound (Sakura, Tokyo, Japan) and 8- or 10-μm-thick cryosection slides of the colon tissues were prepared for immunofluorescence staining.

8. Preparation of bone marrow-derived macrophages (BMDMs)

The femur and tibia were obtained from 8–12-week-old WT or *Ninj1*$^{-/-}$ mice. After sacrificing the mice by cervical dislocation, the hind legs were

dissected and the skin and muscle from the leg were removed using sterile scissors and forceps. Under sterile conditions, epiphyses were removed, and the bones were flushed with 25 mL of ice-cold sterile PBS using a 22-gauge needle syringe through a 70-μm strainer (BD Falcon, Franklin Lakes, NJ, USA) into a 50-mL tube. The filtrates were centrifuged at 500 × *g* for 5 min at 4 °C, and the supernatants were discarded. The pellets were resuspended in RPMI (GenDEPOT, Barker, TX, USA), supplemented with 10% FBS (GenDEPOT), 100 U/mL penicillin (GenDEPOT), 100 μg/mL streptomycin (GenDEPOT), and 0.25 μg/mL amphotericin B (GenDEPOT) and added to cell culture flasks. After 6 h of incubation at 37 °C, nonadherent cells were collected and resuspended in complete RPMI containing 30% L929 conditioned media. The resuspended cell suspension was filtered through a 40-μm strainer, plated on Petri dishes, and allowed to differentiate at 37 °C for six days with a single addition of complete RPMI containing 30% L929-conditioned media.

9. Isolation of colonic lamina propria (cLP) cells

The gut pieces was cut into 2–3 mm pieces and incubated in Hanks' balanced salt solution (HBSS) containing 5 mM EDTA and 1 mM DTT for 20 min in a shaking incubator at 37 °C two or three times to remove the epithelial layer. After incubation, the gut pieces were incubated with 1 mg/mL collagenase D (Roche, Basel, Switzerland), 1 mg/mL dispase II (Sigma-Aldrich), and 25 U/mL DNase I (Sigma-Aldrich) in DMEM (GenDEPOT) for

60 min in a shaking incubator at 37 °C twice. Single-cell suspensions were harvested by filtering through a 40-μm strainer. Then, cLP suspensions were purified with 40%–75% discontinuous Percoll gradient (Sigma-Aldrich) at 1000 × *g* for 20 min at 20 °C.

10. THP-1 cell culture and macrophage differentiation

THP-1 cells from the American Type Culture Collection (ATCC, Manassas, VA, USA) were cultured in complete RPMI-1640 medium at 37 °C in an atmosphere of 95% O2 and 5% CO2. The macrophage-like state was obtained by treating THP-1 cells for 48 h with 100 ng/mL phorbol 12-myristate 13-acetate (PMA, Sigma-Aldrich). Differentiated, adherent cells were washed and rested for an additional 24 h in complete RPMI-1640 medium to obtain the resting state of M0 macrophages.

11. Small interfering RNA (siRNA) Transfection

When M0 BMDMs or PMA-differentiated THP-1 macrophages reached 60–70% confluency, they were transfected with a Ninj1 siRNA (20 nM) or negative control siRNA (20 nM) with Lipofectamine RNAi MAX (Invitrogen) according to manufacturer's instructions. After 24 h of transfection, media were changed with presence or absence of LPS (1 μg/mL; Sigma-Aldrich) or IL-4 (50 ng/mL; BioLegend, San Diego, CA, USA). The siRNA sequences are listed

in Table 1.

12. Macrophage stimulation

For bacterial stimulation, macrophages were stimulated with heat-killed *Bacteroides fragilis* (HKBF), heat-killed *Lactobacillus rhamnosus* (HKLR), heat-killed *Listeria monocytogenes* (HKLM), heat-killed *Porphyromonas gingivalis* (HKPG), heat-killed *Escherichia coli 0111:B4* (HKEB), heat-killed *Salmonella typhimurium* (HKST) (10^8 cells/mL; InvivoGen, San Diego, CA, USA), lipopolysaccharide (LPS)-EB, and LPS-ST (1 μg/mL, Sigma-Aldrich) for 4 h. For M1 or M2 macrophage polarization, macrophages were stimulated with LPS (1 μg/mL; Sigma-Aldrich) or recombinant mouse or human IL-4 (50 ng/mL; BioLegend, San Diego, CA, USA) for 6 or 24 h.

13. Immunofluorescence

The frozen colon sections were blocked with 5% normal donkey or goat serum (Sigma-Aldrich) and 0.5% Triton X-100 (Amresco, Fountain Parkway, Solon, OH, USA) in PBS, and incubated overnight at 4 °C with primary antibodies for $Ninj1_{1-15}$ (AbFrontier, Seoul, Korea), F4/80 (AbD Serotec, Oxford, UK), EpCAM (BD Biosciences, San Jose, CA), CD31 (BD Biosciences), NIMP-R14 (Abcam, Cambridge, MA, USA), CD3 (R&D Systems, Minneapolis, MN, USA), iNOS (BD Biosciences), arginase I (Santa

Cruz Biotechnology, Santa Cruz, CA, USA), and CD206 (R&D Systems), TNF-α (Abcam) and IL-10 (Abcam). After extensive washing in PBS containing 0.1% Tween-20 solution, the sections were treated with Alexa-488 or 546-conjugated secondary antibodies (1:500, Invitrogen, Carlsbad, CA, USA) for 1 h at 20–25 °C followed by counter staining with Hoechst (Sigma). Fluorescent images were obtained under confocal microscopy (Carl Zeiss AG, Oberkochen, Germany), and immuno-positive areas were quantified using ImageJ software. Unless otherwise specified, three images from a single animal were quantified and the mean value was considered as a representative for the animal.

14. Flow cytometry

The cLP suspensions were incubated with CD16/32 (BD Biosciences) in FACS buffer (1.5% FBS in PBS) for 30 min at 4 °C to block the Fcγ receptors and were then surface-stained with antibodies for 30 min at 4 °C. Antibodies to V450-CD11b (BD Biosciences) or Alexa Fluor 700-CD11b (M1/70) (BioLegend), PE or PerCP/Cy5.5-F4/80 (BM8), FITC or APC-CD206 (C068C2), and PE or PerCP/Cy5.5-CD86 (GL-1) were used. All antibodies were used at 1:100 dilution. The cells were then washed with FACS buffer and analyzed. The samples were analyzed with FACSVerse or FACSAriaII (BD Bioscience) and the data were analyzed using FACSuite (BD Bioscience) or FlowJo (Tree Star, Ashland, OR, USA).

15. RNA isolation and qPCR

The total RNA from the colon tissues or cells was extracted using TRIzol Reagent (Invitrogen) according to the manufacturer's instructions. Two micrograms of RNA from each sample were reverse-transcribed with an oligo (dT) primer using Moloney murine leukemia virus (MMLV) reverse transcriptase (Promega, Madison, WI, USA). Quantitative real-time PCR was then performed using the StepOnePlus Real-Time PCR System (Applied Biosystems, Foster City, CA, USA) and the RealHelix qPCR Kit (NanoHelix, Daejeon, Korea). The comparative Ct ($2^{-\Delta\Delta Ct}$) method was used to quantify the mRNA levels. The relative mRNA levels were normalized using the housekeeping gene *Gapdh*. Primer sequences used in this study are provided in Table 1.

16. Immunoblotting

The cells used were homogenized and lysed in buffer [20 mM Tris-HCl (pH 7.5), 150 mM NaCl, 1 mM Na2EDTA, 1 mM EGTA, 1% Triton, 2.5 mM sodium pyrophosphate, 1 mM beta-glycerophosphate, 1 mM Na3VO4, 1 μg/mL leupeptin, and protease inhibitor cocktail]. Subsequently, 50 μg of protein lysate was subjected to SDS-PAGE and immunoblot analyses. Immunoblotting was performed using the primary antibodies against IKKβ (D30C6), p65 (D14E12), SAPK/JNK, p38 MAPK (D13E1), p-IKKα/β

(Ser176/180), p-p65 (Ser536), p-SAPK/JNK (Thr183/Tyr185) (81E11), p-p38 MAPK (Thr180/Tyr182) (D3F9) (Cell Signaling Technology, Danvers, MA, USA), Ninj11-15 (AbFrontier), α-Tubulin, and β-Actin (Sigma-Aldrich). HRP-conjugated antibodies were used as the secondary antibodies. Quantification of western blots was performed with ImageJ software.

17. Enzyme-linked immunosorbent assay (ELISA)

Media supernatants were collected, and cytokines were quantified using ELISA kits (BioLegend) for mouse or human TNF-α, IL-6 and IL-1β, according to the manufacturer's protocol.

18. Adoptive transfer of macrophages

BMDMs were suspended at a concentration of 4×10^7 cells/mL in PBS. Next, 50 μL (2×10^6 cells) of the prepared samples was intravenously injected into each *Ninj1*$^{-/-}$ mouse on the 2nd and 4th day, following the start of DSS treatment. To trace the transferred BMDMs *in vivo*, BMDMs were labeled with carboxyfluorescein succinimidyl ester (CFSE) (Invitrogen). After 8 days of DSS treatment, the proportion of CFSE$^+$ F4/80$^+$ macrophages was analyzed using confocal microscopy.

19. Data analysis and statistics

All data are expressed as mean ± SEM. One-way ANOVAs followed by Tukey's tests (for multiple comparisons) or two-tailed Student's *t*-tests (for single comparisons) were used for statistical analyses. The results with a *P* value of < 0.05 were considered statistically significant. All statistical analyses were performed using GraphPad Prism V.8.2.0 (GraphPad Software, San Diego, CA, USA).

Table 1. Oligonucleotide information

siRNA sequences used for knockdown			
Host	Gene	sense (5'->3')	antisense (5'->3')
Mouse	Control	GCGAAAGAGAAAGCAA	UUGCUUUCUCUUUCGC
	Ninj1 #1	CAGGGCAAUGAUUUCGCCUUCUUCG	CGAAGAAGGCGAAAUCAUUGCCCUG
	Ninj1 #2	ACCGGCCCAUCAAUGUAAACCAUUA	UAAUGGUUUACAUUGAUGGGCCGGU
Human	Control	CGUUAAUCGCGUAUAAUACGCUGAT	AUACGCGUAUUAUACGCGAUUAACGAC
	NDN1 #1	GCCGUAGACCCUUGUAUAUACCCUGC	GCAGGGUAUAUACAAGGUCUACGGCCC
	NDN1 #2	AGCACGCCAAGCUGGACUUCCUCAA	UUGAGGAAGUCCAGCUUGGCGUGCUUG
Primer sequences for qPCR detection			
Host	Gene	sense (5'->3')	antisense (5'->3')
Mouse	*Gapdh*	AGGTCGGTGTGAACGGATTTG	GGGGTCGTTGATGGCAACA
	Tnf	ATCCGGCGACGTGGAACTG	TGGGAGTAGACAAGGTACAACCC
	Il6	TAGTCCTTCCTACCCCAATTTCC	TTGGTCCTTAGCCACTCCTTC
	Nos2	GGCAGCCTGTGAGACCTTTG	TGCATTGGAAGTGAAGCGTTT
	Il1b	CTACAGGCTCCGAGATGAACAAC	TCCATTGAGGTGGAGAGCTTTC
	Il10	AGCCGGGAAGACAATAACTG	GGAGTCGGTTAGCAGTATGTTG
	Atg1	TGGCTTGCGAGACGTAGAC	GCTCAGGTGAATCGGCCTTTT
	Mrc1	GCTGAATCCCAGAAATTCCGC	ATCACAGGCATACAGGGTGAC
	Retnla	CCAATCCAGCTAACTATCCCTCC	CCAGTCAACGAGTAAGCACAG
	Ninj1	AGTCGGGCACTGAGGAGTAT	TACATTGATGGGCCGGTTCC
Human	*GAPDH*	TCTCCCTCTGACTTCAACAGCGACA	CCCTGTTGCTGTAGCCAAATTCGT
	TNF	GCCTCTTCTCCTTCCTGATCG	TCGAGAAGATGATCTGACTGCC
	IL6	TGCAATAACCACCCCTGACC	AGCTGCGCAGAATGAGATGA
	IL1B	GTGGCAATGAGGATGACTTGTTCT	TGTAGTGGTGGTCGGAGATTCG
	MRC1	GGGTTGCTATCACTCTCTATGC	TTTCTTGTCTGTTGCCGTAGTT
	CD209	TCAAGCAGTATTGGAACAGAGGA	CAGGAGGCTGCGGACTTTTT
	CCL22	ATTACGTCCGTTACCGTCTG	TAGGCTCTTCATTGGCTCAG
	NDNJ1	CCAGTACGACCTTAACAACCG	AGGCCGTGATGAAGATGTTG

Table 2. Number and proportion of iNOS$^+$ or Arg-1$^+$ macrophages and TNF-α$^+$ or IL-10$^+$ macrophages in normal or DSS-treated colon tissues detected using immunofluorescence.

Data are expressed as mean ± SD, with five mice in each group. *P < 0.05 vs. Normal WT group; $^{\#}P$ < 0.05, $^{\#\#}P$ < 0.01, $^{\#\#\#}P$ < 0.001 vs. DSS WT group.

Group	iNOS$^+$ F4/80$^+$ macrophages			Arg-1$^+$ F4/80$^+$ macrophages		
	F4/80$^+$ cells	iNOS$^+$ cells	iNOS$^+$ F4/80$^+$	F4/80$^+$ cells	Arg-1$^+$ cells	Arg-1$^+$ F4/80$^+$
	(n / 0.025mm^2)		(%)	(n / 0.025mm^2)		(%)
Normal WT	18.86±3.39	2.53±0.83	13.53±2.38	18.33±4.80	11.33±4.25	61.42±4.38
Normal *Nlrp1*$^{-/-}$	19.73±6.66	3.60±1.50*	18.67±4.01*	19.93±3.17	10.80±3.03	54.84±3.19*
DSS WT	22.73±4.34	8.33±3.99	36.92±6.41	23.40±1.55	13.13±3.20	55.95±5.92
DSS *Nlrp1*$^{-/-}$	23.20±5.45	12.73±4.01##	55.31±8.33##	24.53±2.78	7±2.45###	29.48±8.74###

Group	TNF-α$^+$ F4/80$^+$ macrophages			IL-10$^+$ F4/80$^+$ macrophages		
	F4/80$^+$ cells (n / 0.025mm^2)	TNF-α$^+$ cells (n / 0.025mm^2)	TNF-α$^+$ F4/80$^+$ (%)	F4/80$^+$ cells (n / 0.025mm^2)	IL-10$^+$ cells (n / 0.025mm^2)	IL-10$^+$ F4/80$^+$ (%)
Normal WT	18.73±3.99	4.27±1.62	23.36±1.27	18.80±1.64	4.80±1.47	25.56±2.99
Normal *Nin1*$^{-/-}$	19.86±2.52	5.47±1.41*	27.40±2.60*	19.60±3.28	4.07±1.28	21.00±2.95*
DSS WT	24.67±1.97	8.80±1.82	36.68±4.59	25.93±2.60	6.40±1.88	24.60±2.73
DSS *Nin1*$^{-/-}$	25.93±2.20	15.60±5.59$^{\#\#\#}$	60.61±6.49$^{\#\#}$	27.80±3.19	5.07±1.53$^{\#}$	18.44±2.64$^{\#\#\#}$

RESULTS

1. Enhanced susceptibility of *Ninj1*$^{-/-}$ mice to colitis is dependent on gut microbiota

To investigate the relationship between the gut microbiota and Ninj1 in the development of colitis, I administered wild-type (WT) and *Ninj1*$^{-/-}$ mice with 2% dextran sulfate sodium (DSS) in the presence of normal gut microbiota or after disrupting the microbiota by treatment with antibiotics (Figure 8). There was no significant difference in DSS consumption between the groups (Figure 9). On day 10 after colitis induction, all WT mice with normal gut microbiota survived; meanwhile only 60% of the *Ninj1*$^{-/-}$ mice survived (Figure 10A). This was accompanied by dramatic weight loss (Figure 10B). The disease activity index (DAI) (Siegmund et al., 2001), which is calculated as the sum of scores for weight loss, stool consistency, and rectal bleeding, was also higher in *Ninj1*$^{-/-}$ mice than in WT mice in the presence of the gut microbiota (Figure 10C). Additionally, colon length, which indicates the degree of colon damage, was shorter in *Ninj1*$^{-/-}$ mice than in WT mice (Figure 11). Consistent with the clinical parameters mentioned above (Figure 10), histopathological analyses of colons revealed considerable differences in tissue architecture between WT and

Ninj1$^{-/-}$ mice, with crypt loss, increased ulceration, and infiltration of inflammatory cells (Figure 12). However, these clinical or histopathological differences between WT and *Ninj1*$^{-/-}$ mice disappeared in the absence of the gut microbiota (Figure 10–12), indicating that *Ninj1*$^{-/-}$ mice are hypersusceptible to colitis in the presence of the gut microbiota. Furthermore, disease severity was not significantly different between WT mice in the presence and absence of the gut microbiota (Figure 10–12). These results suggest that microbiota composition shaped by Ninj1 deficiency promotes colitis development.

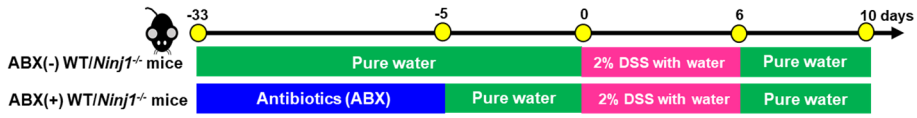

Figure 8. Schedule for the comparing the colitis development of WT and *Ninj1*$^{-/-}$ mice under ABX-untreated or ABX-treated conditions.

Wild-type (WT) and *Ninj1*$^{-/-}$ mice were provided antibiotic cocktails (ABX) dissolved in water or fresh water for four weeks, fed 2% DSS in drinking water for six days, followed by normal drinking water for four days

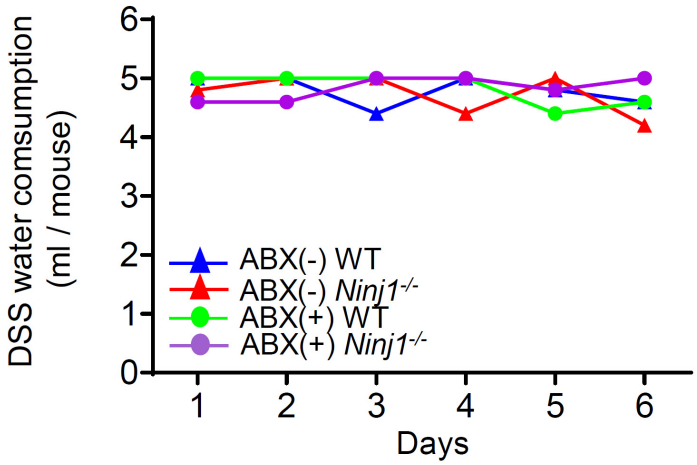

Figure 9. **Comparison of consumption of DSS in drinking water by WT and *Ninj1*$^{-/-}$ mice.**

Consumption of DSS in drinking water was calculated from the decrease in water volume divided by the number of mice (n = 5 per group).

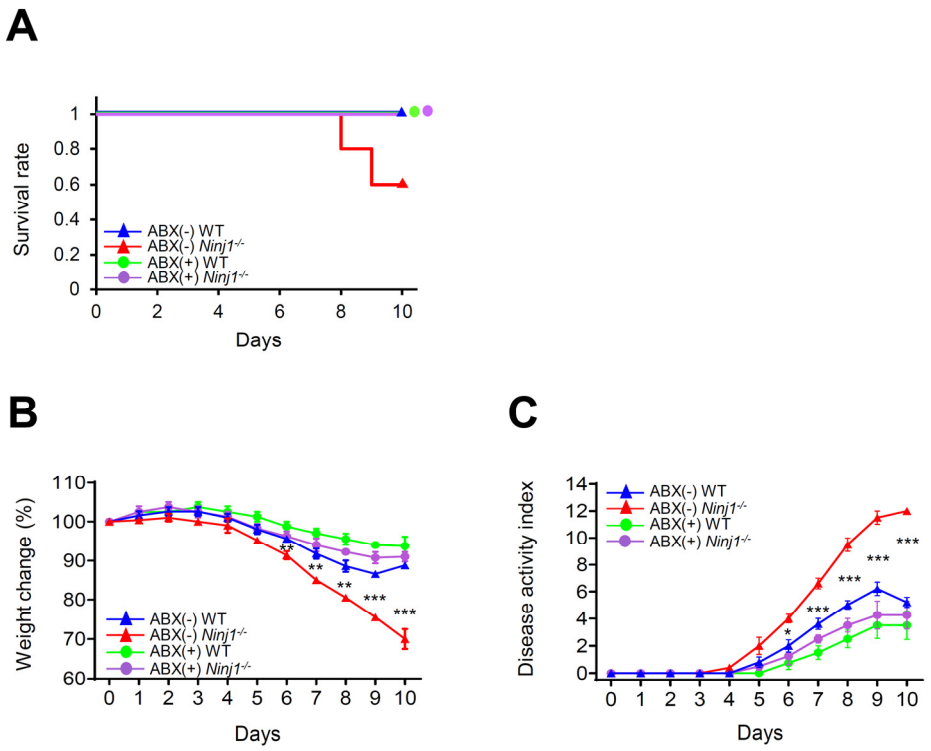

Figure 10. In the presence of gut microbiota, clinical symptoms of DSS-induced colitis were more severe in *Ninj1*$^{-/-}$ mice than in WT mice.

Survival rate (A), weight change (B), and disease activity index (DAI) scores (C) (*, ABX(-) WT vs. ABX(-) *Ninj1*$^{-/-}$ mice) were screened daily. $n_{0day} = 5$, $n_{8\sim10days} = 3$–5 per ABX(-) group; $n_{0\sim10days} = 4$ per ABX(+) group. The data represent the mean ± SEM. $^{**}P < 0.01$; $^{***}P < 0.001$. (-): untreated, (+): treated.

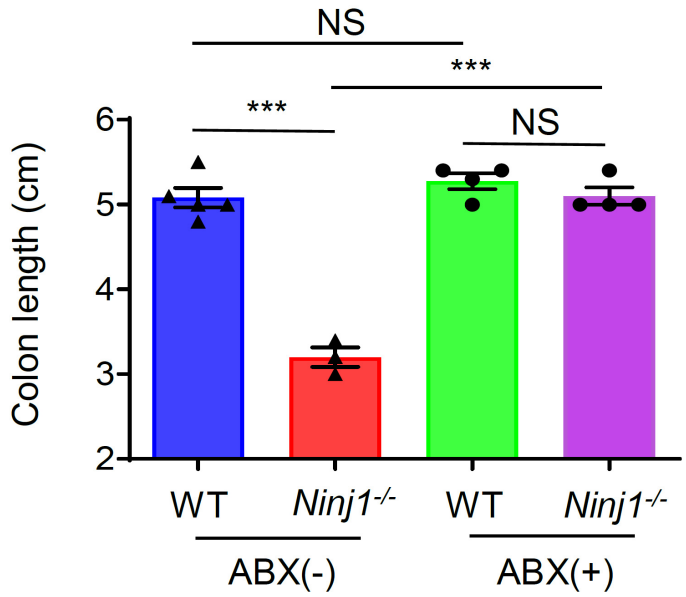

Figure 11. In the presence of gut microbiota, colon length was shorter in DSS-treated *Ninj1*$^{-/-}$ mice than in DSS-treated WT mice

Colon length was recorded using a ruler on day 10 (n = 3–5 per group). The data represent the mean ± SEM. **P < 0.01; ***P < 0.001. (-): untreated, (+): treated.

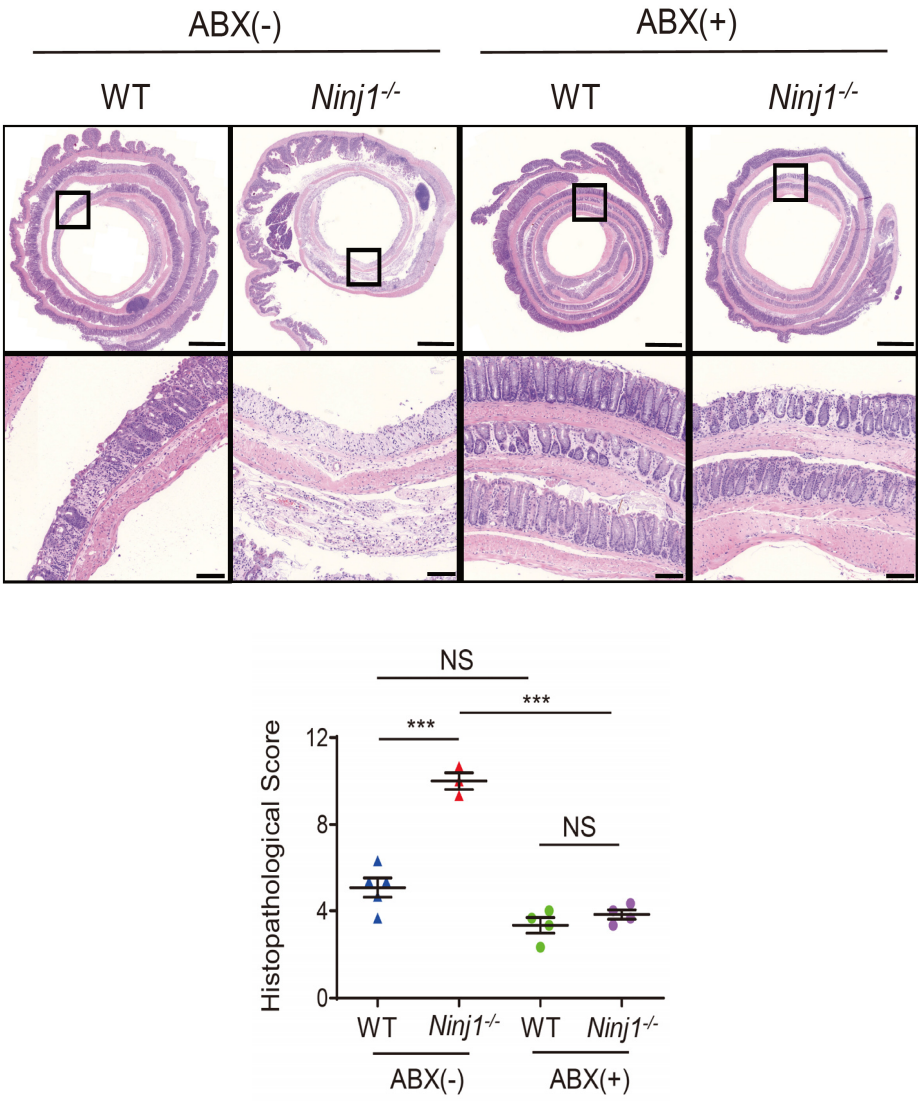

Figure 12. In the presence of gut microbiota, histological damage was more severe in DSS-treated colon of *Ninj1*$^{-/-}$ mice than in that of WT mice.

Representative image and histopathology score obtained from H&E-stained colonic sections (n = 3–5 per group). Scale bar = 1000 μm (upper) or 100 μm (bottom). The data represent the mean ± SEM. ***P < 0.001. (-): untreated, (+): treated.

2. Alteration of the gut microbiome by Ninj1 deficiency

The disruption of intestinal homeostasis can lead to gut dysbiosis, making a crucial contribution to the pathogenesis of IBD (Levy et al., 2017). Therefore, microbiota alteration by Ninj1 deficiency might promote colitis development. I compared the microbial composition in fecal samples from normal or DSS-treated WT and *Ninj1*$^{-/-}$ mice by 16S ribosomal RNA (rRNA) gene sequencing. Microbial diversity differed slightly between the normal groups (Figure 13). The proportion of the *Lachnospiraceae* family (Atarashi et al., 2011; Chen et al., 2017), which includes butyrate-producing immunoregulatory bacteria that limit colon inflammation, was significantly lower in *Ninj1*$^{-/-}$ mice; however, that of the *Prevotellaceae* family (Elinav et al., 2011; Lucke et al., 2006; Tang et al., 2018), which includes colitogenic bacteria, was higher in *Ninj1*$^{-/-}$ mice than in the WT mice (Figure 14). A lower proportion of *Unclassified (UC) Lachnospiraceae* and *Coprococcus,* and a higher proportion of *Prevotella* genera was observed in normal *Ninj1*$^{-/-}$ mice than in normal WT mice (Figure 15A).

After DSS treatment, microbial diversity differed significantly between WT and *Ninj1*$^{-/-}$ mice (Figure 13). The abundance of colitogenic bacteria, such as *Paraprevotellaceae* (Walters et al., 2014) and *Erysipelotrichaceae* families (Chen et al., 2017; Dinh et al., 2015; Handley et al., 2016), and rare bacteria, such as the *UC YS2* family, increased significantly, and the abundance of

immunoregulatory bacteria such as *Ruminococcaceae* (Atarashi et al., 2011) and *Lachnospiraceae* families decreased in *Ninj1*$^{-/-}$ mice (Figure 14). In particular, *Ninj1*$^{-/-}$ mice exhibited an increase in *Paraprevotella*, *Allobaculum*, and *UC YS2* genera and a decrease in *Oscillospira*, *Coprococcus*, and *Ruminococcus* genera (Figure 15B). These results suggest that microbial imbalance in *Ninj1*$^{-/-}$ mice becomes exacerbated after the induction of colitis, which may accelerate severe colitis development.

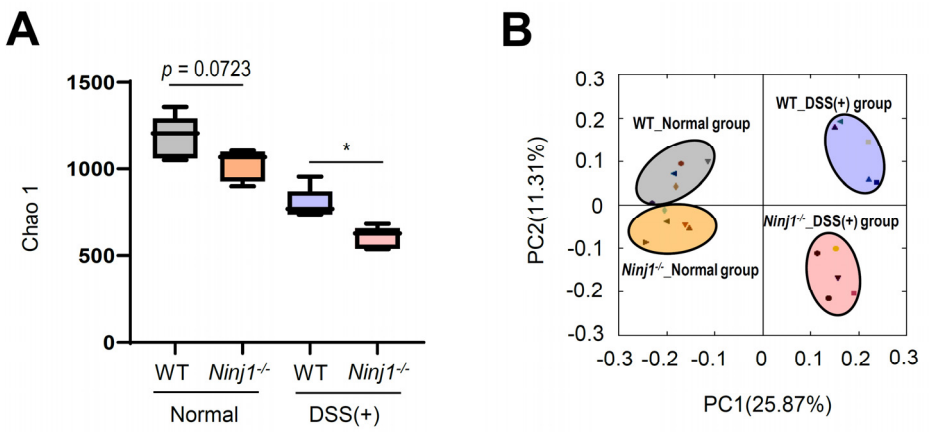

Figure 13. Effect of Ninj1 deficiency on microbial diversity under homeostatic condition and during colitis development.

Gut microbial Chao diversity analysis (**A**) and principal-coordinate analysis (**B**) based on unweighted UniFrac distances of the microbiota composition in WT and *Ninj1*$^{-/-}$ mice before and on day 6 after DSS treatment. Each symbol represents an individual mouse (n = 5 per group).

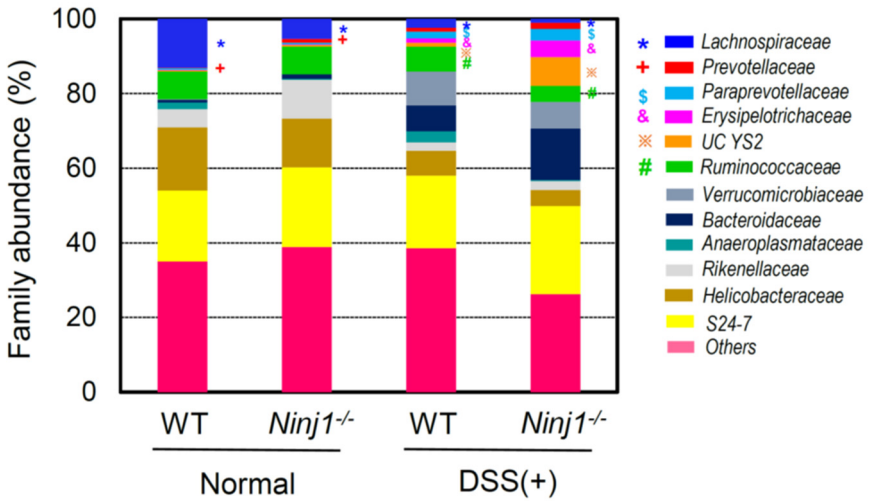

Figure 14. Effect of Ninj1 deficiency on microbial composition at the family level under homeostatic condition and during colitis development.

Microbiota composition in WT and *Ninj1*$^{-/-}$ mice before and on day 6 after DSS treatment at the family level (n = 5 per group). UC: unclassified, OTU: operational taxonomic unit.

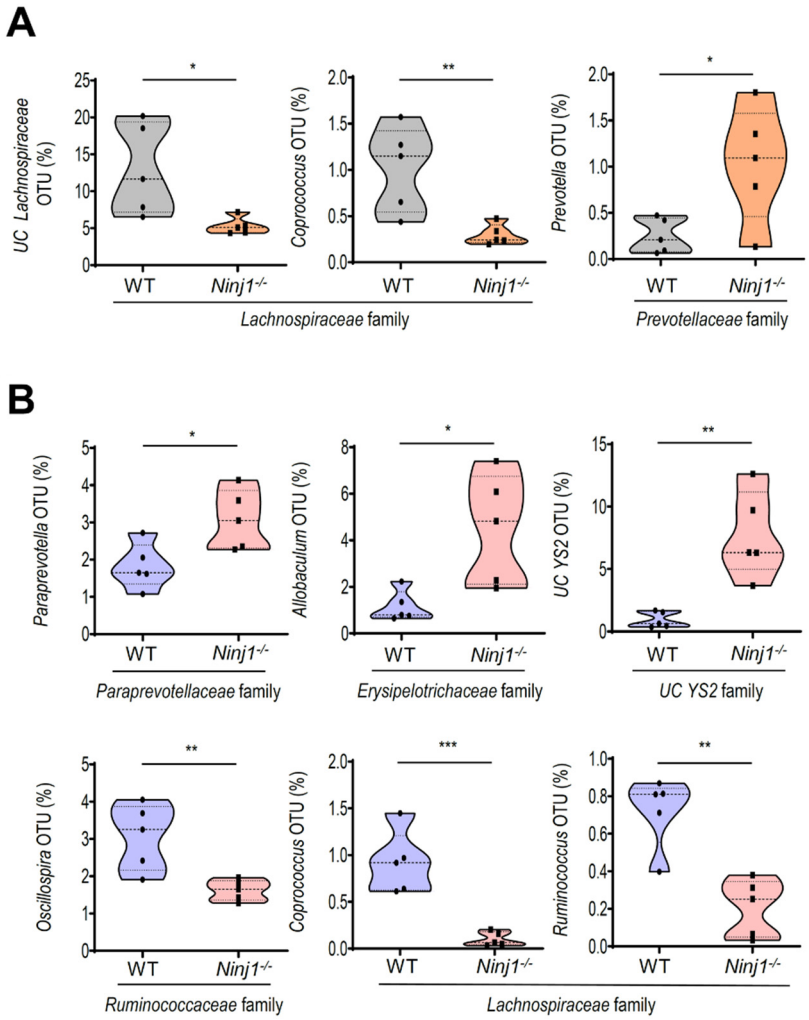

Figure 15. Effect of Ninj1 deficiency on microbial composition at the genus level under homeostatic condition and during colitis development.

Microbiota composition in WT and *Ninj1*$^{-/-}$ mice before **(A)** and on day 6 after DSS treatment **(B)** at the genus level (n = 5 per group). The data represent the mean ± SEM. *P < 0.05; **P < 0.01, ***P < 0.001. UC: unclassified, OTU: operational taxonomic unit.

3. Reconstitution of *Ninj1*$^{-/-}$ mice by WT fecal microbiota attenuates colon inflammation

To determine whether the altered microbiota in *Ninj1*$^{-/-}$ mice is associated with severe colitis development, I performed microbiome transfer by co-housing mice, which leads to the natural exchange of the microbiota through feces consumption. WT and *Ninj1*$^{-/-}$ mice were either singly-housed (SiH) or co-housed (CoH) — SiH WT(*Ninj1*$^{-/-}$): WT(*Ninj1*$^{-/-}$) mice housed with WT(*Ninj1*$^{-/-}$) mice, CoH WT(*Ninj1*$^{-/-}$): WT(*Ninj1*$^{-/-}$) mice housed with *Ninj1*$^{-/-}$ (WT) mice — for 6 weeks prior to DSS treatment (Figure 16). As expected, SiH *Ninj1*$^{-/-}$ mice exhibited a substantial weight loss (Figure 17A), and elevated clinical scores (Figure 17B), compared with SiH WT mice. This culminated in significantly high mortality (Figure 17C) and reduction in colon length (Figure 18). Interestingly, CoH WT mice exhibited severe clinical parameters (Figure 17) and reduced colon length (Figure 18) compared with SiH WT mice. In addition, CoH *Ninj1*$^{-/-}$ mice exhibited a substantially improved degree of colitis severity compared with SiH *Ninj1*$^{-/-}$ mice (Figure 17 and 18). These data suggest that the development of severe colitis of *Ninj1*$^{-/-}$ mice is reversed by the transfer of WT microbiota.

To verify this, I compared the microbial composition in WT and *Ninj1*$^{-/-}$ mice after single- or co-housing. Following 6 weeks of co-housing, the microbial

composition of CoH *Ninj1*$^{-/-}$ mice was similar to the microbial composition of the SiH WT mice and CoH WT mice, yet was distinct from that of SiH *Ninj1*$^{-/-}$ mice (Figure 19). Next, I determined if the changes in specific bacteria after co-housing translated to amelioration of severe colitis in *Ninj1*$^{-/-}$ mice. Surprisingly, the frequency of *Lachnospiraceae* family was significantly higher, while *Prevotellaceae* family were lower in CoH *Ninj1*$^{-/-}$ mice compared to that in the SiH *Ninj1*$^{-/-}$ mice (Figure 20). Furthermore, a higher proportion of *Coprococcus* and *Ruminococcus,* and a lower proportion of *Prevotella* genera was observed in CoH *Ninj1*$^{-/-}$ mice than in the SiH *Ninj1*$^{-/-}$ mice (Figure 21). These results indicate that specific microbiota transferred from WT mice alleviated the severity of colitis in *Ninj1*$^{-/-}$ mice in a co-housing setting.

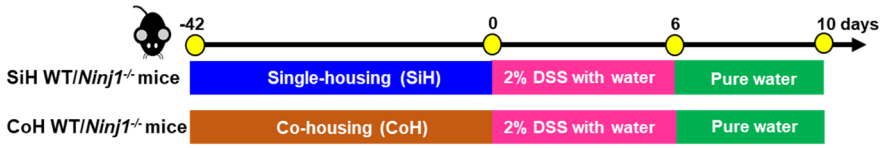

Figure 16. Schedule of the SiH (Single housing)/CoH (Co-housing) strategy.

WT and *Ninj1*$^{-/-}$ mice were either singly housed (SiH) or co-housed (CoH) for six weeks prior to treatment with 2% DSS.

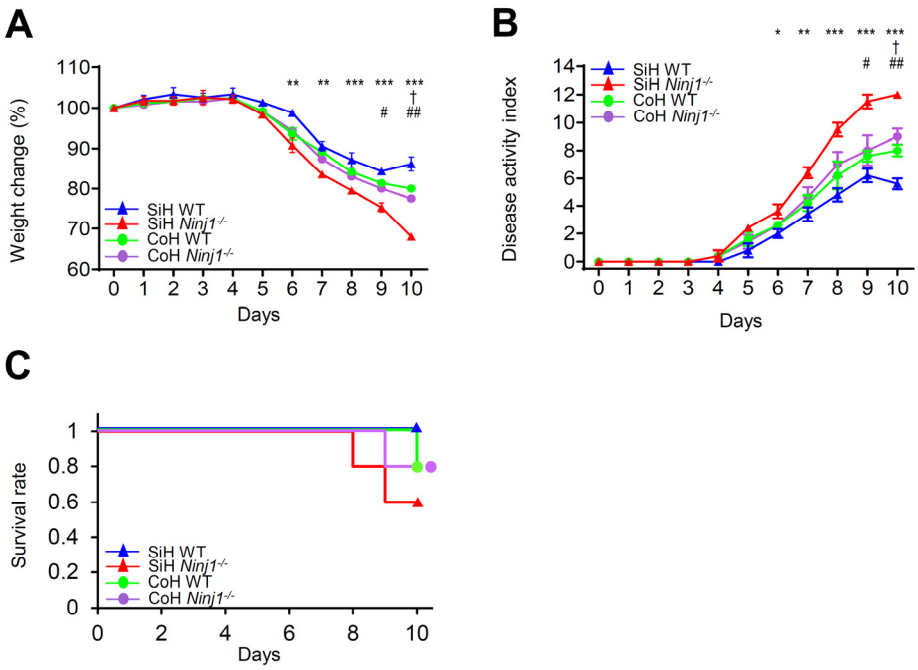

Figure 17. After colitis induction, *Ninj1*$^{-/-}$ mice co-housed with WT mice showed less severe clinical symptoms than single-housed *Ninj1*$^{-/-}$ mice.

Weight loss **(A)**, DAI scores **(B)** (*, SiH WT vs. SiH *Ninj1*$^{-/-}$; †, SiH WT vs. CoH WT; $^{\#}$, SiH *Ninj1*$^{-/-}$ vs. CoH *Ninj1*$^{-/-}$), and survival rate **(C)** were checked daily. $n_{0day} = 5$ per group, $n_{8\sim10days} = 3$–5 per group. The data represent the mean ± SEM. *$^{,\dagger,\#}$ $P < 0.05$; **$^{,\#\#}$ $P < 0.01$; *** $P < 0.001$.

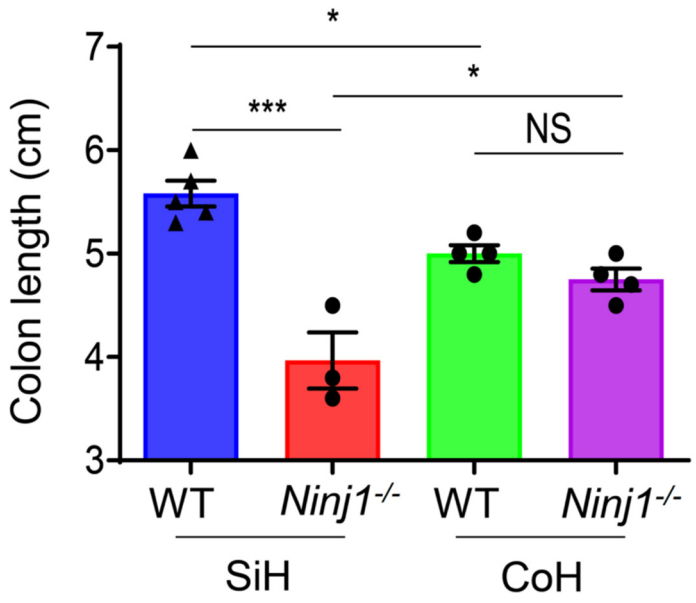

Figure 18. After colitis induction, colon length was longer in *Ninj1*$^{-/-}$ mice co-housed with WT mice than single-housed *Ninj1*$^{-/-}$ mice.

On day 10, mice were sacrificed, and colon length was measured (n = 3–5 per group). The data represent the mean ± SEM. *P < 0.05; ***P < 0.001; NS, non-significance.

.

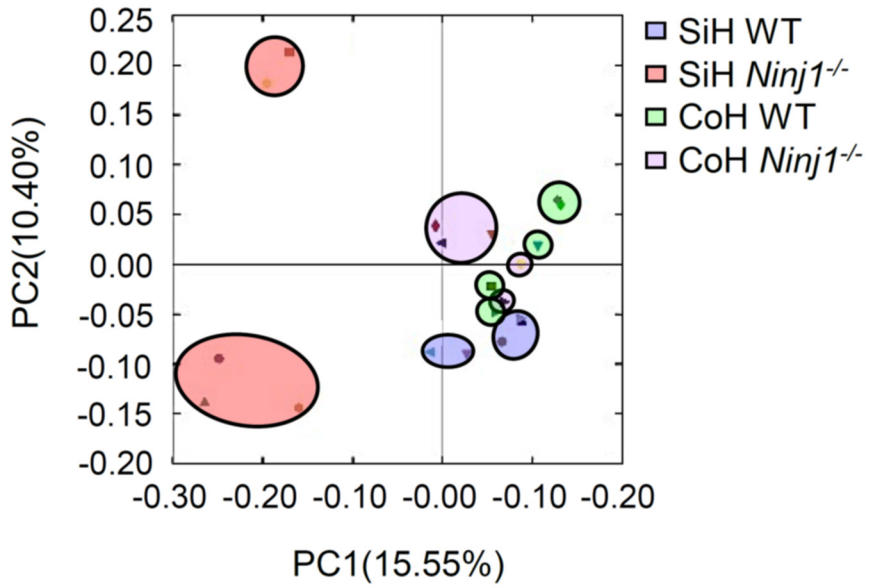

Figure 19. Effect of co-housing on microbial diversity.

Principal-coordinate analysis based on unweighted UniFrac distances of the microbiota composition in WT and *Ninj1*$^{-/-}$ mice after single or co-housing conditions. Each symbol represents an individual mouse (n = 5 per group).

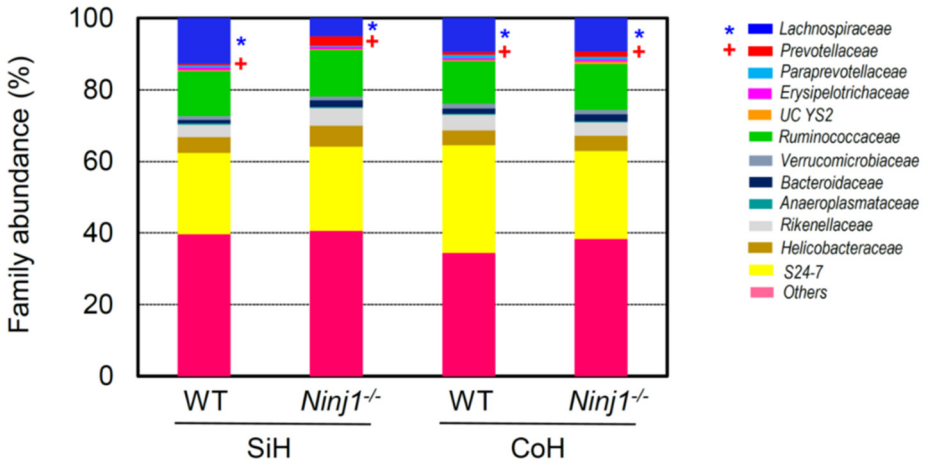

Figure 20. Effect of co-housing on microbial composition at the family level.

Microbiota composition in WT and *Ninj1*$^{-/-}$ mice after single or co-housing conditions at the family level (n = 5 per group). UC: unclassified, OTU: operational taxonomic unit.

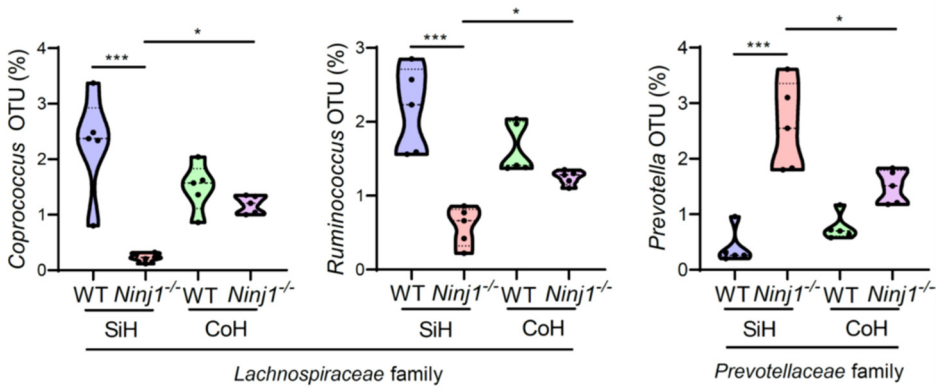

Figure 21. Effect of co-housing on microbial composition at the genus level.

Microbiota composition in WT and *Ninj1*$^{-/-}$ mice after single or co-housing conditions at the genus level (n = 5 per group). The data represent the mean ± SEM. *P < 0.05; **P < 0.01, ***P < 0.001. UC: unclassified, OTU: operational taxonomic unit.

4. Host Ninj1 deficiency and gut dysbiosis shaped by Ninj1 deficiency cooperatively accelerate severe colitis development

Next, to further explore the mutual effect of the altered microbiota in *Ninj1*$^{-/-}$ mice and host Ninj1 deficiency in severe colitis development, I conducted reciprocal fecal microbiota transplantation (FMT) in microbiota-depleted WT or *Ninj1*$^{-/-}$ mice, followed by colitis induction (Figure 22). A larger increase in histopathological score was observed after colonization with *Ninj1*$^{-/-}$ microbiota in the same host mice than that with WT microbiota (Figure 23), accompanied by reduced colon length (Figure 24), high mortality (Figure 25A), increased weight loss (Figure 25B), and elevated DAI scores (Figure 25C), indicating that microbial imbalance in *Ninj1*$^{-/-}$ mice could contribute to severe colitis. In addition, *Ninj1*$^{-/-}$ mice showed more colon histopathology and severe clinical symptoms than WT mice after colonization with WT or *Ninj1*$^{-/-}$ microbiota (Figure 23–25), implying that genetic deficiency of Ninj1 confers hypersusceptibility to colitis. Interestingly, there were no significant histopathological or clinical differences between *Ninj1*$^{-/-}$ mice colonized with WT microbiota and WT mice colonized with *Ninj1*$^{-/-}$ microbiota (Figure 23–25), and both presented less severe clinical signs or histopathological score than *Ninj1*$^{-/-}$ mice colonized with *Ninj1*$^{-/-}$ microbiota (Figure 23–25). Collectively, these results indicate that genetic deficiency of Ninj1 and gut dysbiosis shaped by Ninj1 deficiency cooperatively result in the progression of severe colitis in *Ninj1*$^{-/-}$ mice.

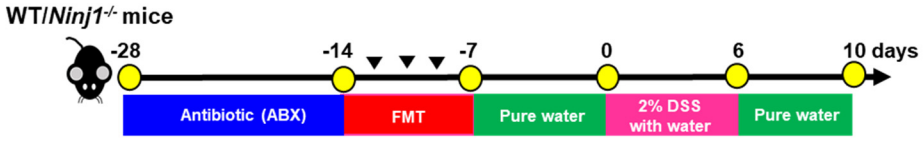

Figure 22. Schedule of the fecal microbiota transplantation strategy.

Microbiota-depleted WT and *Ninj1*$^{-/-}$ mice received normal fecal microbiota (FM) from WT and *Ninj1*$^{-/-}$ mice for one week, followed by treatment with 2% DSS.

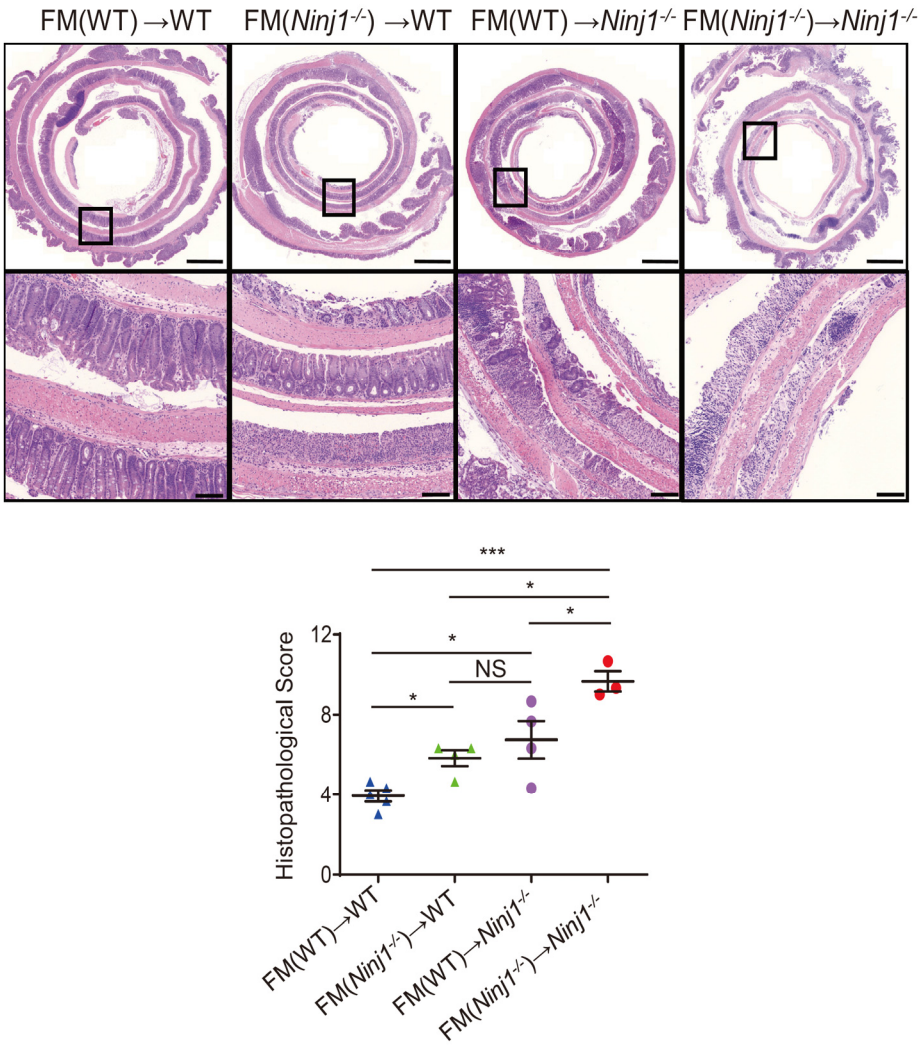

Figure 23. DSS-induced histological colon damage of *Ninj1*$^{-/-}$ mice was ameliorated by the transfer of WT microbiota.

Representative H&E-stained colonic sections and histopathologic score (n = 3–5 per group). Scale bar = 1000 μm (upper) or 100 μm (bottom). The data represent the mean ± SEM. *P < 0.05; ***P < 0.001; NS, non-significance.

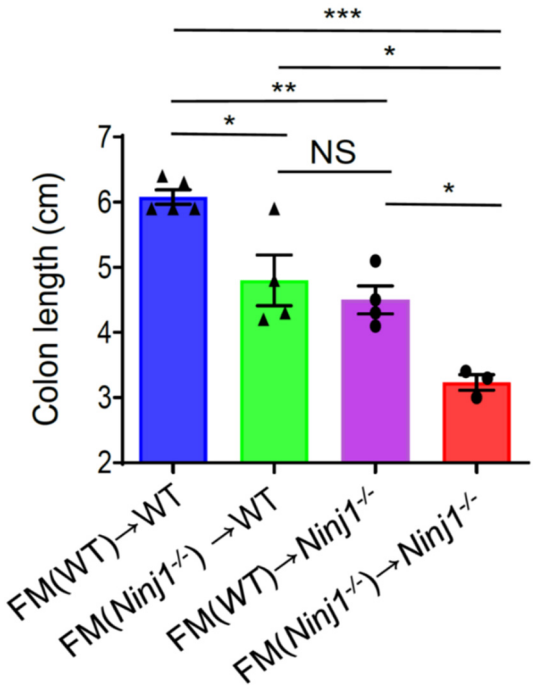

Figure 24. Transfer of WT fecal microbiota to *Ninj1*$^{-/-}$ mice was improved the shortness of colon length from *Ninj1*$^{-/-}$ mice under DSS-induced colitis conditions.

Colon length was measured on day 10 (n = 3–5 per group). The data represent the mean ± SEM. *P < 0.05; **P < 0.01; ***P < 0.001; NS, non-significance.

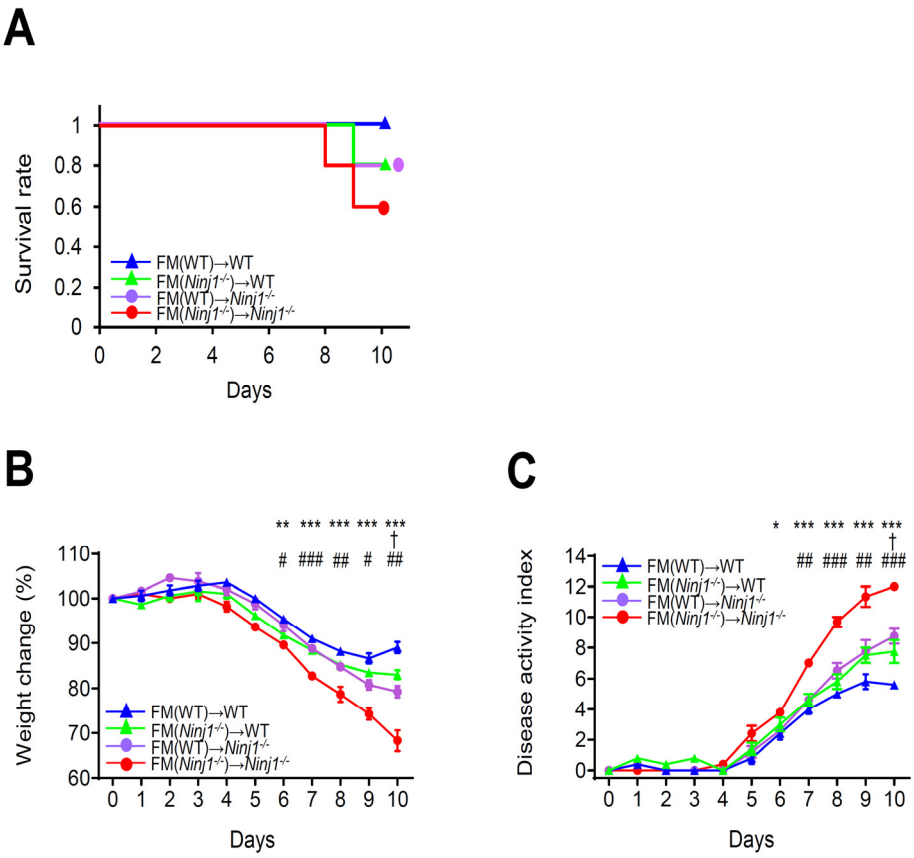

Figure 25. Reconstitution of *Ninj1*$^{-/-}$ mice by WT fecal microbiota attenuates colitis development.

Survival rate **(A)**, weight change **(B)**, and DAI scores **(C)** were determined daily ((**B, C**) *, FM(WT)→WT mice vs. FM (*Ninj1*$^{-/-}$)→*Ninj1*$^{-/-}$ mice; †, FM(WT)→WT mice vs. FM (*Ninj1*$^{-/-}$)→WT mice; $^{\#}$, FM(WT)→*Ninj1*$^{-/-}$ mice vs. FM (*Ninj1*$^{-/-}$)→*Ninj1*$^{-/-}$ mice. n_{0day} = 5 per group, $n_{8\sim10days}$ = 3–5 per group The data represent the mean ± SEM. *$^{,\dagger,\#}$ $P < 0.05$; **$^{,\#\#}$ $P < 0.01$; ***$^{,\#\#\#}$ $P <$ 0.001.

5. Ninj1 deficiency establishes pro-inflammatory colonic environment by increasing the numbers of M1 macrophages

Recently, inflammation was reported to deplete butyrate-producing immunoregulatory bacteria (Tye et al., 2018). In addition, several colitogenic bacteria arising under inflammatory conditions contribute to the perpetuation of inflammation, thereby preserving conditions that favor their own growth (Zeng et al., 2017). To investigate whether microbial imbalance of *Ninj1*$^{-/-}$ mice under homeostatic conditions was related to the pro-inflammatory colon environment, I compared the expression of basal pro-inflammatory or anti-inflammatory mediators between WT and *Ninj1*$^{-/-}$ mice. The expression of pro-inflammatory mediators, such as *Tnf*, *Il6*, *Nos2*, and *Ifng,* was higher in the colon of *Ninj1*$^{-/-}$ mice than in the colon of WT mice (Figure 26). However, the expression of the anti-inflammatory cytokine *Il10* was lower in the colon of *Ninj1*$^{-/-}$ mice than in the colon of WT mice (Figure 26). These results suggest that the pro-inflammatory environment in the colon promoted by Ninj1 deficiency may contribute to microbial imbalance. Intriguingly, Ninj1 was expressed in F4/80^{+} colonic macrophages, and not in other colonic cells such as CD3^{+} T cells, NIMP-R14^{+} neutrophils, EpCAM^{+} epithelial cells, or CD31^{+} endothelial cells (Figure 27, Figure 28). Ninj1 deficiency did not affect the expression of these cell markers (Figure 29A). In addition, no significant difference was observed in the numbers of colonic immune cells in WT and

Ninj1$^{-/-}$ mice (Figure 29B). As a result, I did not detect histological differences between WT and *Ninj1*$^{-/-}$ mice under homeostatic conditions (Figure 29C).

In the steady state, colonic macrophages initially develop an M1/pro-inflammatory phenotype, however, gradually acquire an M2/anti-inflammatory phenotype to maintain immune homeostasis (Isidro and Appleyard, 2016). I, therefore, sought to investigate whether the Ninj1 deficiency in macrophages resulted in an aberrant macrophage phenotype, which may account for the observed pro-inflammatory colon environment in *Ninj1*$^{-/-}$ mice. An increase in the number of CD86^{+} M1 macrophages and a decrease in the number of CD206^{+} M2 macrophages was observed in the colon of *Ninj1*$^{-/-}$ mice compared with those in the colon of WT mice (Figure 30 and 31). In addition, I confirmed that a higher proportion of iNOS^{+} M1 macrophages and a lower proportion of Arginase-1 (Arg-1)$^{+}$ M2 macrophages was observed in the colon of *Ninj1*$^{-/-}$ mice (Figure 32, Table 2). Consistent with the macrophage phenotype observed above, the population of TNF-α^{+} macrophages was higher, however, that of IL-10^{+} macrophages was lower in the colon tissue of *Ninj1*$^{-/-}$ mice compared to WT mice (Figure 33, Table 2). These results indicate that Ninj1 deficiency promotes the basal pro-inflammatory colonic environment by increasing the population of M1 macrophage phenotype.

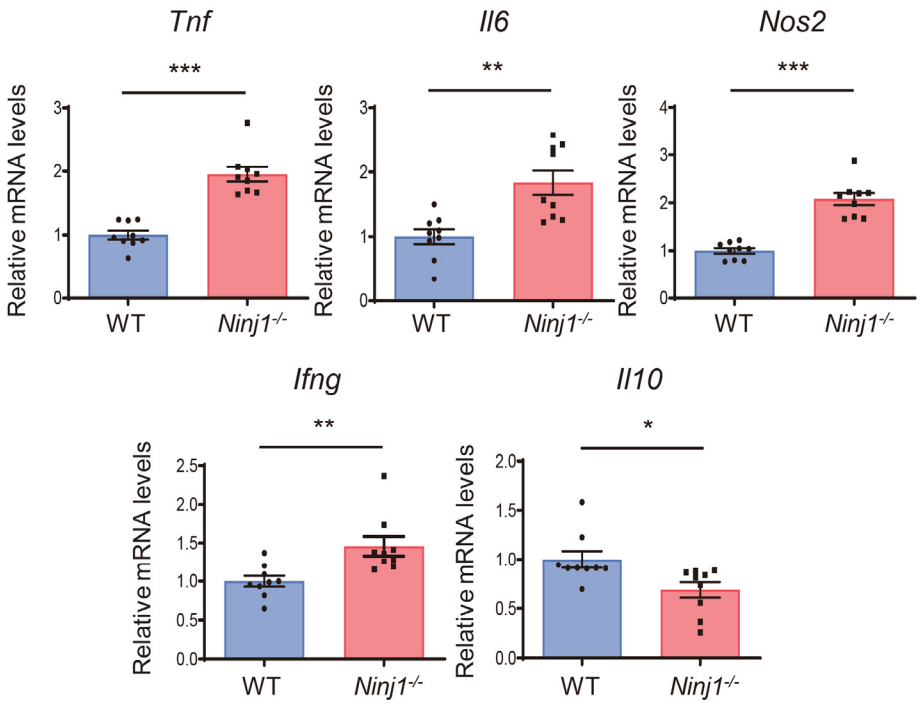

Figure 26. Ninj1 deficiency promotes pro-inflammatory colonic environment under homeostatic conditions.

Relative mRNA levels of *Tnf*, *Il6, Nos2*, *Ifng,* and *Il10* in the normal colon from WT and *Ninj1*$^{-/-}$ mice (n = 9 per group). The data represent the mean ± SEM. *P < 0.05; **P < 0.01; ***P < 0.001.

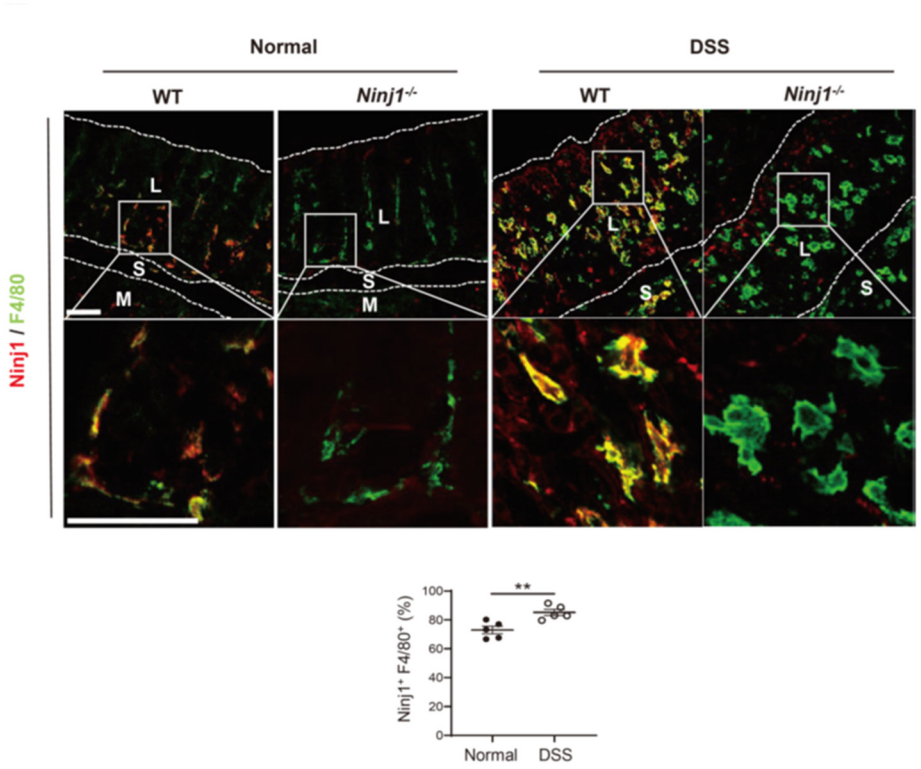

Figure 27. Ninj1 is primarily expressed in colonic macrophages.

Co-immunostaining of the colon sections from WT mice under normal or DSS-induced colitis conditions for Ninj1 (red) and F4/80 (green). Graphs show percent frequency of $Ninj1^+$ $F4/80^+$ macrophages in the lamina propria (per 0.1 mm^2 of colonic images). Scale bar = 50 μm. L: lamina propria (mucosa), S: submucosa, M: muscularis externa.

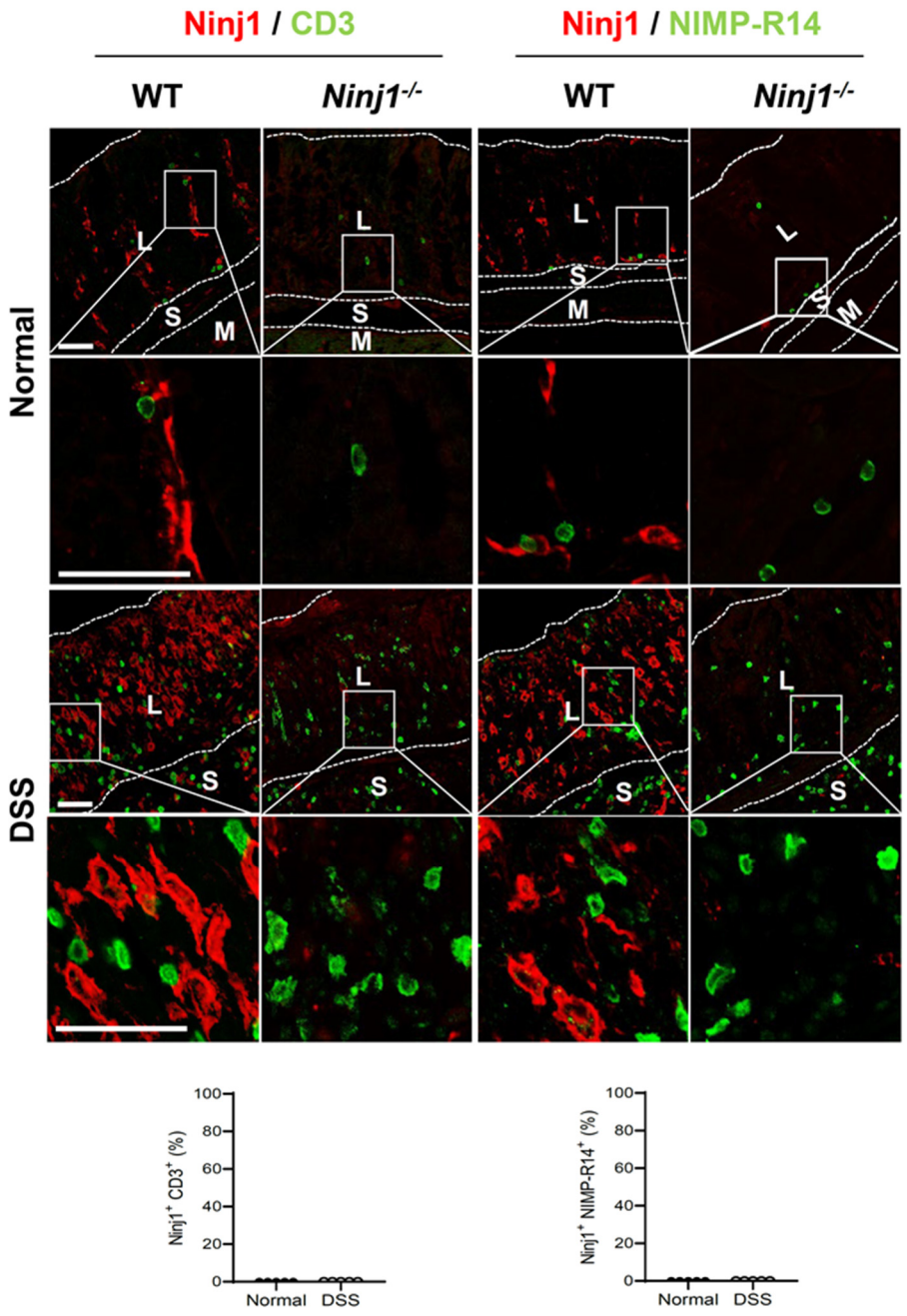
Ninj1 / CD3
Ninj1 / NIMP-R14
WT
Ninj1-/-
WT
Ninj1-/-
Normal
DSS
L
S
M
Ninj1+ CD3+ (%)
Ninj1+ NIMP-R14+ (%)
100
80
60
40
20
0
Normal
DSS

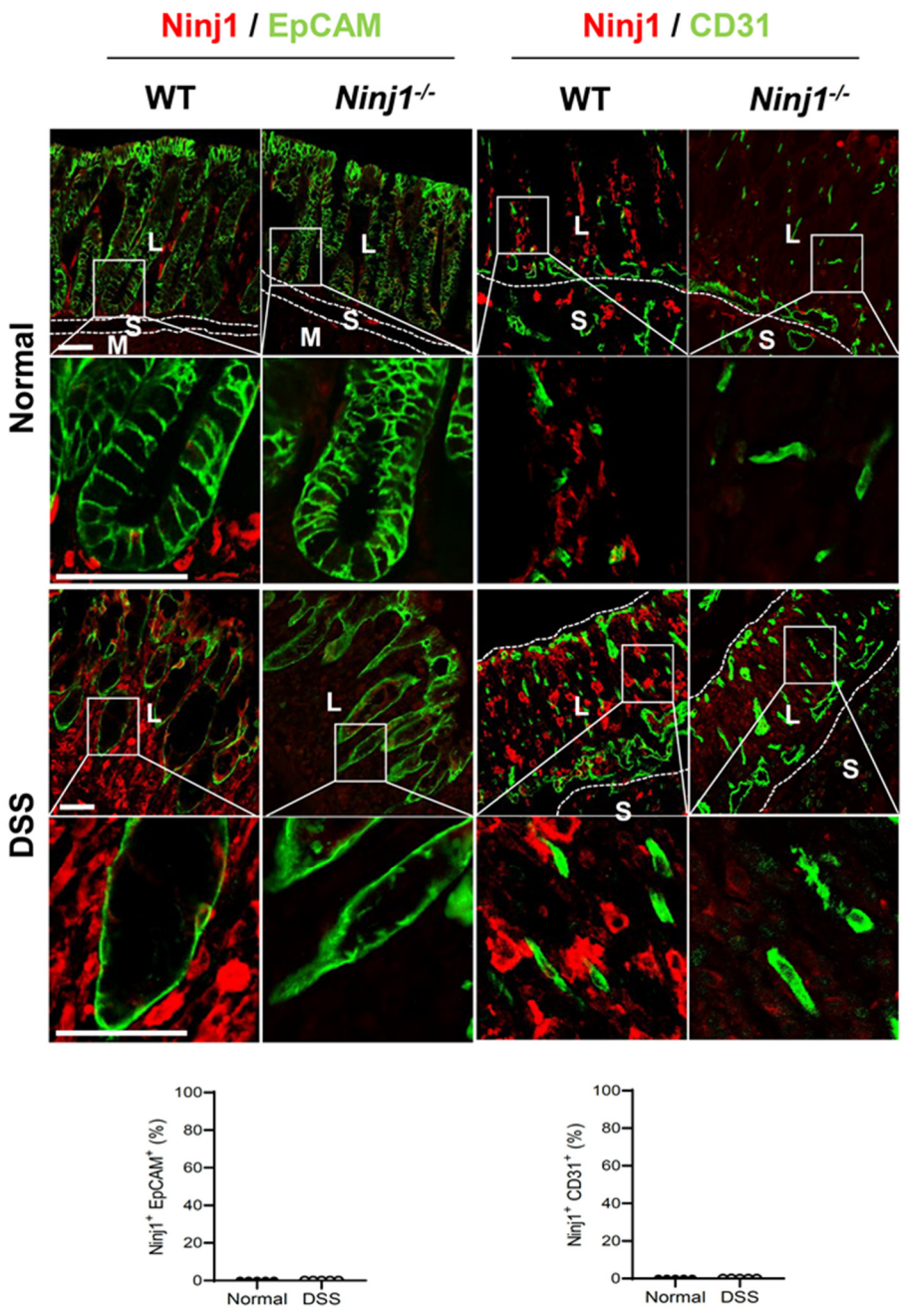
Ninj1 / EpCAM
Ninj1 / CD31
WT
Ninj1-/-
WT
Ninj1-/-
Normal
DSS
L
S
M
L
S
M
L
S
L
S
L
L
S
L
L
S
L
S
Ninj1+ EpCAM+ (%)
100
80
60
40
20
0
Normal
DSS
Ninj1+ CD31+ (%)
100
80
60
40
20
0
Normal
DSS

Figure 28. Ninj1 is not expressed in $CD3^+$, NIMP-$R14^+$, $EpCAM^+$ or $CD31^+$ cells in the colon.

Co-immunostaining of the colon sections from WT and *Ninj1*$^{-/-}$ mice under normal or DSS-induced colitis conditions for Ninj1 (red) and other cell markers (green). Graphs show percent frequency of $Ninj1^+$ $CD3^+$, NIMP-$R14^+$, $EpCAM^+$, and $CD31^+$ cells in the normal or DSS-treated lamina propria (per $0.1mm^2$ of colonic images). n = 5 mice per group (n = 3 fields/mice). The data represent the mean ± SEM. NS: non-significance. Scale bar = 50 μm. L: lamina propria (mucosa), S: submucosa, M: muscularis externa.

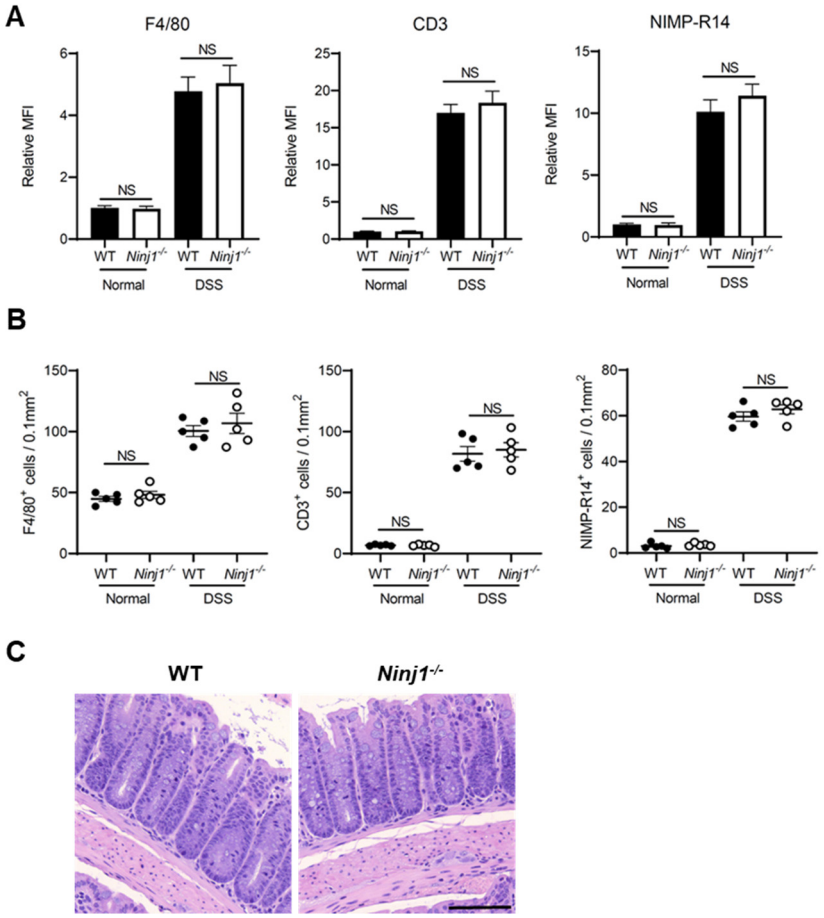

Figure 29. Ninj1 deficiency does not affect histological changes in normal colonic tissue of mice. A) Relative mean fluorescence intensity (MFI) of F4/80 CD3, NIMP-R14, EpCAM and CD31 in normal or DSS-treated colons of WT and *Ninj1*$^{-/-}$ mice. **B)** Quantification of the absolute number of F4/80, CD3 and NIMP-R14^{+} immune cells per 0.1 mm^{2} from colon images of WT or *Ninj1*$^{-/-}$ mice under normal or DSS-treated conditions. **C**) Representative histological images from normal colonic tissues of WT and *Ninj1*$^{-/-}$ mice. (**A**, **B**) n = 5 per mice group (n = 3 fields/mice). The data represent the mean ± SEM. NS: non-significance.

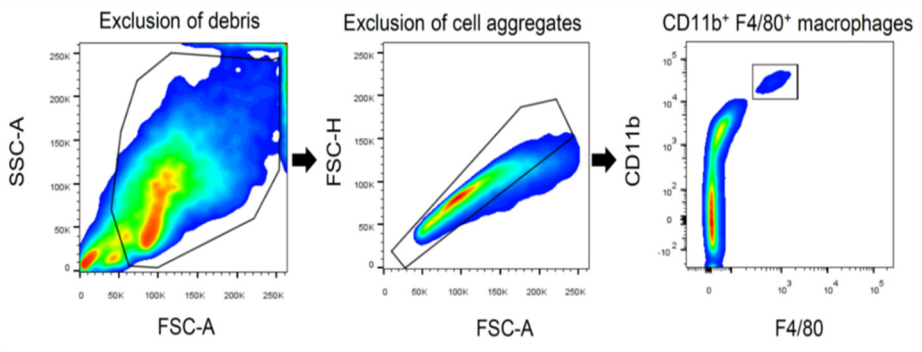

Figure 30. Gating strategy for isolating the macrophage population under homeostatic conditions.

Whole prepared cell population were first gated by excluding debris (FSC-A vs SSC-A) and cell aggregates (FSC-A vs FSC-H). Then the gated cell population takes only $CD11b^{+}$ $F4/80^{+}$ macrophage population.

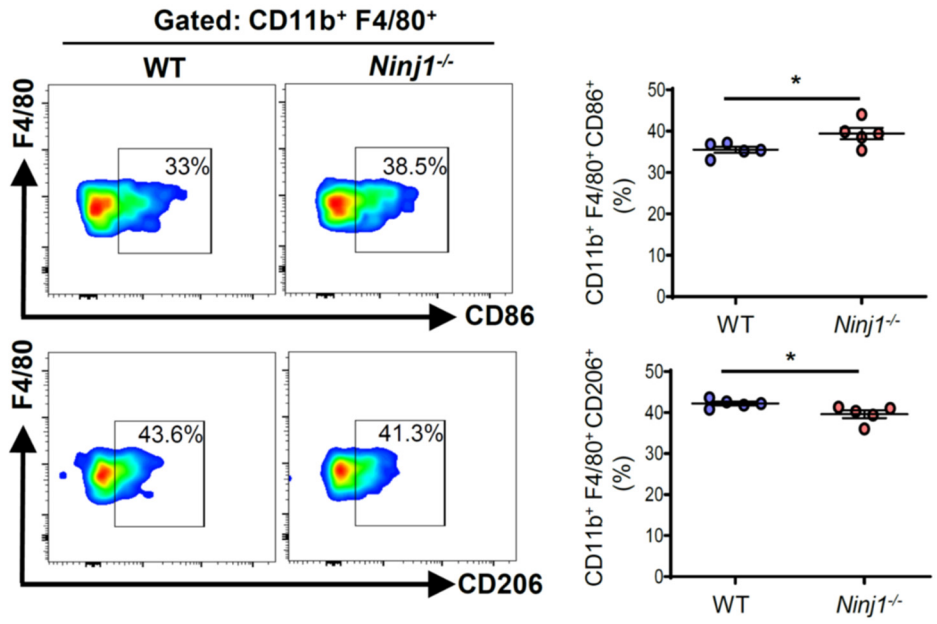

Figure 31. A higher proportion of CD86^{+} M1 macrophages and a lower proportion of CD206^{+} M2 macrophages was observed in normal colons of *Ninj1*$^{-/-}$ mice than in those of WT mice.

Representative plot of flow cytometry (left panel) and frequency (right panel) of CD86^{+} or CD206^{+} CD11b^{+} F4/80^{+} macrophages in normal colonic tissues from WT and *Ninj1*$^{-/-}$ mice (n = 5 mice per group). The data represent the mean ± SEM. *$P < 0.05$.

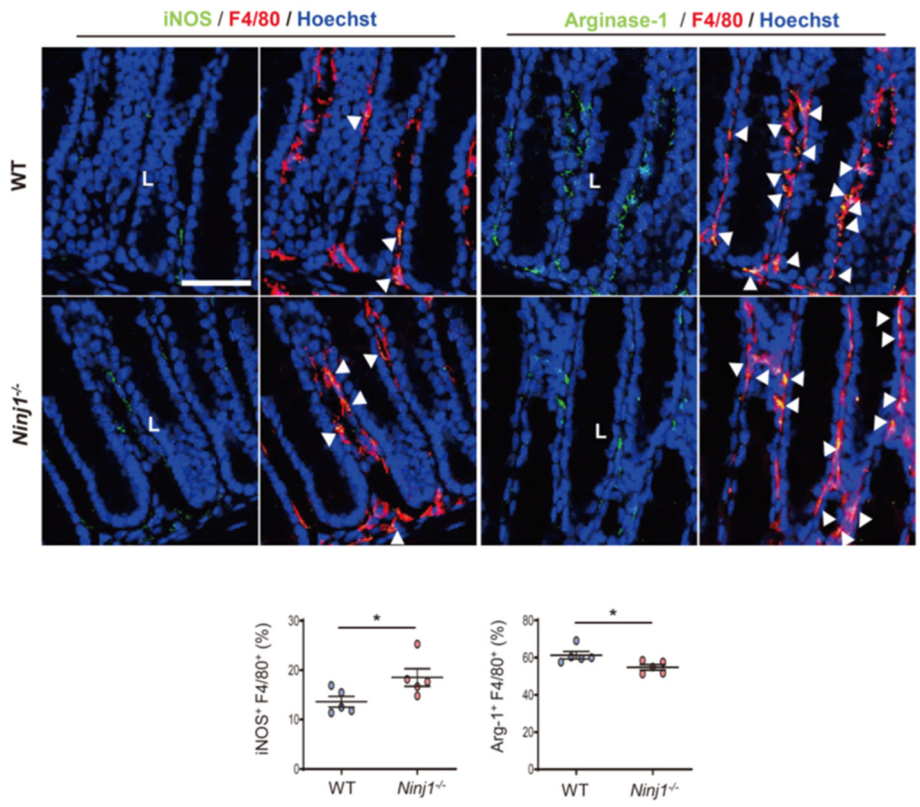

Figure 32. A higher proportion of iNOS^{+} M1 macrophages and a lower proportion of Arginase-1^{+} M2 macrophages was observed in normal muscosa of *Ninj1*$^{-/-}$ mice than in those of WT mice.

Immunostaining of iNOS^{+} or Arg-1^{+} F4/80^{+} macrophages in normal lamina propria from WT or *Ninj1*$^{-/-}$ mice. iNOS^{+} or Arg-1^{+} F4/80^{+} macrophages are indicated by arrowheads (upper panel). The proportion of iNOS^{+} or Arg-1^{+} F4/80^{+} macrophages was calculated (bottom panel; n = 3 fields/mice). n = 5 mice per group. The data represent the mean ± SEM. *P < 0.05. L: lamina propria (mucosa).

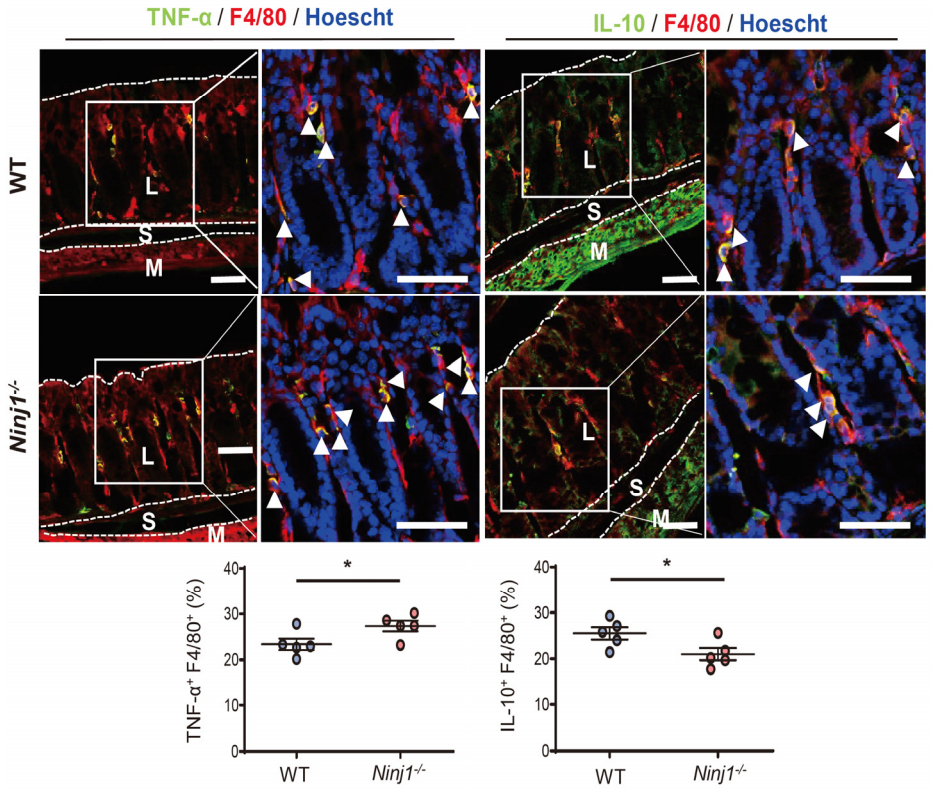

Figure 33. A higher proportion of TNF-α^{+} macrophages and a lower proportion of IL-10^{+} macrophages was observed in normal mucosa of *Ninj1*$^{-/-}$ mice than in those of WT mice.

Immunostaining for TNF-α^{+} or IL-10^{+} F4/80^{+} macrophages in normal colonic tissues from WT and *Ninj1*$^{-/-}$ mice. TNF-α^{+} or IL-10^{+} F4/80^{+} macrophages are indicated by arrowheads (left panel). The proportion of TNF-α^{+} or IL-10^{+} F4/80^{+} macrophages was calculated (right panel; $n = 3$ fields/mice). $n = 5$ mice per group. The data represent the mean ± SEM. *$P < 0.05$. L: lamina propria (mucosa), S: submucosa, M: muscularis externa.

6. Ninj1 deficiency increases inflammatory response to bacteria in macrophages via activation of chronic inflammatory signaling *in vitro*

Next, I examined whether the increased M1 phenotype in *Ninj1*$^{-/-}$ mice is associated with an excessive inflammatory response to the microbes. To determine whether Ninj1 deficiency promotes an aberrant inflammatory response in macrophages by interacting with the gut-resident bacteria, I exposed WT or *Ninj1*$^{-/-}$ macrophages to various heat-killed bacteria to mimic the macrophage–bacterial interaction *in vivo*. The inflammatory response was highly induced by colitogenic bacteria (Gradel et al., 2009; Martin et al., 2004; Nakajima et al., 2015; Santos-Antunes et al., 2014), such as *Listeria monocytogenes, Porphyromonas gingivalis*, *Escherichia coli 0111:B4,* and *Salmonella typhimurium,* but was weakly induced by immunoregulatory bacteria (Goyal and Shukla, 2013; Mazmanian et al., 2005), such as *Bacteroides fragilis* and *Lactobacillus rhamnosus,* in WT macrophages (Figure 34). Indeed, *Ninj1*$^{-/-}$ macrophages expressed high levels of pro-inflammatory factors, such as *Tnf*, *Il6*, *Nos2,* and *Il1b*, and low levels of anti-inflammatory factors, such as *Il10,* after stimulation by colitogenic bacteria or immunoregulatory bacteria, compared with those in WT macrophages (Figure 34), indicating that Ninj1 deficiency increases inflammatory response to bacteria in macrophages.

Next, to compare the efficiency of phagocytosis, I exposed WT or *Ninj1*$^{-/-}$ macrophages to Alexa488-conjugated *E.coli*. As shown in Figure 35, the efficiency of phagocytosis was not different between the two groups. Phagosome maturation is closely related to the strongly acidic environment in the phagosome lumen. Defective phagosome maturation may result in dysfunctional bacterial lysis in the phagosome, resulting in chronic expression of pro-inflammatory mediators. Based on previous findings, I exposed macrophages to pHrodo (pH-sensitive dye)-tagged *Escherichia coli*. *Ninj1*$^{-/-}$ macrophages showed fewer pHrodo-positive cells than that in WT macrophages (Figure 36), suggesting that defective bacterial lysis promotes chronic inflammatory signaling activation.

To elucidate the underlying inflammatory signaling in connection with a defective bacterial lysis, I examined the activation of NF-κB or MAPK signaling molecules in response to LPS in WT or *Ninj1*$^{-/-}$ macrophages. The initial phase of NF-κB or JNK/p38 MAPK activation, immediately after LPS stimulation, was comparable between WT and *Ninj1*$^{-/-}$ macrophages (Figure 37). Intriguingly, the NF-κB and JNK/p38 MAPK activities subsided in WT macrophages 2 h after stimulation, whereas those in *Ninj1*$^{-/-}$ macrophages were maintained (Figure 37). These results suggest that *Ninj1*$^{-/-}$ macrophages promote M1 polarization by activating chronic inflammatory response via dysfunctional bacterial lysis.

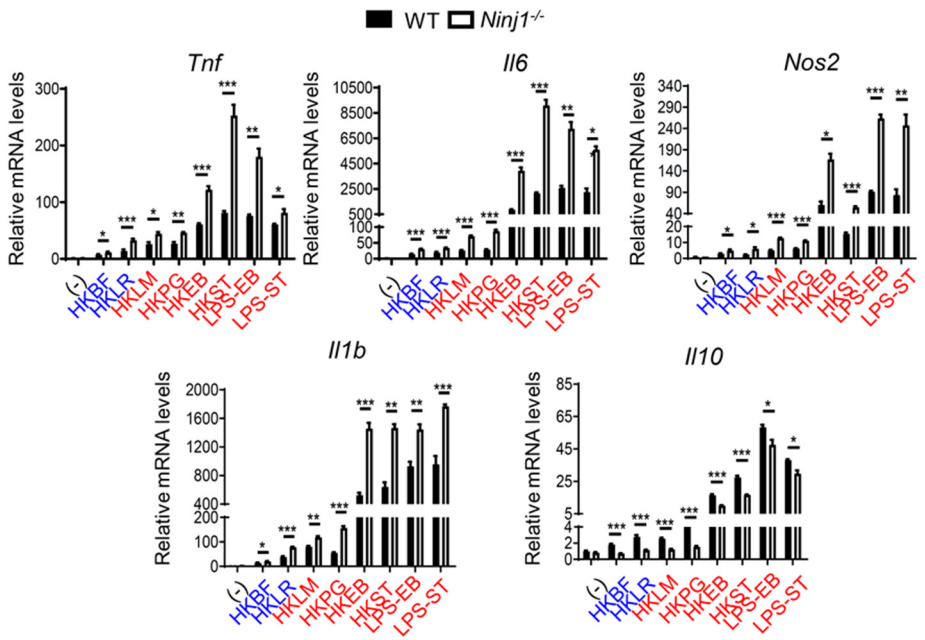

Figure 34. *Ninj1*$^{-/-}$ macrophages expressed high levels of pro-inflammatory mediators after stimulation by immunoregulatory or colitogenic bacteria. Relative mRNA levels of *Tnf*, *Il6*, *Nos2*, *Il1b*, and *Il10* in BMDMs from WT and *Ninj1*$^{-/-}$ mice without or with stimulation of HKBF, HKLR, HKLM, HKPG HKEB, HKST, LPS-EB, and LPS-ST (n = 3 per group). Blue: immunoregulatory bacteria, Red: colitogenic bacteria. BMDMs: bone marrow-derived macrophages HK: heat-killed, BF: *Bacteroides fragilis*, LR: *Lactobacillus rhamnosus*, LM: *Listeria monocytogenes*, PG: *Porphyromonas gingivalis*, EB: *Escherichia coli 0111:B4*, ST: *Salmonella typhimurium*.

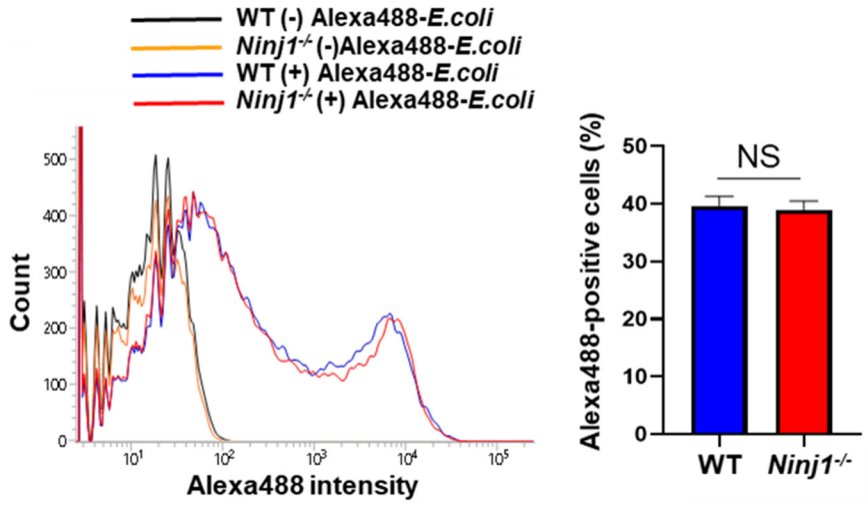

Figure 35. Ninj1 deficiency does not affect Alexa488-conjugated *E.coli* phagocytosis in macrophages.

Bone marrow-derived macrophages (BMDM) from WT or *Ninj1*$^{-/-}$ mice were stimulated with Alexa488-conjugated *E. coli* particles for 60 minutes. The percentage of WT and Ninj1 macrophages showing Alexa488-positive signals was measured by flow cytometry (n = 3 per group). The data represent the mean ± SEM.

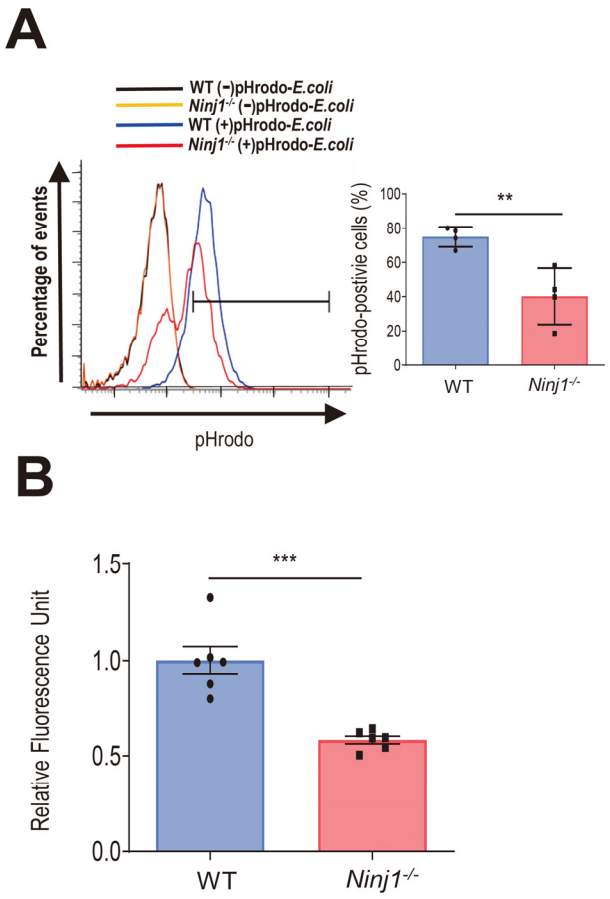

Figure 36. *Ninj1*$^{-/-}$ macrophages showed fewer pHrodo-positive cells than that in WT macrophages.

(A) Percent of WT and *Ninj1*$^{-/-}$ macrophages containing pHrodo-positive signals was measured by FACS (n = 4 per group). (B) Fluorescence from ingested *E. coli* particles was detected by ELISA (n = 6 per group). The data represent the mean ± SEM. *$P < 0.05$; **$P < 0.01$; ***$P < 0.001$.

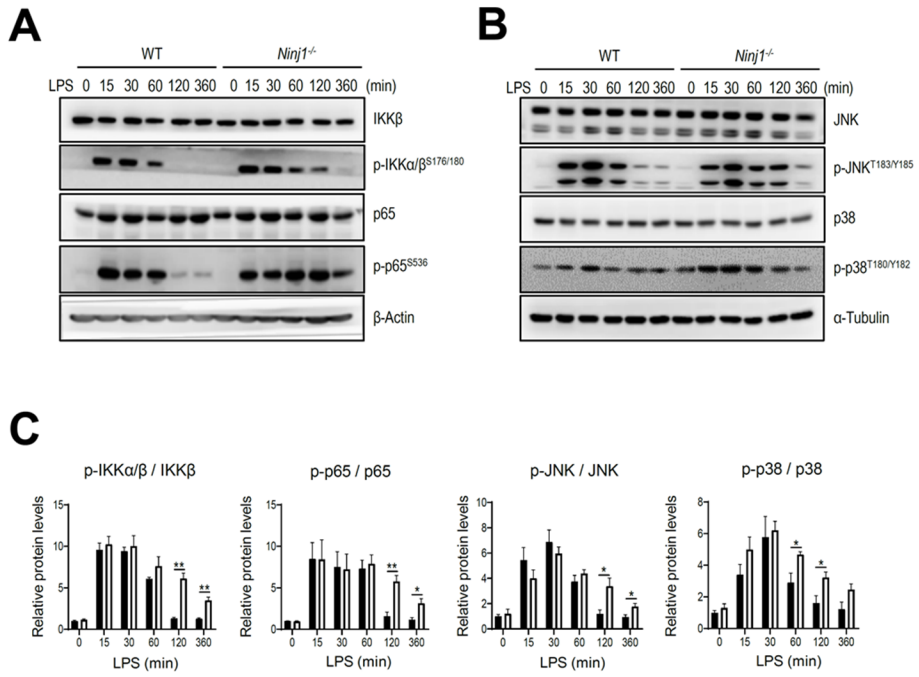

Figure 37. Ninj1 deficiency promotes chronically NF-κB or JNK/p38 MAPK signaling in macrophages.

Immunoblotting of NF-κB **(A)** and MAPK signaling molecules **(B)** in WT and *Ninj1*$^{-/-}$ BMDMs untreated or treated with LPS. (**C**) The quantitative analysis of the ratios of p-IKKα/β/IKKβ, p-p65/p65, pJNK/JNK and p-p38/p38 normalized with β-actin or α-tubulin. Data represent the mean ± SEM. **P* < 0.05; ***P* < 0.01

7. *Ninj1*$^{-/-}$ mice exhibited impaired colitis recovery

As mentioned above, microbial imbalance, such as an increase in colitogenic and rare bacteria and a decrease in immunoregulatory bacteria in *Ninj1*$^{-/-}$ mice, was higher after DSS treatment. (Figure 14, 15). Interestingly, the clinical difference in the body weight changes, DAI score, and survival rate between WT and *Ninj1*$^{-/-}$ mice gradually increased in the later stage after DSS withdrawal (Figure 10), suggesting that the escalated dysbiosis in *Ninj1*$^{-/-}$ mice after DSS treatment may lead to impaired recovery. To assess the potential effect of escalated microbial imbalance in *Ninj1*$^{-/-}$ mice on the impaired gut healing process, WT and *Ninj1*$^{-/-}$ mice were given drinking water with 2% DSS for 6 days, followed by fresh water for an additional 6 days (Figure 38). When the clinical signs were compared after providing fresh water, the WT mice showed an increase in weight loss (Figure 39A) and the DAI score (Figure 39B) after 3 days, which were gradually suppressed thereafter (Figure 39A, B). In contrast, *Ninj1*$^{-/-}$ mice displayed a spontaneous decrease in body weight (Figure 39A) and elevated DAI scores (Figure 39B), accompanied by low survival rate (Figure 39C). Additionally, *Ninj1*$^{-/-}$ mice exhibited a significant reduction in colon length (Figure 40) and increased crypt loss, ulceration, and inflammatory cell infiltration highlighted by an increased histopathological score (Figure 41). These results indicate that the escalated dysbiosis in *Ninj1*$^{-/-}$ mice may delay the colitis recovery process.

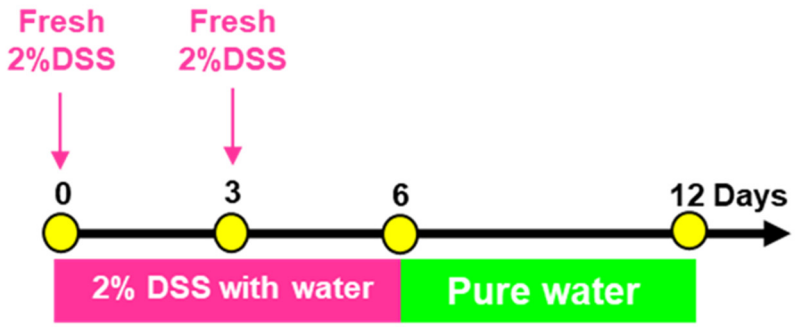

Figure 38. Schedule for directly comparing the ability of WT and *Ninj1*$^{-/-}$ mice to recover from colitis.

WT and *Ninj1*$^{-/-}$ mice were provided drinking water containing 2% DSS for 6 days, followed by fresh water for an additional 6 days ($n_{0\sim7\text{days}}$ = 10 per group; $n_{8\sim12\text{days}}$ = 3–10 per group).

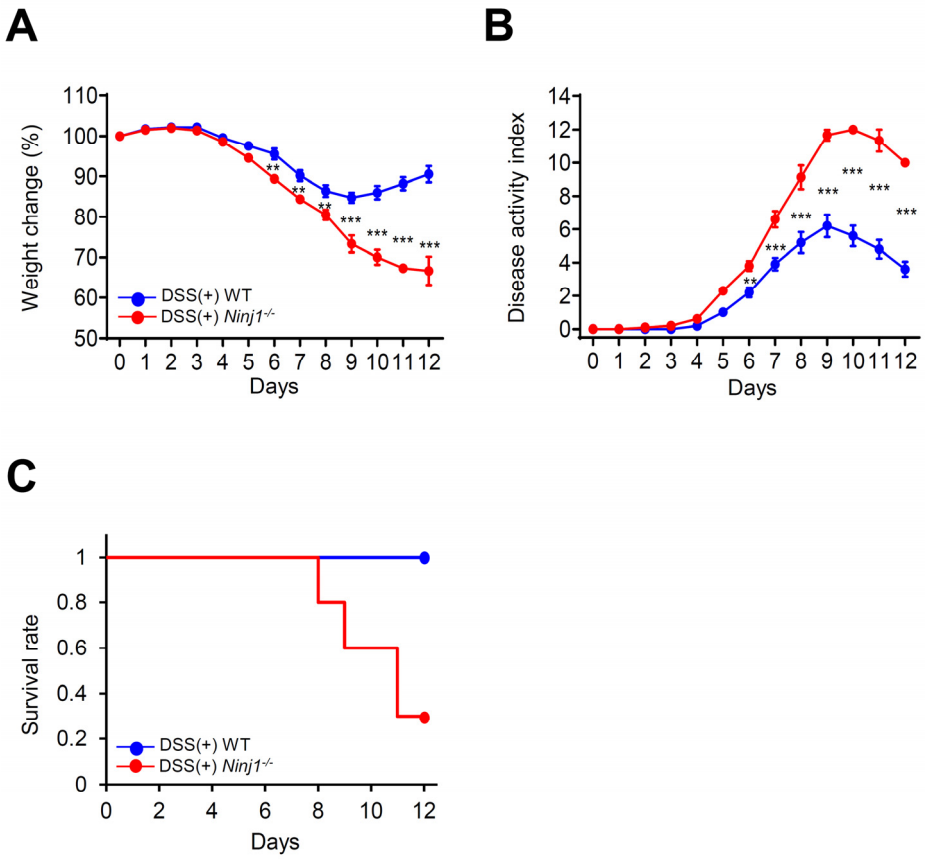

Figure 39. *Ninj1*$^{-/-}$ mice showed impaired colitis recovery.

Body weight changes **(A)** and DAI score **(B)** of WT and *Ninj1*$^{-/-}$ mice are shown. **(C)** The proportion of mice that survived to the total number of mice in each group was recorded on each day. $n_{0\sim7\text{days}}$ = 10 per group; $n_{8\sim12\text{days}}$ = 3–10 per group. The data represent the mean ± SEM. $^{**}P < 0.01$; $^{***}P < 0.001$.

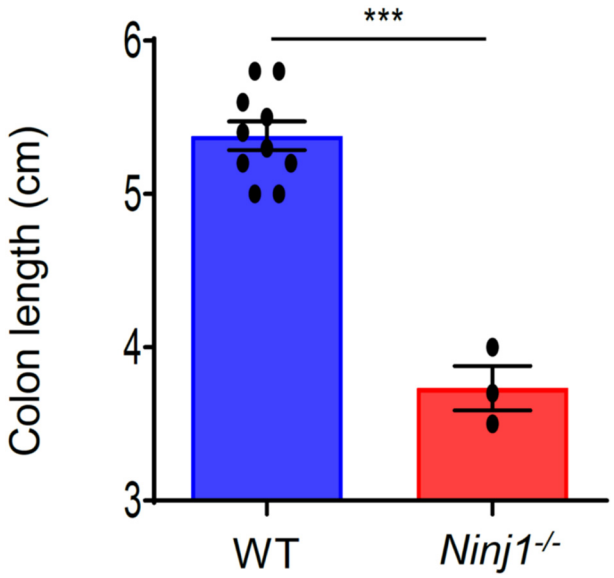

Figure 40. Colon length was shorter in *Ninj1*$^{-/-}$ mice than in WT mice during recovery phase.

Colon length was measured on day 12. The data represent the mean ± SEM. ***$P < 0.001$.

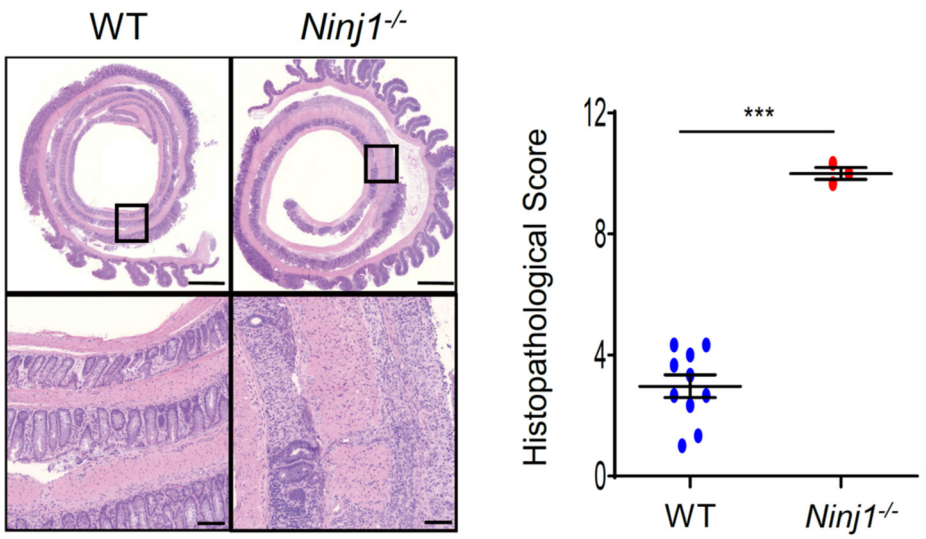

Figure 41. Histological damage was more severe in *Ninj1*$^{-/-}$ mice than in WT mice during recovery phase.

Representative histopathology images and scores from colonic tissue. Scale bar = 1000 μm (upper) or 100 μm (bottom). The data represent the mean ± SEM. ***$P < 0.001$.

8. Reduction of M2 macrophages in *Ninj1*$^{-/-}$ mice delays colitis recovery

M2 macrophages antagonize inflammation and promote tissue repair (Mantovani et al., 2013; Sica and Mantovani, 2012). I therefore investigated whether a decrease in the M2 macrophage phenotype was related to impaired colitis recovery in *Ninj1*$^{-/-}$ mice (Figure 42). After DSS treatment, the number of CD206^{+} M2 macrophages was significantly increased in the colon of WT mice compared to that in *Ninj1*$^{-/-}$ mice (Figure 43). Conversely, the number of CD86^{+} M1 macrophages was drastically increased in *Ninj1*$^{-/-}$ mice compared to that in WT mice (Figure 43). In the inflamed colon mucosa, I also confirmed that Ninj1 deficiency accelerates the accumulation of iNOS^{+} M1 macrophages and decreases the proportion of Arg-1^{+} and CD206^{+} M2 macrophages (Figure 44, Table 2). Consistently, the proportion of TNF-α^{+} macrophages was increased significantly, whereas that of IL-10^{+} macrophages was decreased in the inflamed mucosa of *Ninj1*$^{-/-}$ mice compared to WT mice (Figure 45, Table 2). These results suggest that the impaired colitis recovery observed in *Ninj1*$^{-/-}$ mice is associated with reduced M2 macrophage population.

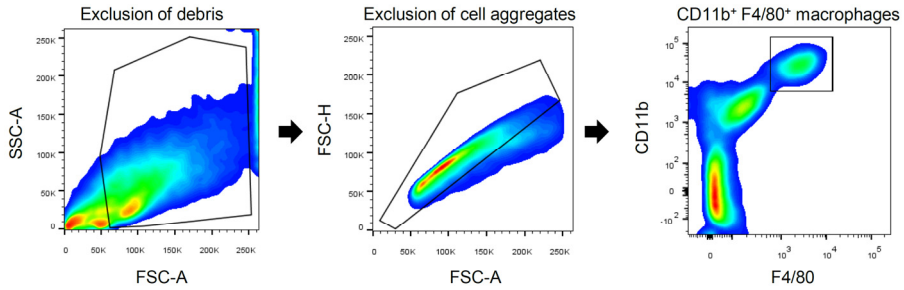

Figure 42. Gating strategy for isolating the macrophage population after colitis induction

Whole prepared cell population were first gated by excluding debris (FSC-A vs SSC-A) and cell aggregates (FSC-A vs FSC-H). Then the gated cell population takes only $CD11b^{+}$ $F4/80^{+}$ macrophage population.

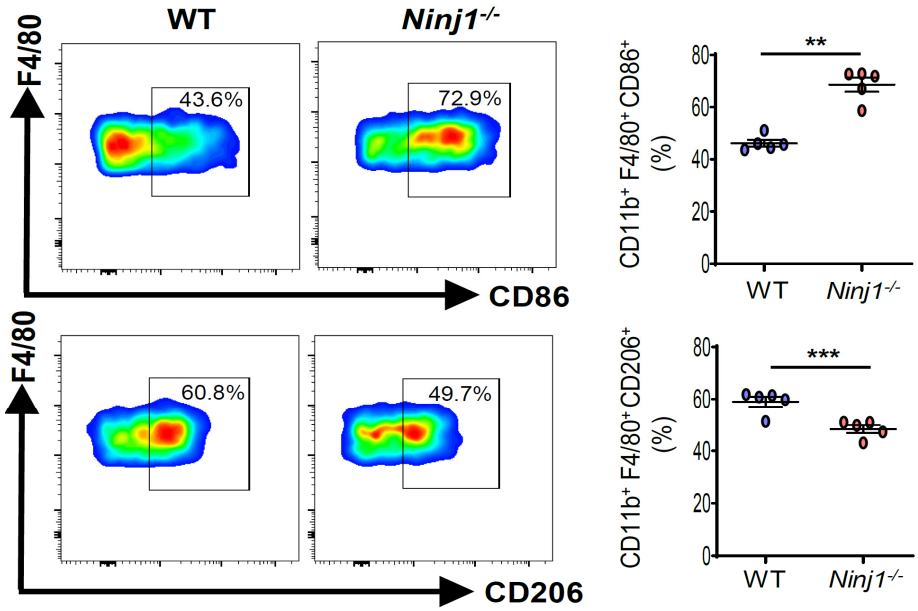

Figure 43. An accumulation of CD86^{+} M1 macrophages and a lower proportion of CD206^{+} M2 macrophages was observed in DSS-treated colons of *Ninj1*$^{-/-}$ mice than in those of WT mice.

Representative plot of flow cytometry (left panel) and frequency (right panel) of CD86^{+} or CD206^{+} CD11b^{+} F4/80^{+} macrophages in DSS-treated inflamed colonic tissues from WT and *Ninj1*$^{-/-}$ mice. The data represent the mean ± SEM. $^{**}P < 0.01$; $^{***}P < 0.001$.

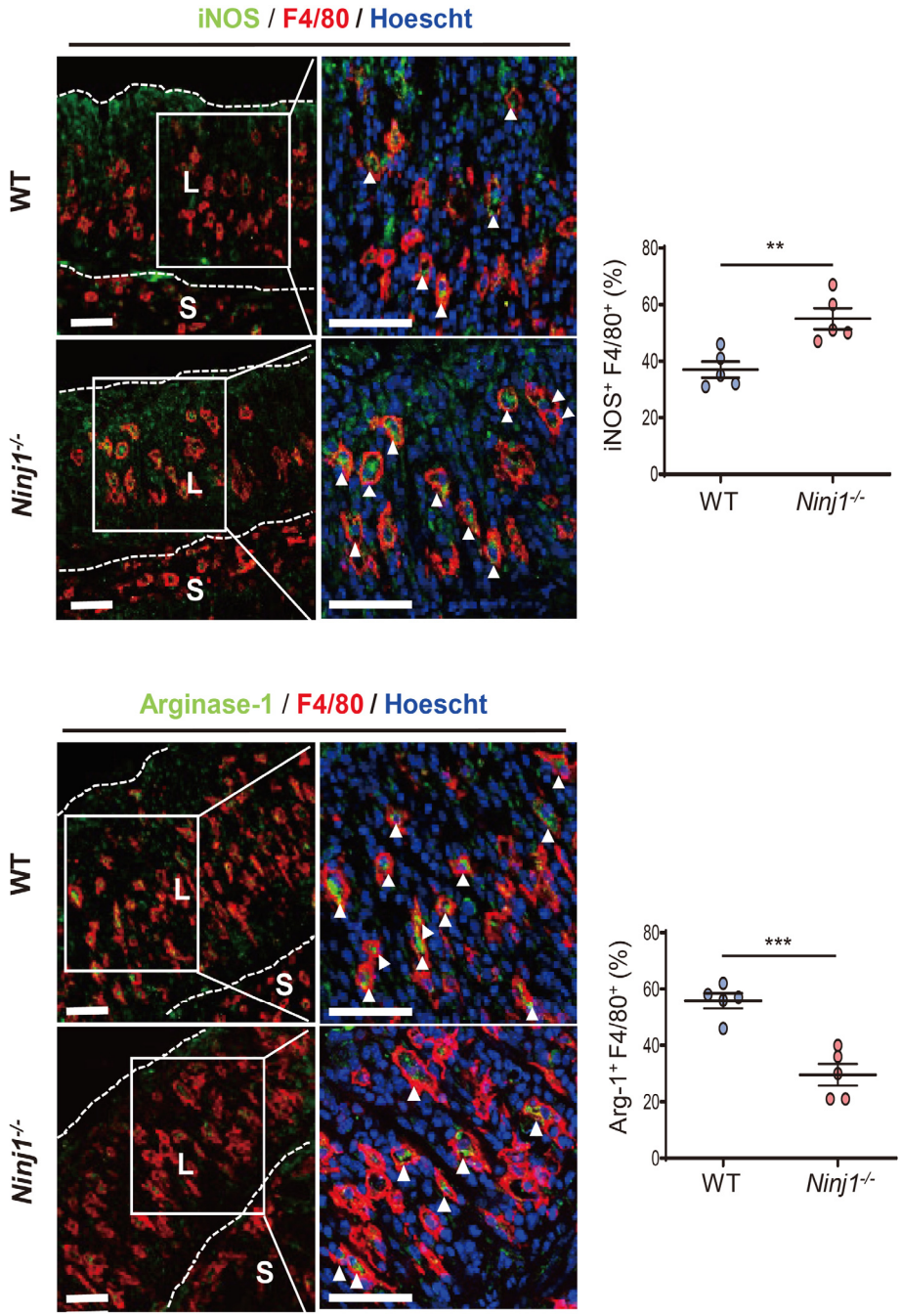
iNOS / F4/80 / Hoescht
WT
Ninj1-/-
L
S
iNOS+ F4/80+ (%)
**
WT
Ninj1-/-
Arginase-1 / F4/80 / Hoescht
WT
Ninj1-/-
L
S
Arg-1+ F4/80+ (%)
***
WT
Ninj1-/-

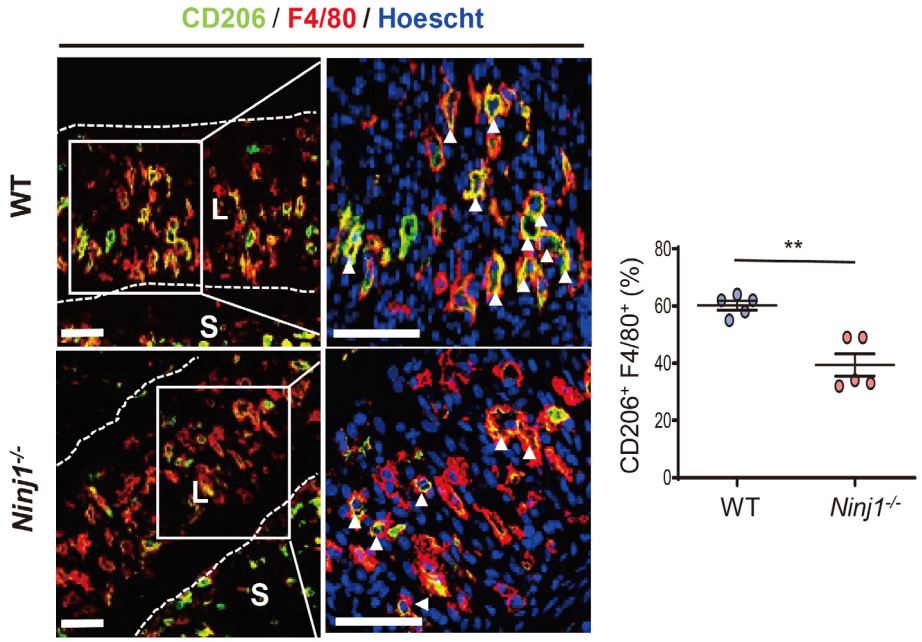

Figure 44. An accumulation of iNOS^{+} M1 macrophages and a lower proportion of Arginase-1 or CD206^{+} M2 macrophages was observed in inflamed mucosa of *Ninj1*$^{-/-}$ mice than in those of WT mice.

Immunostaining for M1 (iNOS) and M2 (Arginase-1; Arg-1 and CD206^{+}) macrophage markers in inflamed colon mucosa of WT and *Ninj1*$^{-/-}$ mice. iNOS^{+}, Arg-1^{+} and CD206^{+} F4/80^{+} macrophages are indicated by arrowheads (left panel). The proportion of iNOS^{+}, Arg-1^{+} and CD206^{+} macrophages was calculated (right panel; n = 3 fields/mice). n = 5 per group. Scale bar = 50 μm. The data represent the mean ± SEM. $^{**}P < 0.01$; $^{***}P < 0.001$.

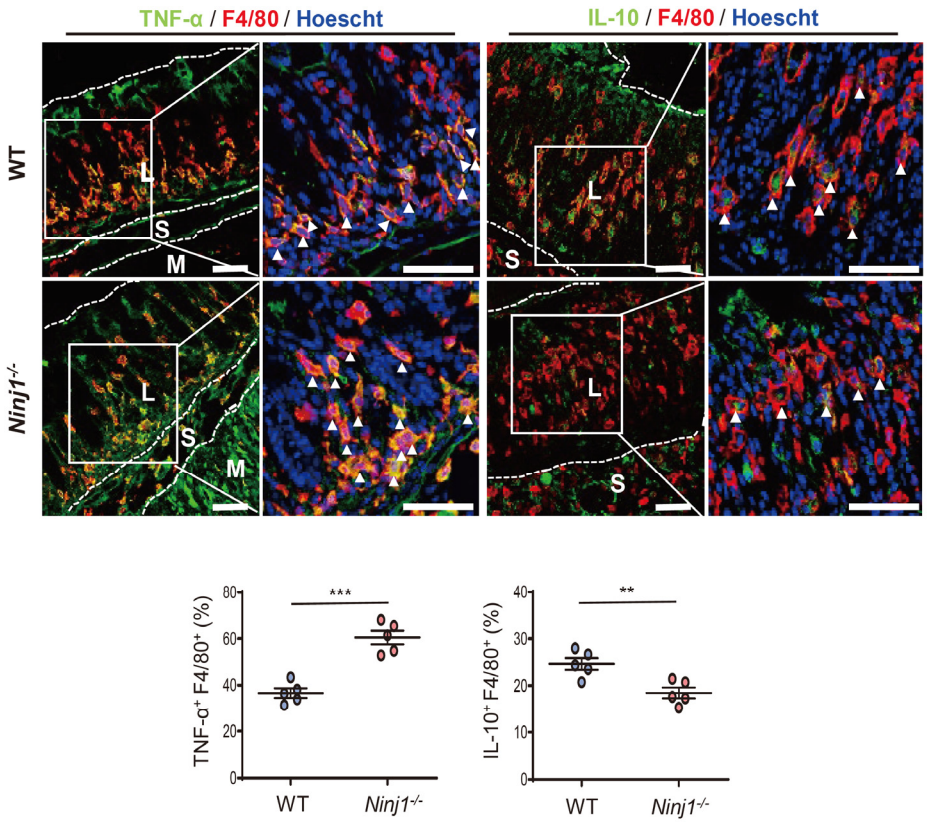

Figure 45. An accumulation of TNF-α^{+} macrophages and a lower proportion of IL-10^{+} macrophages was observed in inflamed mucosa of *Ninj1*$^{-/-}$ mice than in those of WT mice.

Immunostaining of TNF-α^{+} or IL-10^{+} F4/80^{+} macrophages in colonic tissues from DSS-induced WT and *Ninj1*$^{-/-}$ mice. TNF-α^{+} or IL-10^{+} F4/80^{+} macrophages are indicated by arrowheads (left panel). The proportion of TNF-α^{+} or IL-10^{+} F4/80^{+} macrophages was calculated (right panel; $n = 3$ fields/mice). $n = 5$ per group. Scale bar = 50 μm. The data represent the mean ± SEM. *$P <$ 0.05. L: lamina propria (mucosa), S: submucosa, M: muscularis externa.

9. Ninj1 restricts M1 macrophage polarization but activates M2 polarization *in vitro*

Following colitis induction, the proportion of Ninj1-expressing F4/80^{+} macrophages was increased compared to that under homeostatic conditions (Figure 27). In addition, Ninj1 expression was significantly increased by 3.8-fold compared to that in the normal colon (Figure 46). Simultaneously, the number of M1 macrophages was drastically increased in the colon of *Ninj1*$^{-/-}$ mice compared to that of WT mice. Conversely, the number of M2 macrophages was significantly increased in the WT mice compared to that in *Ninj1*$^{-/-}$ mice (Figure 43 and Figure 44). These results suggest that the increased expression of Ninj1 in macrophages during colitis development restricts M1 polarization and promotes M2 polarization, thereby preventing the development of severe colitis and promoting colitis recovery. Next, I stimulated BMDMs with various stimuli, including LPS to induce the M1 phenotype or IL-4 to generate the M2 phenotype. Interestingly, the expression of Ninj1 was induced by both LPS and IL-4. Consistent with *in vivo* result, these results suggest that increased Ninj1 expression in macrophages is associated with the regulation of M1/M2 polarization. To test this hypothesis, I used siRNA to knockdown Ninj1 expression in the naïve WT macrophages. siRNA treatment markedly decreased the expression of Ninj1 in unstimulated, or LPS and IL-4-stimulated macrophages (Figure 47A). Furthermore, Ninj1 knockdown

macrophages showed higher levels of mRNAs of M1 markers, such as *Tnf*, *Nos2*, and *Il6*, with a corresponding higher production of TNF-α, IL-6, and IL-1β (Figure 47B, C), in comparison to those in the control macrophages. However, Ninj1 knockdown decreased the M2 marker levels, such as those of *Arg1*, *Mrc1*, and *Retnla* (Figure 47A). Furthermore, *Ninj1*$^{-/-}$ macrophages showed high mRNA levels of M1 markers and low mRNA levels of M2 markers (Figure 48A). At the protein level, higher levels of CD86 and lower levels of CD206 were expressed in the *Ninj1*$^{-/-}$ macrophages (Figure 48B). Collectively, these results indicate that increased Ninj1 expression in macrophages limits M1 polarization and promotes M2 polarization.

Next, to further investigate the role of NINJ1 in regulating M1/M2 macrophage polarization in human macrophages, I knocked down NINJ1 expression in PMA-differentiated THP-1 macrophages using siRNA (Figure 49A). Consistent with the results in mice, the expression of NINJ1 was increased by both LPS and IL-4. NINJ1 knockdown increased the levels of M1 marker genes such as *TNF*, *IL6*, and *IL1B* (Figure 49B, C), and decreased M2 marker gene levels, such as those of *MRC1*, *CD209*, and *CCL22* (Figure 49B). Overall, these results indicate that increased Ninj1 expression in macrophages during colitis development restricts M1 polarization and activates M2 polarization, thereby preventing the development of severe colitis and promoting recovery.

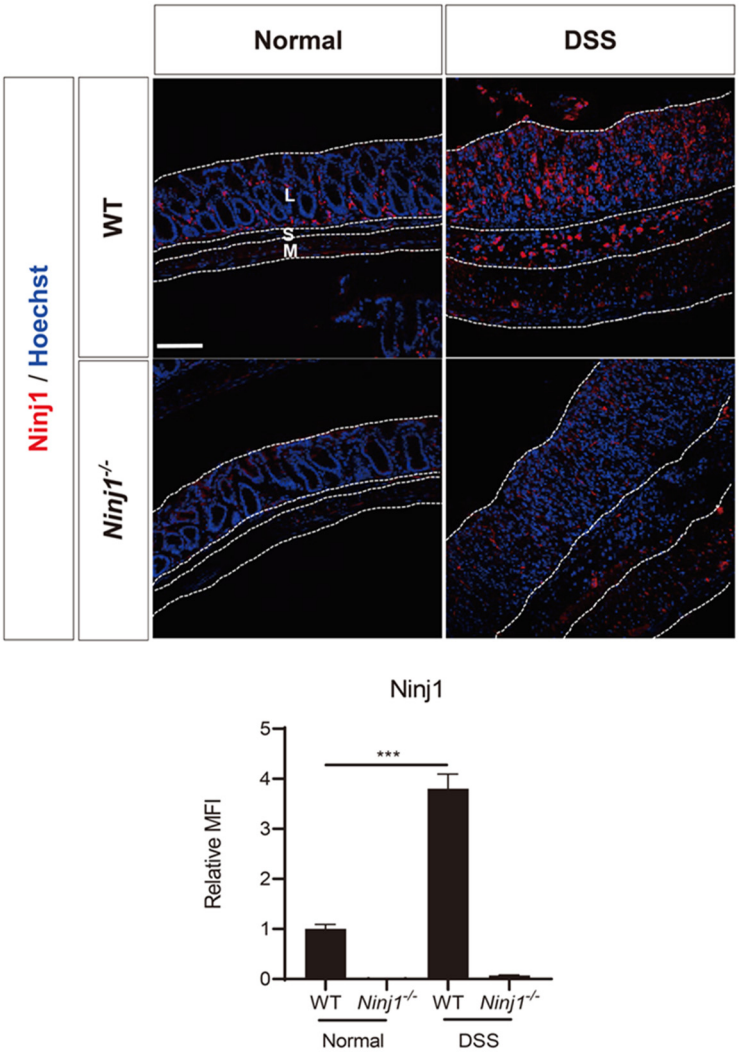

Figure 46. Ninj1 expression in macrophages is increased after colitis induction. Confocal images of Ninj1 expression (upper) and relative mean fluorescence intensity (MFI) of Ninj1 (bottom) in normal or DSS-treated colons in WT and *Ninj1*$^{-/-}$ mice. n = 5 mice per group. The data represent the mean ± SEM. Scale bar = 50 μm. ***$P < 0.001$.

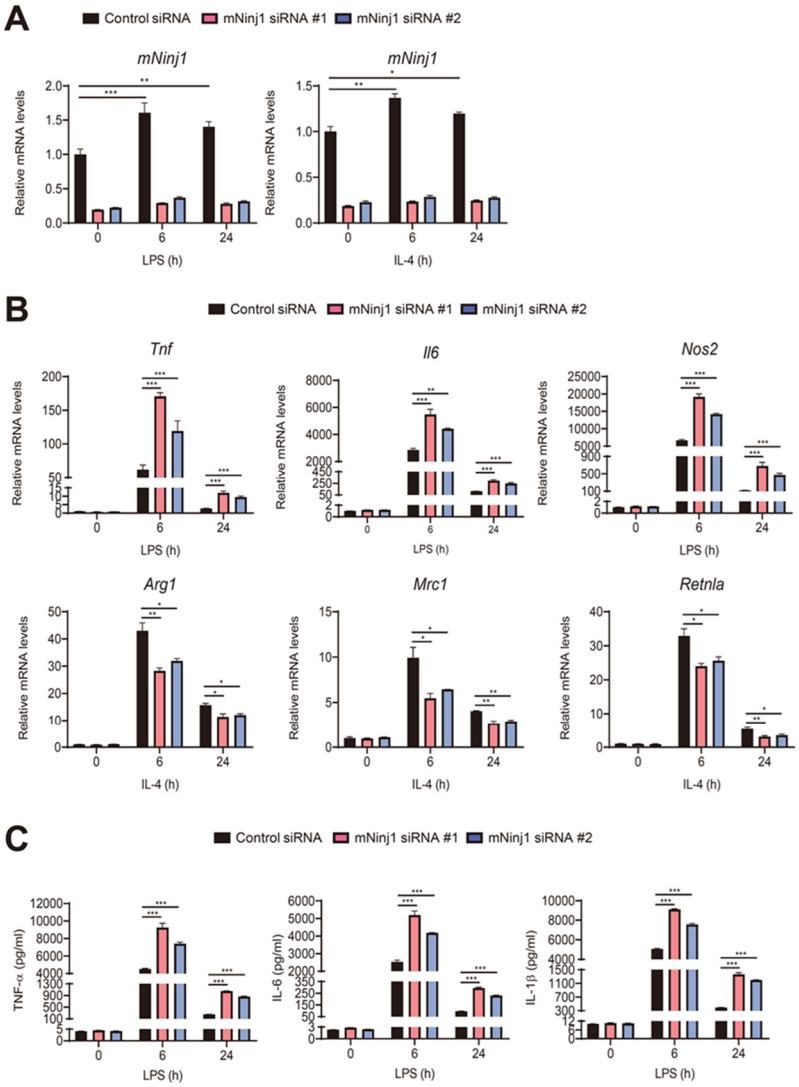

Figure 47. Ninj1 knockdown in primary murine macrophages promotes M1 polarization but inhibits M2 polarization *in vitro*. A–C) WT BMDMs were transfected with siRNA for Ninj1 (Ninj1 siRNA #1 or #2) or non-targeting control siRNA (control siRNA), followed by stimulation with LPS or IL-4 for 6 or 24 h ($n = 3$ repeats). The mRNA levels of *mNinj1* (**A**), M1-associated genes, and M2-related genes (**B**) were measured using qPCR. (**C**) The protein expression of mTNF-α, mIL-6 and mIL-1β was measured using ELISA.

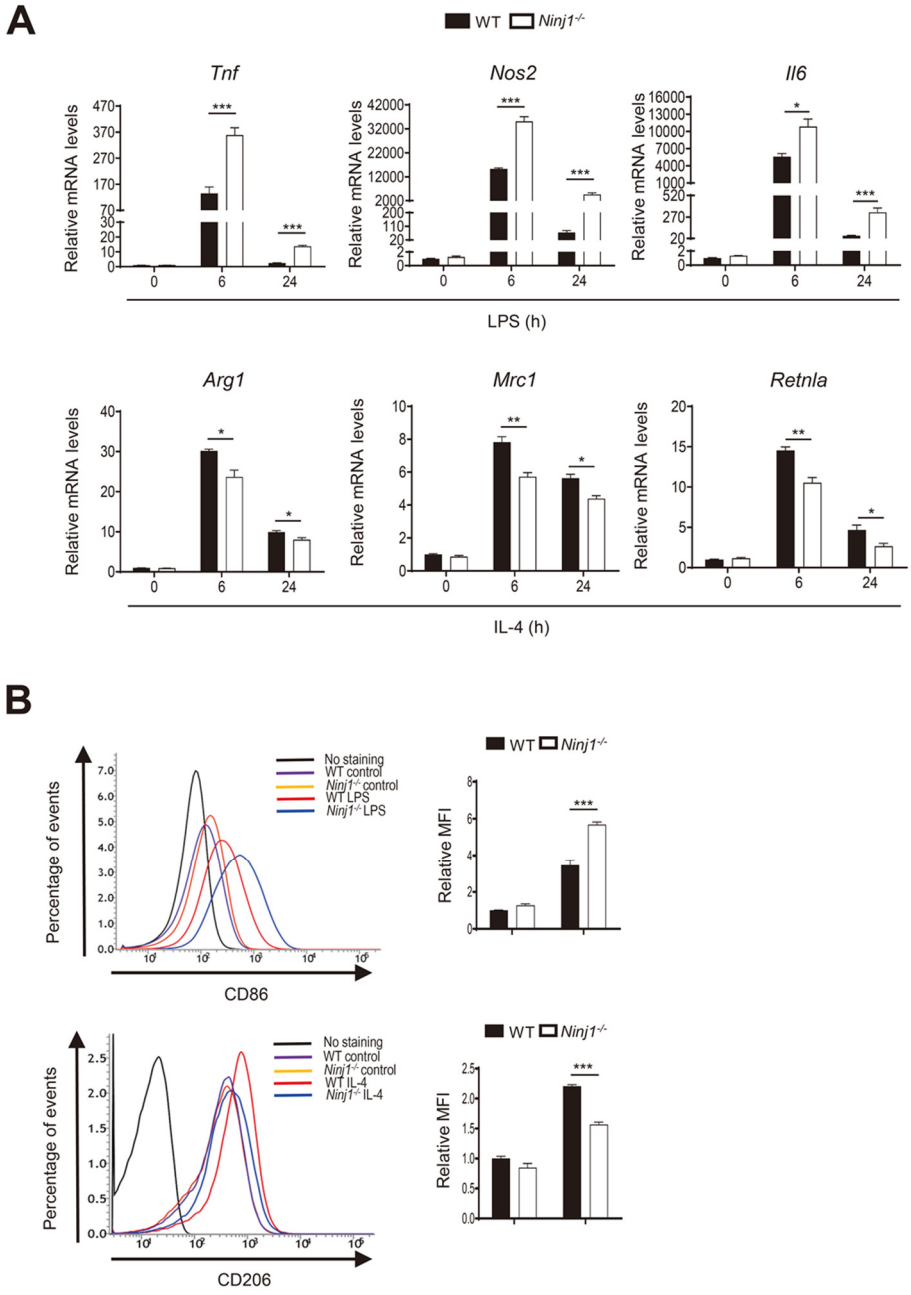
A
WT
Ninj1-/-
Tnf
Nos2
Il6
Relative mRNA levels
LPS (h)
Arg1
Mrc1
Retnla
IL-4 (h)
B
No staining
WT control
Ninj1-/- control
WT LPS
Ninj1-/- LPS
Percentage of events
CD86
Relative MFI
WT IL-4
Ninj1-/- IL-4
CD206

Figure 48. Ninj1 deficiency suppresses the activation of M2 macrophage programming *in vitro*.

A) The relative mRNA levels of *Tnf*, *Nos2,* and *Il6* (upper panel) or *Arg1*, *Mrc1*, and *Retnla* (bottom panel) in BMDMs from WT and *Ninj1*$^{-/-}$ mice with or without stimulation with LPS or IL-4 for 6 or 24 h. **B)** Representative flow cytometry plots (left panel) and relative mean fluorescence intensity (MFI; right panel) for CD86 (upper panel) or CD206 (bottom panel) in WT and *Ninj1*$^{-/-}$ BMDMs with or without stimulation by LPS or IL-4 for 24 h. **(A, B)** $n = 3$ repeats. The data represent the mean ± SEM. *$P < 0.05$; **$P < 0.01$; ***$P < 0.001$.

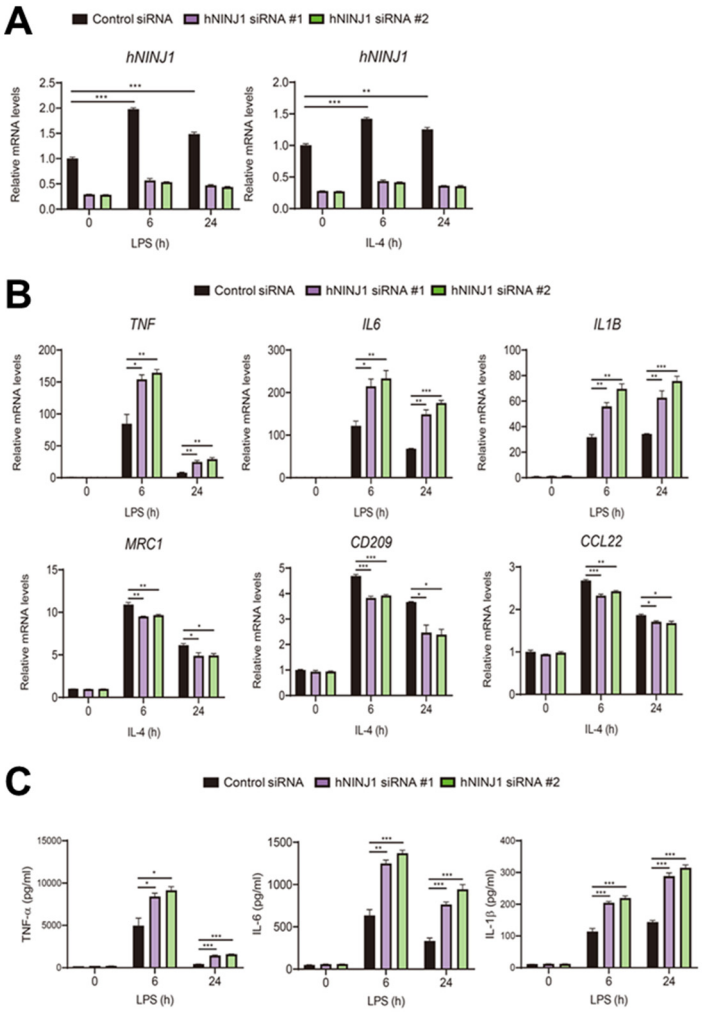

Figure 49. Ninj1 knockdown in human macrophages promotes M1 polarization but inhibits M2 polarization *in vitro*. A-C) PMA-differentiated THP-1 macrophages were treated with control siRNA, Ninj1 siRNA #1 or #2, followed by exposure to LPS or IL-4 for 6 or 24 h (n = 3 repeats). The mRNA levels of *hNINJ1* (**D**), M1-associated genes, and M2-related genes (**E**) were measured by qPCR. (**F**) ELISA was used to assess the production of hTNF-α, hIL-6, and hIL-1β cytokines. The data represent the mean ± SEM. *$P < 0.05$; **$P < 0.01$; ***$P < 0.001$.

10. Transfer of WT macrophages ameliorated severe colitis development of *Ninj1*$^{-/-}$ mice

Lastly, I examine whether transfer of Ninj1-expressing macrophages into *Ninj1*$^{-/-}$ mice could improve the development of colitis by modulating aberrant macrophage polarization. To this end, PBS and CFSE-labeled BMDMs from WT or *Ninj1*$^{-/-}$ mice were administered into *Ninj1*$^{-/-}$ mice in a DSS-induced colitis model (Figure 50). Adoptively transferred macrophages from each genotype were equivalently located in the colonic tissue after injection (Figure 51). Administration of WT macrophages significantly suppressed the loss of body weight (Figure 52A) and DAI (Figure 52B) from day 6 after DSS treatment compared to that in response to the administration of PBS or *Ninj1*$^{-/-}$ macrophages. Additionally, the shortness of colon length (Figure 53) or increased histologic score (Figure 54) was ameliorated by the administration of WT macrophages. These results were confirmed by decreased mRNA levels of M1-associated genes, such as *Nos2,* and increased levels of M2-associated genes, such as *Arg*, *Mrc1*, and *Retnla,* in lamina propria cells from WT macrophage-transferred *Ninj1*$^{-/-}$ mice (Figure 55), suggesting that Ninj1-expressing macrophages elicit a protective role against the development of colitis via promotion of M2 polarization.

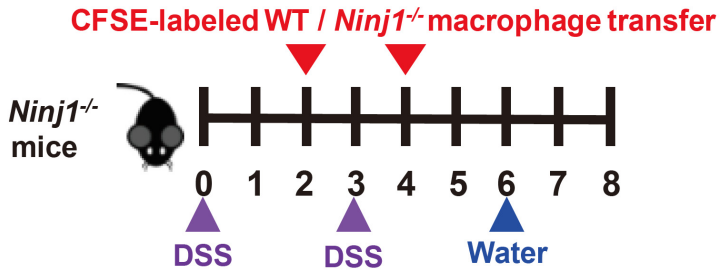

Figure 50. Experimental schedule for the evaluation of adoptive WT or *Ninj1*$^{-/-}$ macrophage transfer in DSS-treated *Ninj1*$^{-/-}$ mice.

CFSE-labeled BMDMs from WT and *Ninj1*$^{-/-}$ mice were intravenously injected into *Ninj1*$^{-/-}$ mice at 2 and 4 days after the start of DSS treatment. CFSE: carboxyfluorescein succinimidyl ester.

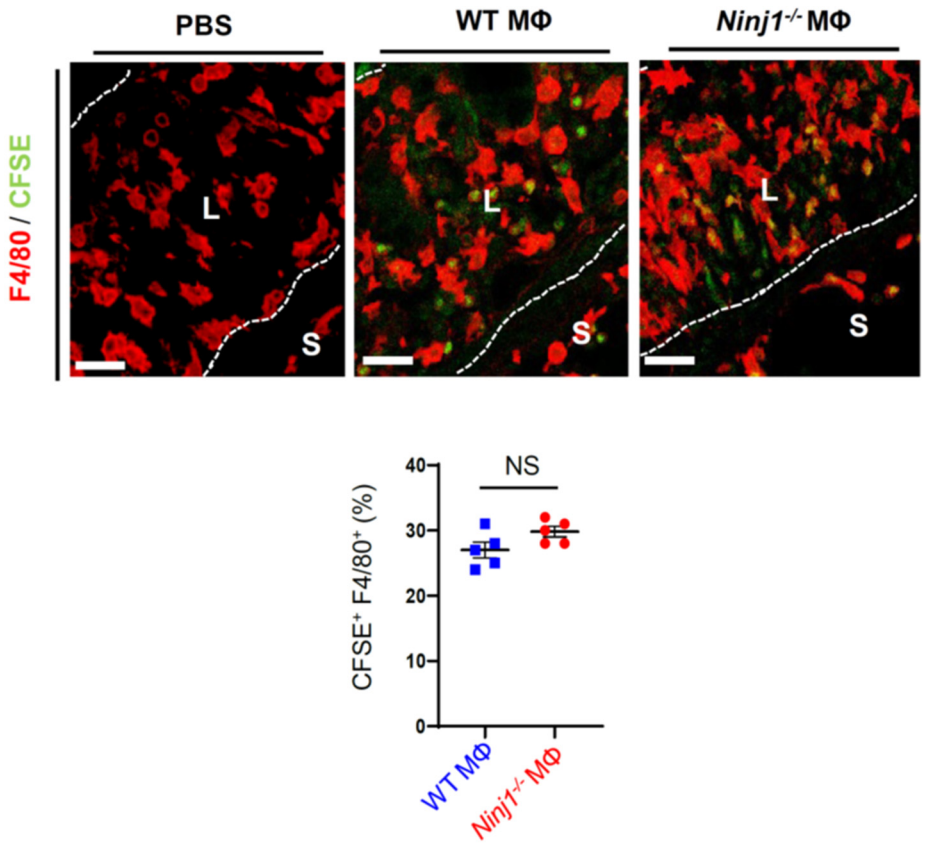

Figure 51. Adoptively transferred WT or *Ninj1*$^{-/-}$ macrophages were equivalently located in the colonic tissue after injection.

The proportion of CFSE^{+} F4/80^{+} macrophages was calculated (right panel; n = 3 fields/mice). n = 5 per group. The data represent the mean ± SEM. NS: Non-significance, MΦ: macrophages.

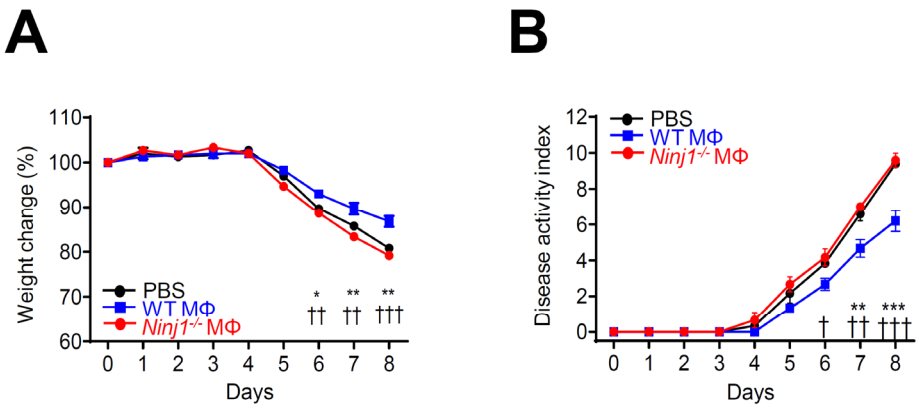

Figure 52. The administration of WT macrophages significantly suppressed severe colitis development

Weight change **(A)**, DAI scores **(B)** were obtained daily (*, PBS vs. WT MΦ; †, WT MΦ vs. *Nin1*$^{-/-}$ MΦ). $n_{0day} = 6$ per group, $n_{7\sim8days} = 5$ per group. The data represent the mean ± SEM. *,† $P < 0.05$; **,†† $P < 0.01$; ***,††† $P < 0.001$.

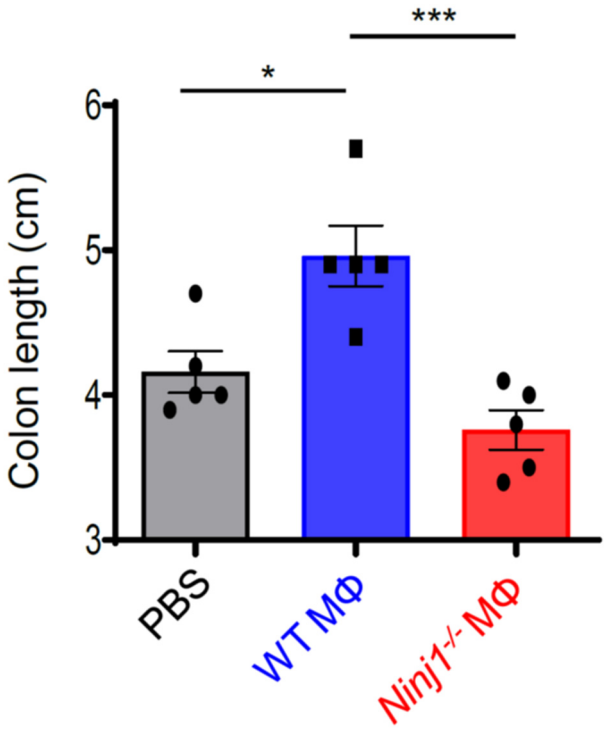

Figure 53. Transfer of WT macrophages to *Ninj1*$^{-/-}$ mice was improved the shortness of colon length from *Ninj1*$^{-/-}$ mice under DSS-induced colitis conditions.

Colon length was recorded using a ruler on day 8 (n = 5 per group). The data represent the mean ± SEM. *$P < 0.05$; ***$P < 0.001$.

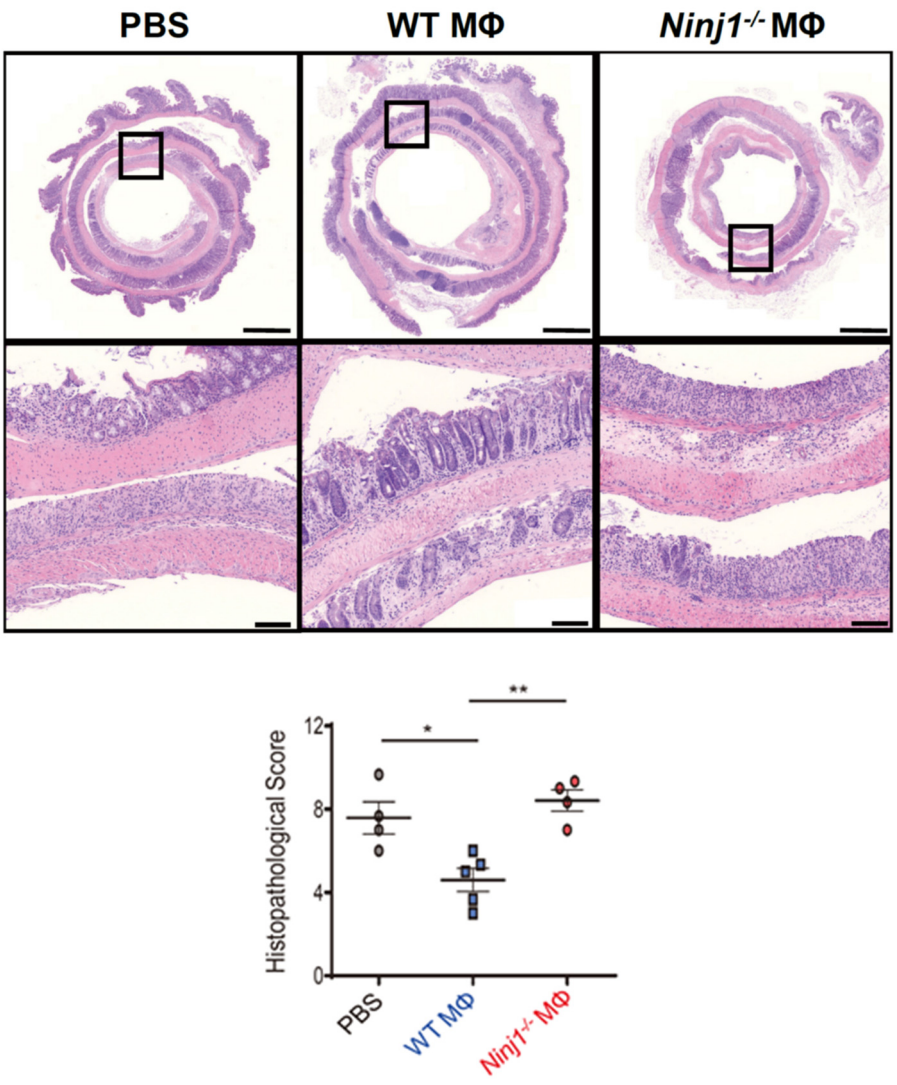

Figure 54. DSS-induced histological damage of *Ninj1*$^{-/-}$ mice was ameliorated by the transfer of WT macrophages

Representative histological images and scores from each colonic tissue (n = 5 per group). Scale bar = 1000 μm (upper) or 100 μm (bottom). The data represent the mean ± SEM. *P < 0.05; **P < 0.01.

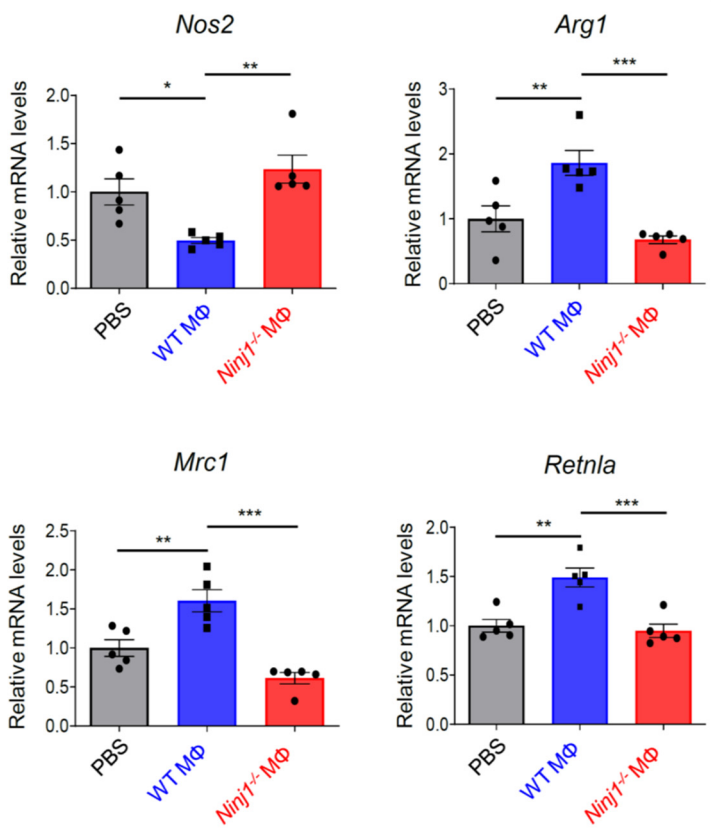

Figure 55. The expression levels of M2-associated genes was increased by the transfer of WT macrophages

The relative mRNA levels of *Nos2, Arg1, Mrc1*, and *Retnla* in the lamina propria cells from PBS, WT, and *Ninj1*$^{-/-}$ BMDMs-transferred *Ninj1*$^{-/-}$ mice (n = 5 per group). The data represent the mean ± SEM. *P < 0.05; **P < 0.01; ***P < 0.001.

DISCUSSION

Ninj1 is a transmembrane protein that functions as a cell adhesion molecule (CAM). Certain CAMs, including integrins, cadherins, and immunoglobulin-related cell adhesion molecule (IgCAM) family members, function as sensors of the surrounding environment to detect specific bacterial components, while also participating in cell-cell adhesion (Mengaud et al., 1996; Relman et al., 1990; Schmitter et al., 2004). Hence, Ninj1 may have the potential to act as a mediator between host and gut microbiota to maintain colon homeostasis.

IBD patients frequently experience a breakdown in gut homeostasis that is reflected by dysregulated immune homeostasis and a dominance of dysbiotic bacterial communities. Therefore, an understanding of the mechanisms required for maintenance and restoration of gut homeostasis is important for prevention and treatment of IBD. In this study, I identified Ninj1 as a key mediator that promotes colonic homeostasis by influencing the M1/M2 macrophage phenotype and microbial homeostasis.

Specifically, I found that *Ninj1*$^{-/-}$ mice had an increased proportion of the colitogenic *Prevotellaceae* family and decreased proportion of the butyrate-producing *Lachnospiraceae* family in the normal colon, which led to hyper-susceptibility to DSS-induced colitis. The *Lachnospiraceae* family, which was preferentially enriched in the mucosal sites compared to the central lumen,

prevents enteric pathogen adhesion and colonization (Nava et al., 2011), suggesting that Ninj1 may promote colonization of *Lachnospiraceae* to prevent adhesion or colonization of colitogenic *Prevotellaceae* in or near the colonic mucosa. Indeed, compared with the single-housed *Ninj1*$^{-/-}$ mice, *Ninj1*$^{-/-}$ mice co-housed with WT mice showed improved colitis phenotypes associated with the elevated abundance of *Lachnospiraceae* and decreased *Prevotellaceae*. *Lachnospiraceae* are primarily responsible for butyrate production, which limits colonic inflammation. Thus the increased abundance of *Lachnospiraceae* family in co-housed *Ninj1*$^{-/-}$ mice resulted in an increase in butyrate, which could be associated with an improved colitis phenotype in co-housed *Ninj1*$^{-/-}$ mice.

A precise and complex balance in macrophage polarization has proven important in maintaining gut homeostasis. Therefore, the accumulation of M1 macrophages is frequently observed in IBD mice or patients. This finding was consistent with those of the current present study, in which the relative number of M1 macrophage was drastically accumulated in the DSS-treated colon of *Ninj1*$^{-/-}$ mice. DSS treatment in mice leads to disruption of the colon epithelial barrier, which promotes the entry of lumen bacteria and their components or metabolites such as LPS and butyrate. Simultaneously, Ninj1 expression is increased in F4/80^{+} macrophages. Thus, basis on the increased Ninj1 expression and M1 macrophage accumulation observed in *Ninj1*$^{-/-}$ mice, I hypothesized that Ninj1 deficiency in macrophages led to M1 macrophage polarization,

which was also supported by these observation that Ninj1 expression is induced by stimulation with microbial LPS alone or in concert with butyrate (Figure 56), and that loss of Ninj1 expression in BMDMs enhances LPS-induced M1 polarization *in vitro*.

However, previous studies have reported that the peptide-mediated inhibition of trans-interactions between Ninj1 in human macrophages or siRNA-mediated Ninj1 silencing in the Raw 264.7 monocyte/macrophage cell lines, negatively regulate LPS-induced inflammatory responses (Jennewein et al., 2015; Shin et al., 2016). Although it is difficult to ascertain the precise cause of this discrepancy, a possible explanation may be that the constitutive absence of Ninj1 may affect transcriptional reprogramming of myeloid progenitor cells, which may in turn influence the hyper-inflammatory response to bacterial antigens. Nevertheless, I confirmed that Ninj1 knockdown in naïve WT BMDMs or PMA-differentiated THP-1 macrophages promoted LPS-induced M1 macrophage polarization. Meanwhile, the population of the M1 phenotype is expanded by pro-inflammatory cytokines during colitis development. I also confirmed that Ninj1 knockdown in macrophages enhances the expression and secretion of LPS-induced pro-inflammatory cytokines. The stimulation of TLR4 by LPS activates the NF-κB and JNK/p38 MAPK signaling molecules, which are necessary to induce the expression of the pro-inflammatory cytokines. I have shown that Ninj1 deficiency in macrophages chronically activates NF-κB and JNK/p38 MAPK signaling molecules. These results suggest that Ninj1

can regulate pro-inflammatory cytokine expression by acting as a negative regulator of the TLR-4-induced NF-κB and JNK/p38 MAPK signaling pathways.

I also found that *Ninj1*$^{-/-}$ mice exhibited impaired colitis recovery, which was closely associated with a reduction in M2 macrophages compared with those in WT mice. Ninj1 knockdown or knockout macrophages also exhibited impaired M2 programming *in vitro*, suggesting that Ninj1 is required for M2 macrophage activation in a cell-intrinsic manner. p53 has been previously reported to act as a brake to inhibit M2 macrophage polarization (Li et al., 2015). Interestingly, Ninj1 was reported to repress p53 translation (Cho et al., 2013), suggesting that Ninj1 might potentially promote M2 macrophage polarization by repressing p53 translation. Additionally, butyrate is a novel activator of STAT6-mediated transcription through H3K9 acetylation, which induces M2 macrophage polarization (Ji et al., 2016). *Ninj1*$^{-/-}$ mice exhibited significantly reduced abundance of butyrate-producing *Lachnospiraceae* and *Ruminococcaceae* families compared with WT mice following DSS treatment, suggesting that reduced butyrate may be partially associated with decreased M2 macrophage differentiation.

Inflammation promotes instability of the intestinal epithelial barrier and alters the expression of antimicrobial peptides resulting in a dysbiotic microbiome (Gallo and Hooper, 2012; Wellman et al., 2017). Several

colitogenic bacteria promote inflammatory conditions that favor their own growth. Hence, inefficient clearance of bacteria results in non-resolving inflammation, followed by increased pro-inflammatory responses (Kaufmann and Dorhoi, 2016; Kim et al., 2019; Na et al., 2019). In this regard, I suggested that bacterial lysis is not functioning properly as a cause of chronic inflammation activation in *Ninj1*$^{-/-}$ macrophages, contributing to increased basal colonic inflammation and microbial imbalance. Recent studies have demonstrated that dysfunctional bacterial lysis in aged macrophages was associated with increased inflammation and dysbiosis (Thevaranjan et al., 2018). Interestingly, Yang *et al.* reported that Ninj1 deficiency increases systemic inflammation and reduces the survival rate of mice with age (Yang et al., 2017), implying that *Ninj1*$^{-/-}$ mice exhibit higher levels of malfunctioning bacterial lysis in macrophages with age, leading to increased intestinal microbial imbalance and possibly contributing to the development of chronic colitis and colon cancer. Woo *et al.* reported that Ninj1 overexpression on macrophages plays a negative role in the azoxymethane (AOM)/DSS model of colitis-associated colon cancer (CAC) (Woo et al., 2016). However, further studies are required to identify the precise mechanism underlying microbial imbalance caused by Ninj1 deficiency.

Generation of a dysbiotic microbiome, through the production of metabolites and toxins, can influence distal organ-related disease, such as obsessive-compulsive disorder (OCD), asthma, rheumatoid arthritis, and atherosclerosis

as well as local IBD development (Levy et al., 2017). Our group previously reported that Ninj1 deficiency also leads to OCD-like neuropsychiatric disorders in mice (Le et al., 2017). IBD and OCD symptoms are closely associated (Nahon et al., 2012), suggesting that Ninj1 may play a broad role in modulating bidirectional communication between the brain cells and gut microbiome.

In the present study, I focused primarily on the critical role of Ninj1 on macrophages in limiting the development of colitis. However, I lack understanding of the role of Ninj1 in other colonic cells in regulating the development of colitis, because I used systemic Ninj1-deficient mice. Therefore, further studies will need to be performed to clarify the role of cell-specific Ninj1 in colitis development using conditional Ninj1-deficient or transgenic mice.

In summary, under homeostatic conditions, Ninj1 deficiency increases the proportion of M1 macrophages and triggers microbial imbalance, inducing colitis hyper-susceptibility. Further, during colitis development, Ninj1 deficiency accelerates M1 macrophage accumulation and escalates dysbiosis, contributing to severe colitis development and impaired recovery. These study sheds light on the role of Ninj1 in preventing an imbalance in M1/M2 macrophage phenotypes and extensive dysbiosis to promote gut homeostasis. Further, this work provide insights into designing improved therapeutic approaches that include the use of Ninj1 agonists to prevent or treat IBD.

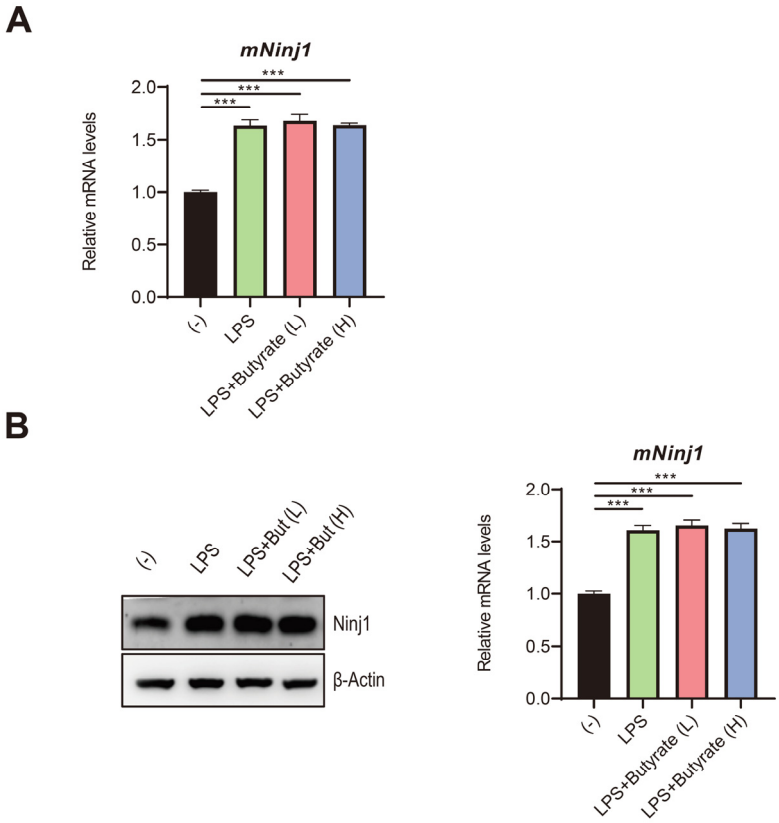

Figure 56. Ninj1 expression is increased in macrophages by treatment with LPS and butyrate.

A–B) BMDMs were unstimulated or stimulated with LPS (1 μg/mL) for 6 h in the presence or absence of butyrate (L, 0.1mM; H, 1 mM). (A) The relative mRNA levels of *Ninj1*. The levels of the Ninj1 protein were shown in (B) were quantified using a densitometer and normalized against the density of β-Actin. $n = 3$ repeats. The data represent the mean ± SEM. ***$P < 0.001$.

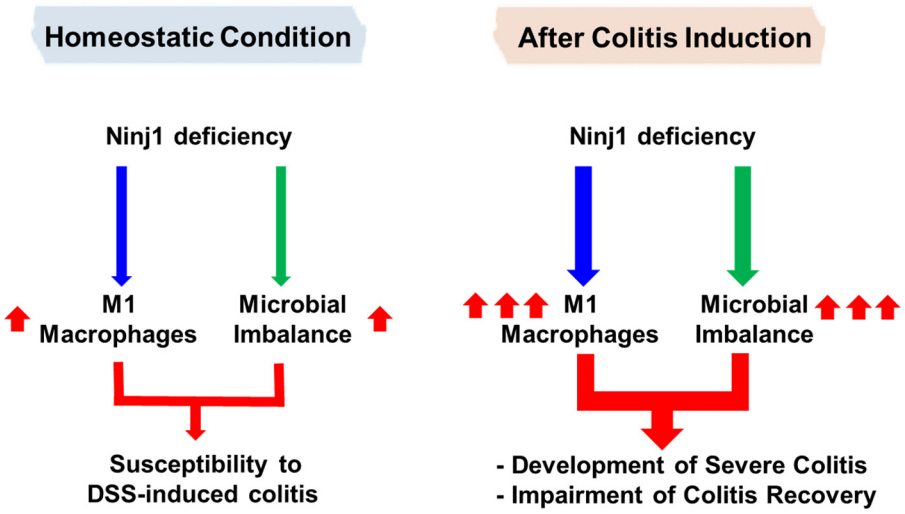

Figure 57. Summary illustration of the role of Ninj1 in mediating colonic homeostasis under homeostatic condition and after colitis induction.

REFERENCES

Ahn, B.J., Le, H., Shin, M.W., Bae, S.J., Lee, E.J., Wee, H.J., Cha, J.H., Lee, H.J., Lee, H.S., Kim, J.H.*, et al.* (2014). Ninjurin1 deficiency attenuates susceptibility of experimental autoimmune encephalomyelitis in mice. J Biol Chem *289*, 3328-3338.

Ahn, B.J., Lee, H.J., Shin, M.W., Choi, J.H., Jeong, J.W., and Kim, K.W. (2009). Ninjurin1 is expressed in myeloid cells and mediates endothelium adhesion in the brains of EAE rats. Biochem Biophys Res Commun *387*, 321-325.

Amit, I., Winter, D.R., and Jung, S. (2016). The role of the local environment and epigenetics in shaping macrophage identity and their effect on tissue homeostasis. Nat Immunol *17*, 18-25.

Araki, T., and Milbrandt, J. (1996). Ninjurin, a novel adhesion molecule, is induced by nerve injury and promotes axonal growth. Neuron *17*, 353-361.

Araki, T., Zimonjic, D.B., Popescu, N.C., and Milbrandt, J. (1997). Mechanism of homophilic binding mediated by ninjurin, a novel widely expressed adhesion molecule. J Biol Chem *272*, 21373-21380.

Atarashi, K., Tanoue, T., Shima, T., Imaoka, A., Kuwahara, T., Momose, Y., Cheng, G., Yamasaki, S., Saito, T., Ohba, Y.*, et al.* (2011). Induction of colonic regulatory T cells by indigenous Clostridium species. Science *331*, 337-341.

Bae, S.J., Shin, M.W., Son, T., Lee, H.S., Chae, J.S., Jeon, S., Oh, G.T., and Kim, K.W. (2019). Ninjurin1 positively regulates osteoclast development by enhancing the survival of prefusion osteoclasts. Exp Mol Med *51*, 7.

Bain, C.C., Scott, C.L., Uronen-Hansson, H., Gudjonsson, S., Jansson, O., Grip, O., Guilliams, M., Malissen, B., Agace, W.W., and Mowat, A.M. (2013). Resident and pro-inflammatory macrophages in the colon represent alternative context-dependent fates of the same Ly6Chi monocyte precursors. Mucosal Immunol *6*, 498-510.

Belkaid, Y., and Hand, T.W. (2014). Role of the microbiota in immunity and inflammation. Cell *157*, 121-141.

Bernardo, D., Marin, A.C., Fernandez-Tome, S., Montalban-Arques, A., Carrasco, A., Tristan, E., Ortega-Moreno, L., Mora-Gutierrez, I., Diaz-Guerra, A., Caminero-Fernandez, R.*, et al.* (2018). Human intestinal pro-inflammatory CD11c(high)CCR2(+)CX3CR1(+) macrophages, but not their tolerogenic CD11c(-)CCR2(-)CX3CR1(-) counterparts, are expanded in inflammatory bowel disease. Mucosal Immunol *11*, 1114-1126.

Carvalho, F.A., Koren, O., Goodrich, J.K., Johansson, M.E., Nalbantoglu, I., Aitken, J.D., Su, Y., Chassaing, B., Walters, W.A., Gonzalez, A.*, et al.* (2012). Transient inability to manage proteobacteria promotes chronic gut inflammation in TLR5-deficient mice. Cell Host Microbe *12*, 139-152.

Cerovic, V., Bain, C.C., Mowat, A.M., and Milling, S.W. (2014). Intestinal macrophages and dendritic cells: what's the difference? Trends Immunol *35*, 270-277.

Chang, P.V., Hao, L., Offermanns, S., and Medzhitov, R. (2014). The microbial metabolite butyrate regulates intestinal macrophage function via histone deacetylase inhibition. Proc Natl Acad Sci U S A *111*, 2247-2252.

Chassaing, B., Aitken, J.D., Malleshappa, M., and Vijay-Kumar, M. (2014). Dextran sulfate sodium (DSS)-induced colitis in mice. Curr Protoc Immunol *104*, Unit 15.25.

Chen, L., Wilson, J.E., Koenigsknecht, M.J., Chou, W.C., Montgomery, S.A., Truax, A.D., Brickey, W.J., Packey, C.D., Maharshak, N., Matsushima, G.K.*, et al.* (2017). NLRP12 attenuates colon inflammation by maintaining colonic microbial diversity and promoting protective commensal bacterial growth. Nat Immunol *18*, 541-551.

Cho, S.J., Rossi, A., Jung, Y.S., Yan, W., Liu, G., Zhang, J., Zhang, M., and Chen, X. (2013). Ninjurin1, a target of p53, regulates p53 expression and p53-dependent cell survival, senescence, and radiation-induced mortality. Proc Natl Acad Sci U S A *110*, 9362-9367.

Choi, S., Woo, J.K., Jang, Y.S., Kang, J.H., Hwang, J.I., Seong, J.K., Yoon, Y.S., and Oh, S.H. (2018). Ninjurin1 Plays a Crucial Role in Pulmonary Fibrosis by Promoting Interaction between Macrophages and Alveolar Epithelial Cells. Sci

Rep *8*, 17542.

Couturier-Maillard, A., Secher, T., Rehman, A., Normand, S., De Arcangelis, A., Haesler, R., Huot, L., Grandjean, T., Bressenot, A., Delanoye-Crespin, A., *et al.* (2013). NOD2-mediated dysbiosis predisposes mice to transmissible colitis and colorectal cancer. J Clin Invest *123*, 700-711.

Denning, T.L., Wang, Y.C., Patel, S.R., Williams, I.R., and Pulendran, B. (2007). Lamina propria macrophages and dendritic cells differentially induce regulatory and interleukin 17-producing T cell responses. Nat Immunol *8*, 1086-1094.

Di Sabatino, A., Morera, R., Ciccocioppo, R., Cazzola, P., Gotti, S., Tinozzi, F.P., Tinozzi, S., and Corazza, G.R. (2005). Oral butyrate for mildly to moderately active Crohn's disease. Aliment Pharmacol Ther *22*, 789-794.

Dinh, D.M., Volpe, G.E., Duffalo, C., Bhalchandra, S., Tai, A.K., Kane, A.V., Wanke, C.A., and Ward, H.D. (2015). Intestinal microbiota, microbial translocation, and systemic inflammation in chronic HIV infection. J Infect Dis *211*, 19-27.

Elinav, E., Strowig, T., Kau, A.L., Henao-Mejia, J., Thaiss, C.A., Booth, C.J., Peaper, D.R., Bertin, J., Eisenbarth, S.C., Gordon, J.I., *et al.* (2011). NLRP6 inflammasome regulates colonic microbial ecology and risk for colitis. Cell *145*, 745-757.

Flint, H.J., Scott, K.P., Louis, P., and Duncan, S.H. (2012). The role of the gut microbiota in nutrition and health. Nat Rev Gastroenterol Hepatol *9*, 577-589.

Gallo, R.L., and Hooper, L.V. (2012). Epithelial antimicrobial defence of the skin and intestine. Nat Rev Immunol *12*, 503-516.

Gordon, S., and Martinez, F.O. (2010). Alternative activation of macrophages: mechanism and functions. Immunity *32*, 593-604.

Goyal, N., and Shukla, G. (2013). Probiotic Lactobacillus rhamnosus GG modulates the mucosal immune response in Giardia intestinalis-infected BALB/c mice. Dig Dis Sci *58*, 1218-1225.

Gradel, K.O., Nielsen, H.L., Schonheyder, H.C., Ejlertsen, T., Kristensen, B., and Nielsen, H. (2009). Increased short- and long-term risk of inflammatory bowel disease after salmonella or campylobacter gastroenteritis. Gastroenterology *137*, 495-501.

Halfvarson, J., Brislawn, C.J., Lamendella, R., Vazquez-Baeza, Y., Walters, W.A., Bramer, L.M., D'Amato, M., Bonfiglio, F., McDonald, D., Gonzalez, A.*, et al.* (2017). Dynamics of the human gut microbiome in inflammatory bowel disease. Nat Microbiol *2*, 17004.

Handley, S.A., Desai, C., Zhao, G., Droit, L., Monaco, C.L., Schroeder, A.C., Nkolola, J.P., Norman, M.E., Miller, A.D., Wang, D.*, et al.* (2016). SIV Infection-Mediated Changes in Gastrointestinal Bacterial Microbiome and

Virome Are Associated with Immunodeficiency and Prevented by Vaccination. Cell Host Microbe *19*, 323-335.

Hooper, L.V., Littman, D.R., and Macpherson, A.J. (2012). Interactions between the microbiota and the immune system. Science *336*, 1268-1273.

Hoshi, N., Schenten, D., Nish, S.A., Walther, Z., Gagliani, N., Flavell, R.A., Reizis, B., Shen, Z., Fox, J.G., Iwasaki, A.*, et al.* (2012). MyD88 signalling in colonic mononuclear phagocytes drives colitis in IL-10-deficient mice. Nature communications *3*, 1120.

Hume, D.A., Perry, V.H., and Gordon, S. (1984). The mononuclear phagocyte system of the mouse defined by immunohistochemical localisation of antigen F4/80: macrophages associated with epithelia. Anat Rec *210*, 503-512.

Hunter, M.M., Wang, A., Parhar, K.S., Johnston, M.J., Van Rooijen, N., Beck, P.L., and McKay, D.M. (2010). In vitro-derived alternatively activated macrophages reduce colonic inflammation in mice. Gastroenterology *138*, 1395-1405.

Ifergan, I., Kebir, H., Terouz, S., Alvarez, J.I., Lecuyer, M.A., Gendron, S., Bourbonniere, L., Dunay, I.R., Bouthillier, A., Moumdjian, R.*, et al.* (2011). Role of Ninjurin-1 in the migration of myeloid cells to central nervous system inflammatory lesions. Ann Neurol *70*, 751-763.

Isidro, R.A., and Appleyard, C.B. (2016). Colonic macrophage polarization in

homeostasis, inflammation, and cancer. Am J Physiol Gastrointest Liver Physiol *311*, G59-73.

Jennewein, C., Sowa, R., Faber, A.C., Dildey, M., von Knethen, A., Meybohm, P., Scheller, B., Drose, S., and Zacharowski, K. (2015). Contribution of Ninjurin1 to Toll-like receptor 4 signaling and systemic inflammation. Am J Respir Cell Mol Biol *53*, 656-663.

Ji, J., Shu, D., Zheng, M., Wang, J., Luo, C., Wang, Y., Guo, F., Zou, X., Lv, X., Li, Y.*, et al.* (2016). Microbial metabolite butyrate facilitates M2 macrophage polarization and function. Sci Rep *6*, 24838.

Kamada, N., Hisamatsu, T., Okamoto, S., Chinen, H., Kobayashi, T., Sato, T., Sakuraba, A., Kitazume, M.T., Sugita, A., Koganei, K.*, et al.* (2008). Unique CD14 intestinal macrophages contribute to the pathogenesis of Crohn disease via IL-23/IFN-gamma axis. J Clin Invest *118*, 2269-2280.

Kaufmann, S.H.E., and Dorhoi, A. (2016). Molecular Determinants in Phagocyte-Bacteria Interactions. Immunity *44*, 476-491.

Khor, B., Gardet, A., and Xavier, R.J. (2011). Genetics and pathogenesis of inflammatory bowel disease. Nature *474*, 307-317.

Kiesler, P., Fuss, I.J., and Strober, W. (2015). Experimental Models of Inflammatory Bowel Diseases. Cell Mol Gastroenterol Hepatol *1*, 154-170.

Kim, T.S., Jin, Y.B., Kim, Y.S., Kim, S., Kim, J.K., Lee, H.M., Suh, H.W., Choe, J.H., Kim, Y.J., Koo, B.S.*, et al.* (2019). SIRT3 promotes antimycobacterial defenses by coordinating mitochondrial and autophagic functions. Autophagy *15*, 1356-1375.

Kny, M., Csalyi, K.D., Klaeske, K., Busch, K., Meyer, A.M., Merks, A.M., Darm, K., Dworatzek, E., Fliegner, D., Baczko, I.*, et al.* (2019). Ninjurin1 regulates striated muscle growth and differentiation. PLoS One *14*, e0216987.

Kostic, A.D., Xavier, R.J., and Gevers, D. (2014). The microbiome in inflammatory bowel disease: current status and the future ahead. Gastroenterology *146*, 1489-1499.

Krieglstein, C.F., Cerwinka, W.H., Sprague, A.G., Laroux, F.S., Grisham, M.B., Koteliansky, V.E., Senninger, N., Granger, D.N., and de Fougerolles, A.R. (2002). Collagen-binding integrin alpha1beta1 regulates intestinal inflammation in experimental colitis. J Clin Invest *110*, 1773-1782.

Le, H., Ahn, B.J., Lee, H.S., Shin, A., Chae, S., Lee, S.Y., Shin, M.W., Lee, E.J., Cha, J.H., Son, T.*, et al.* (2017). Disruption of Ninjurin1 Leads to Repetitive and Anxiety-Like Behaviors in Mice. Mol Neurobiol *54*, 7353-7368.

Lee, H.J., Ahn, B.J., Shin, M.W., Jeong, J.W., Kim, J.H., and Kim, K.W. (2009). Ninjurin1 mediates macrophage-induced programmed cell death during early ocular development. Cell Death Differ *16*, 1395-1407.

Lee, H.K., Kim, I.D., Lee, H., Luo, L., Kim, S.W., and Lee, J.K. (2018). Neuroprotective and Anti-inflammatory Effects of a Dodecamer Peptide Harboring Ninjurin 1 Cell Adhesion Motif in the Postischemic Brain. Mol Neurobiol *55*, 6094-6111.

Levy, M., Kolodziejczyk, A.A., Thaiss, C.A., and Elinav, E. (2017). Dysbiosis and the immune system. Nat Rev Immunol *17*, 219-232.

Li, L., Ng, D.S., Mah, W.C., Almeida, F.F., Rahmat, S.A., Rao, V.K., Leow, S.C., Laudisi, F., Peh, M.T., Goh, A.M.*, et al.* (2015). A unique role for p53 in the regulation of M2 macrophage polarization. Cell Death Differ *22*, 1081-1093.

Lin, Y., Yang, X., Yue, W., Xu, X., Li, B., Zou, L., and He, R. (2014). Chemerin aggravates DSS-induced colitis by suppressing M2 macrophage polarization. Cell Mol Immunol *11*, 355-366.

Lucke, K., Miehlke, S., Jacobs, E., and Schuppler, M. (2006). Prevalence of Bacteroides and Prevotella spp. in ulcerative colitis. J Med Microbiol *55*, 617-624.

Mantovani, A., Biswas, S.K., Galdiero, M.R., Sica, A., and Locati, M. (2013). Macrophage plasticity and polarization in tissue repair and remodelling. J Pathol *229*, 176-185.

Martin, H.M., Campbell, B.J., Hart, C.A., Mpofu, C., Nayar, M., Singh, R., Englyst, H., Williams, H.F., and Rhodes, J.M. (2004). Enhanced Escherichia

coli adherence and invasion in Crohn's disease and colon cancer. Gastroenterology *127*, 80-93.

Mazmanian, S.K., Liu, C.H., Tzianabos, A.O., and Kasper, D.L. (2005). An immunomodulatory molecule of symbiotic bacteria directs maturation of the host immune system. Cell *122*, 107-118.

Mengaud, J., Ohayon, H., Gounon, P., Mege, R.M., and Cossart, P. (1996). E-cadherin is the receptor for internalin, a surface protein required for entry of L. monocytogenes into epithelial cells. Cell *84*, 923-932.

Minoshima, A., Kabara, M., Matsuki, M., Yoshida, Y., Kano, K., Tomita, Y., Hayasaka, T., Horiuchi, K., Saito, Y., Aonuma, T.*, et al.* (2018). Pericyte-Specific Ninjurin1 Deletion Attenuates Vessel Maturation and Blood Flow Recovery in Hind Limb Ischemia. Arterioscler Thromb Vasc Biol *38*, 2358-2370.

Moolenbeek, C., and Ruitenberg, E.J. (1981). The "Swiss roll": a simple technique for histological studies of the rodent intestine. Lab Anim *15*, 57-59.

Mosser, D.M., and Edwards, J.P. (2008). Exploring the full spectrum of macrophage activation. Nat Rev Immunol *8*, 958-969.

Mottawea, W., Chiang, C.K., Muhlbauer, M., Starr, A.E., Butcher, J., Abujamel, T., Deeke, S.A., Brandel, A., Zhou, H., Shokralla, S.*, et al.* (2016). Altered intestinal microbiota-host mitochondria crosstalk in new onset Crohn's disease.

Nature communications *7*, 13419.

Mowat, A.M. (2018). To respond or not to respond - a personal perspective of intestinal tolerance. Nat Rev Immunol *18*, 405-415.

Na, Y.R., Stakenborg, M., Seok, S.H., and Matteoli, G. (2019). Macrophages in intestinal inflammation and resolution: a potential therapeutic target in IBD. Nat Rev Gastroenterol Hepatol.

Nahon, S., Lahmek, P., Durance, C., Olympie, A., Lesgourgues, B., Colombel, J.F., and Gendre, J.P. (2012). Risk factors of anxiety and depression in inflammatory bowel disease. Inflamm Bowel Dis *18*, 2086-2091.

Nakajima, M., Arimatsu, K., Kato, T., Matsuda, Y., Minagawa, T., Takahashi, N., Ohno, H., and Yamazaki, K. (2015). Oral Administration of P. gingivalis Induces Dysbiosis of Gut Microbiota and Impaired Barrier Function Leading to Dissemination of Enterobacteria to the Liver. PLoS One *10*, e0134234.

Nava, G.M., Friedrichsen, H.J., and Stappenbeck, T.S. (2011). Spatial organization of intestinal microbiota in the mouse ascending colon. Isme j *5*, 627-638.

Okayasu, I., Hatakeyama, S., Yamada, M., Ohkusa, T., Inagaki, Y., and Nakaya, R. (1990). A novel method in the induction of reliable experimental acute and chronic ulcerative colitis in mice. Gastroenterology *98*, 694-702.

Perse, M., and Cerar, A. (2012). Dextran sodium sulphate colitis mouse model: traps and tricks. J Biomed Biotechnol *2012*, 718617.

Postler, T.S., and Ghosh, S. (2017). Understanding the Holobiont: How Microbial Metabolites Affect Human Health and Shape the Immune System. Cell Metab *26*, 110-130.

Relman, D., Tuomanen, E., Falkow, S., Golenbock, D.T., Saukkonen, K., and Wright, S.D. (1990). Recognition of a bacterial adhesion by an integrin: macrophage CR3 (alpha M beta 2, CD11b/CD18) binds filamentous hemagglutinin of Bordetella pertussis. Cell *61*, 1375-1382.

Robertson, S.J., Goethel, A., Girardin, S.E., and Philpott, D.J. (2018). Innate Immune Influences on the Gut Microbiome: Lessons from Mouse Models. Trends Immunol *39*, 992-1004.

Rooks, M.G., and Garrett, W.S. (2016). Gut microbiota, metabolites and host immunity. Nat Rev Immunol *16*, 341-352.

Santos-Antunes, J., Magro, F., and Macedo, G. (2014). Listeria monocytogenes bacteremia and CMV colitis in a patient with Ulcerative Colitis. J Crohns Colitis *8*, 254-255.

Scheppach, W., Sommer, H., Kirchner, T., Paganelli, G.M., Bartram, P., Christl, S., Richter, F., Dusel, G., and Kasper, H. (1992). Effect of butyrate enemas on the colonic mucosa in distal ulcerative colitis. Gastroenterology *103*, 51-56.

Schmitter, T., Agerer, F., Peterson, L., Munzner, P., and Hauck, C.R. (2004). Granulocyte CEACAM3 is a phagocytic receptor of the innate immune system that mediates recognition and elimination of human-specific pathogens. J Exp Med *199*, 35-46.

Shapouri-Moghaddam, A., Mohammadian, S., Vazini, H., Taghadosi, M., Esmaeili, S.A., Mardani, F., Seifi, B., Mohammadi, A., Afshari, J.T., and Sahebkar, A. (2018). Macrophage plasticity, polarization, and function in health and disease. J Cell Physiol *233*, 6425-6440.

Shin, M.W., Bae, S.J., Wee, H.J., Lee, H.J., Ahn, B.J., Le, H., Lee, E.J., Kim, R.H., Lee, H.S., Seo, J.H., *et al.* (2016). Ninjurin1 regulates lipopolysaccharide-induced inflammation through direct binding. Int J Oncol *48*, 821-828.

Sica, A., Erreni, M., Allavena, P., and Porta, C. (2015). Macrophage polarization in pathology. Cell Mol Life Sci *72*, 4111-4126.

Sica, A., and Mantovani, A. (2012). Macrophage plasticity and polarization: in vivo veritas. J Clin Invest *122*, 787-795.

Siegmund, B., Lehr, H.A., Fantuzzi, G., and Dinarello, C.A. (2001). IL-1 beta -converting enzyme (caspase-1) in intestinal inflammation. Proc Natl Acad Sci U S A *98*, 13249-13254.

Smith, P.M., Howitt, M.R., Panikov, N., Michaud, M., Gallini, C.A., Bohlooly,

Y.M., Glickman, J.N., and Garrett, W.S. (2013). The microbial metabolites, short-chain fatty acids, regulate colonic Treg cell homeostasis. Science *341*, 569-573.

Smythies, L.E., Sellers, M., Clements, R.H., Mosteller-Barnum, M., Meng, G., Benjamin, W.H., Orenstein, J.M., and Smith, P.D. (2005). Human intestinal macrophages display profound inflammatory anergy despite avid phagocytic and bacteriocidal activity. J Clin Invest *115*, 66-75.

Tang, C., Kakuta, S., Shimizu, K., Kadoki, M., Kamiya, T., Shimazu, T., Kubo, S., Saijo, S., Ishigame, H., Nakae, S.*, et al.* (2018). Suppression of IL-17F, but not of IL-17A, provides protection against colitis by inducing Treg cells through modification of the intestinal microbiota. Nat Immunol *19*, 755-765.

Tanoue, T., Umesaki, Y., and Honda, K. (2010). Immune responses to gut microbiota-commensals and pathogens. Gut microbes *1*, 224-233.

Thevaranjan, N., Puchta, A., Schulz, C., Naidoo, A., Szamosi, J.C., Verschoor, C.P., Loukov, D., Schenck, L.P., Jury, J., Foley, K.P.*, et al.* (2018). Age-Associated Microbial Dysbiosis Promotes Intestinal Permeability, Systemic Inflammation, and Macrophage Dysfunction. Cell Host Microbe *23*, 570.

Tye, H., Yu, C.H., Simms, L.A., de Zoete, M.R., Kim, M.L., Zakrzewski, M., Penington, J.S., Harapas, C.R., Souza-Fonseca-Guimaraes, F., Wockner, L.F.*, et al.* (2018). NLRP1 restricts butyrate producing commensals to exacerbate inflammatory bowel disease. Nature communications *9*, 3728.

Walters, W.A., Xu, Z., and Knight, R. (2014). Meta-analyses of human gut microbes associated with obesity and IBD. FEBS Lett *588*, 4223-4233.

Wellman, A.S., Metukuri, M.R., Kazgan, N., Xu, X., Xu, Q., Ren, N.S.X., Czopik, A., Shanahan, M.T., Kang, A., Chen, W.*, et al.* (2017). Intestinal Epithelial Sirtuin 1 Regulates Intestinal Inflammation During Aging in Mice by Altering the Intestinal Microbiota. Gastroenterology *153*, 772-786.

Woo, J.K., Jang, Y.S., Kang, J.H., Hwang, J.I., Seong, J.K., Lee, S.J., Jeon, S., Oh, G.T., Lee, H.Y., and Oh, S.H. (2016). Ninjurin1 inhibits colitis-mediated colon cancer development and growth by suppression of macrophage infiltration through repression of FAK signaling. Oncotarget *7*, 29592-29604.

Yang, H.J., Zhang, J., Yan, W., Cho, S.J., Lucchesi, C., Chen, M., Huang, E.C., Scoumanne, A., Zhang, W., and Chen, X. (2017). Ninjurin 1 has two opposing functions in tumorigenesis in a p53-dependent manner. Proc Natl Acad Sci U S A *114*, 11500-11505.

Zeng, M.Y., Inohara, N., and Nunez, G. (2017). Mechanisms of inflammation-driven bacterial dysbiosis in the gut. Mucosal Immunol *10*, 18-26.

Zhou, X., Li, W., Wang, S., Zhang, P., Wang, Q., Xiao, J., Zhang, C., Zheng, X.,

Xu, X., Xue, S.*, et al.* (2019). YAP Aggravates Inflammatory Bowel Disease by Regulating M1/M2 Macrophage Polarization and Gut Microbial Homeostasis. Cell Rep *27*, 1176-1189.e1175.

요약 (국문초록)

비정상적인 M1/M2 대식세포 분극화 및 장내 미생물의 불균형으로 인한 대장 항상성의 파괴는 염증성 장질환 (IBD)의 발병에 기여한다. 그러나, 이러한 대장 항상성을 매개하는 분자 인자는 잘 특성화되어 있지 않다. 현재 연구에서는 Ninjurin1 (Ninj1)이 항상성 또는 대장염을 유도한 조건에서 대식 세포 분극화와 장내 미생물의 구성을 조절하여 과도한 대장 염증을 제한하는 것을 발견하였다. Ninj1 유전자 결핍 생쥐는 대장염을 일으키는 경향(colitogenic)의 *Prevotellaceae* 과의 계통 증가와 면역 조절(immunoregulation)에 관여하는 *Lachnospiraceae* 과의 계통 감소와 함께 대장염에 대한 과민증을 나타냈다. 흥미롭게도, Ninj1 유전자 결핍 생쥐를 WT 생쥐와 공동 거주 시키면 *Lachnospiraceae* 과의 증가와 *Prevotellaceae* 과의 감소를 유도하였고, 이것은 Ninj1 유전자 결핍 생쥐에서 나타나는 심한 대장염의 발생을 상당히 개선시켰다. 항상성 조건에서는, Ninj1 결핍 생쥐의 대장 조직 내에 M1 대식세포의 빈도가 WT 생쥐의 대장 조직과 비교하여 더 높았으며, 이것은 대장 내에 기저 염증의 증가와 장내 미생물의 불균형을 증가시키는 데 기여하는 것으로 보여진다. 대장염을 유도 한 후에는, 항상성 조건과 비교하여 대식세포에서 Ninj1의 발현이 증가된다. 동시에, Ninj1 결핍 생쥐는 WT 생쥐와 비교하여 M2

대식세포의 감소와 광범위한 장내 미생물의 불균형이 관찰되었고, 이것은 심한 대장 염증으로 진행과 대장 염증으로부터 회복 장애와 관련이 있었다. 시험관 내에서, 마우스 및 인간 대식세포에서 Ninj1 녹다운은 대조군과 비교하여 M1 분극화를 활성화 시키고 M2 분극화는 제한시켰다. 마지막으로, Ninj1 결핍 생쥐에 WT 유래 대식세포의 이식은 Ninj1 결핍 생쥐에서 나타나는 심한 대장염을 개선시켰다. 종합해보면, 이러한 연구 결과는 Ninj1이 M1/M2 대식세포의 균형을 조절하고 광범위한 장내 미생물의 불균형 (extensive dysbiosis)을 막아 대장 항상성을 매개한다는 것을 뒷받침하며, IBD의 예방과 치료에 대한 시사점을 제공한다.

주 요 어 : Ninjurin1; inflammatory bowel disease; inflammation; M1 macrophages; M2 macrophages; homeostasis; dysbiosis; colitis development; colitis recovery

학 번 : 2015-30513